UC Berkeley
UC Berkeley Electronic Theses and Dissertations

Title
Exploring the Potential of Autonomous Vehicles in Mixed Autonomy Transportation Systems

Permalink
https://escholarship.org/uc/item/9xt9v883

Author
Li, Ruolin

Publication Date
2023

Peer reviewed|Thesis/dissertation

Exploring the Potential of Autonomous Vehicles in Mixed Autonomy Transportation
Systems

By

Ruolin Li

A dissertation submitted in partial satisfaction of the

requirements for the degree of

Doctor of Philosophy

in

Engineering – Mechanical Engineering

in the

Graduate Division

of the

University of California, Berkeley

Committee in charge:

Professor Roberto Horowitz, Chair
Professor Joan Walker
Professor Murat Arcak

Summer 2023

Exploring the Potential of Autonomous Vehicles in Mixed Autonomy Transportation Systems

Abstract

Exploring the Potential of Autonomous Vehicles in Mixed Autonomy Transportation Systems

by

Ruolin Li

Doctor of Philosophy in Engineering – Mechanical Engineering

University of California, Berkeley

Professor Roberto Horowitz, Chair

Vehicular traffic congestion remains a critical challenge in metropolitan areas around the world. Effectively addressing this problem requires a deep understanding of traffic congestion from a behavioral perspective, as human drivers tend to prioritize their own interests, which leads to selfish behaviors that negatively impact the entire traffic system's efficiency. In contrast, autonomous and connected vehicles, under rapid development, are capable of better coordinating their motion with other neighboring autonomous vehicles and with roadside infrastructure, resulting in potential significant capacity and mobility improvements in the overall transportation networks. However, as a consequence, transportation systems are facing not only unprecedented opportunities but also challenges in the transition to future intelligent transportation systems involving autonomous vehicles.

This dissertation explores the potential improvements that autonomous road vehicles may bring in diverse transportation scenarios and their overall impact on the broader transportation landscape. The study focuses on *two approaches* for the application of autonomous vehicles: first, as altruistic decision-makers, and second, by maintaining a shortened headway. These approaches are analyzed via *four scenarios* that are typical in road vehicle transportation networks: diverges with a bifurcating lane in the middle, highway on-ramps, vehicles' routing on networks, and highway toll lanes. The study emphasizes *three challenges* that are crucial to successfully integrate autonomous vehicles into existing transportation systems that are predominantly transited by human-driven vehicles: first, accurately yet concisely modeling human behavior; second, modeling multi-agent systems that incorporate the key features of autonomous vehicles; and third, developing suitable traffic management and optimization strategies for societal benefits. This dissertation aims to shed light on the complexities of the current transportation revolution and provide valuable insights into the path forward: autonomous vehicles have various potentials to serve for enhanced societal benefits while selfish drivers may exploit the benefits brought by autonomous vehicles.

Therefore, effective management and optimization methods are necessary to boost the performance of transportation networks to pave the way for a safer, more efficient, and more sustainable future transportation system.

Specifically, in this dissertation, a unified game-theoretic framework is first presented to model and examine the selfish lane choice behavior of human-driven vehicles at various traffic merges and diverges, which exhibits promising predictive power with minimal parameter calibration requirements. A systematic method is then proposed to induce altruistic decision-making behavior of autonomous vehicles locally, which configures the costs perceived by autonomous vehicles with a socially aware component. Moreover, a comprehensive theoretical analysis is conducted from both static and dynamic perspectives on the routing of mixed autonomy, where autonomous vehicles are configured with a controllable shorter longitudinal headway compared to human-driven vehicles. This analysis examines the impact and stability of the resulting routing system, providing valuable insights into the potential benefits induced by autonomous vehicles with shortened headway. Furthermore, the coexistence of mixed autonomy and high-occupancy vehicles in a toll lane scenario is investigated and a unified toll lane framework that integrates and compares autonomous vehicles and high-occupancy vehicles is proposed. The effectiveness of this framework is demonstrated across various application situations, including toll design, policy formulation and regulation of autonomy.

Contents

IIIHeadway in Organization   52

List of Figures

Acknowledgments

The past years at UC Berkeley have been a transformative life experience for me, giving me the opportunity to reflect on my own identity and aspirations and to envision the future I am truly passionate about. I would like to first express my sincerest gratitude to my research advisor Roberto Horowitz. I am truly thankful for the exceptional guidance, unwavering encouragement, profound insights, and genuine concern for humanity he has consistently provided me throughout my research journey. Under his mentorship, I have been fortunate to experience the true spirit of research, explore meaningful problems in uncharted territories, and think creatively in awe of science. Roberto's support has been providing me with a strong pillar of stability even during times of extreme uncertainty and challenges.

I extend my heartfelt appreciation to Joan Walker, who questioned me, inspired me and never ceased to encourage me in my research. It was during our conversation at my qualification exam that I found my initial spark to pursue a lifelong career in research. During my doctoral studies, I have been greatly influenced and motivated by Murat Arcak, for whom I hold deep appreciation and gratitude. Murat's commitment to rigorous research, graceful work manner, and compassionate nature toward students have profoundly inspired and impacted my academic journey. I am immensely grateful to Robert Powell. His invaluable assistance persisted until the end of his life and his unwavering dedication to students has served as a constant reminder and motivation for me to strive for excellence as a future educator. I extend my heartfelt thanks to Negar Mehr, an exceptional collaborator and mentor at the beginning of my doctoral studies. I discovered the beauty of research during our collaborations. Her strength and determination have continued to inspire me in countless ways, even if I may not fully realize all of them. I would like to acknowledge Philip Brown for his remarkable qualities of inquisitiveness, perceptiveness, and composure in our online conversations during the pandemic, which have always been a source of inspiration to me.

I consider myself extremely fortunate to have had the opportunity to engage in inspiring conversations with Pravin Varaiya and Masayoshi Tomizuka, who have offered valuable advice that has greatly influenced my research journey. Their wisdom and guidance have been instrumental in shaping my academic development. I would like to express my heartfelt appreciation to Alex Kurzhanskiy and Gabriel Gomez for their mentorship at the initial stage of my graduate studies. Their assistance and mentorship were pivotal in helping me navigate the start in my academic career. I am grateful to Matthew Wright for his selfless assistance and warm heart during the early years of my graduate studies. I extend my deep gratitude to Mark Mueller and Paul Grigas for their invaluable support during my qualification process. Furthermore, I am indebted to Kameshwar Poolla, who taught my first control courses at the beginning of my graduate studies which shaped my trajectory even before my research began. His belief in my potential has been invaluable throughout my academic journey.

I would like to thank the brilliant and kind people who I have worked with: Zahra Amini, Stanley Smith, Mikhail Burov, Prateek Shah, Zhi Chen, Mathias Wulfman, Nikhil Potu Surya, and Joohwan Seo, whose encouragement and friendship have made this journey more rewarding. I am especially grateful to Yeping Hu, for her enjoyable company in the years

and countless memorable discussions on research and life. I would like to extend my utmost gratitude to Jiaxi Liu, for her warm company, remarkable tenderness, and extraordinary tolerance during the most challenging times. I cherish every moment we share on and off campus. I would also like to express my heartfelt appreciation to my selfless friends in all corners of the world for providing me with solace and strength in our conversations and reminding me of the power of human connection and compassion.

I am profoundly grateful to my loving parents, whose support and encouragement have been a constant presence throughout my journey. Their belief in me and the freedom they have granted me to pursue my goals are invaluable. I am especially grateful to my father, Dongming Li, for envisioning an unlimited future for me, for always listening with patience and comprehending the difficulties I have encountered, and for demonstrating courage and responsibility as a role model of a strong character facing life's challenges. I extend my deepest thanks to my mother, Xiaojuan Lin, whose empathy, and optimism have been an endless source of strength and motivation for me. Her dedication to daily life and her nurturing presence have provided me with the resilience and determination needed to overcome obstacles.

I am particularly grateful for the support and companionship of Xudong Frank Wang. His presence has provided me with a profound sense of security, and he has been an endless source of inspiration and encouragement. I want to express my sincere appreciation for his vibrant spirit and boundless energy, as well as his tranquil presence and composed demeanor. The distinct yet harmonious nature of our behavior, perspectives, and styles ignites my passion for the diverse, thriving, and occasionally chaotic world.

Part I

Introduction

Chapter 1

Mixed Autonomy: Human-driven and Autonomous vehicles

Road traffic congestion is a major source of inefficiency in modern society. According to INRIX 2022 Global Traffic Scorecard [1], in 2022, congestion delays in the US alone resulted in drivers collectively losing over 4.8 billion hours and costing the country approximately 81 billion dollars. While the data has not yet reached pre-COVID levels, it is steadily climbing once again following the pandemic. Severe congestion not only results in a significant waste of resources and energy but also constantly interrupts peoples' daily lives and increases drivers' fatigue and road rage, and therefore, becomes the source of anxiety for numerous drivers and passengers.

To improve the efficiency of traffic networks, researchers and engineers have studied various methods such as ramp metering for freeway networks [2]–[4], signaling controls for urban networks [5]–[8] and pricing policies [9]–[11]. Recently, with the development of autonomous vehicles, researchers have also considered controlling the autonomous vehicles on the roads to improve the overall traffic performance [12]–[18].

Decades of research on autonomous vehicles and rapidly developing communication technologies have shed light on the large–scale deployment of autonomous and connected vehicles, which can profoundly alter the way people commute in the future. Autonomous vehicles, as an alternative to human-driven vehicles, are expected to perform in a better way for certain metrics. For example, it is expected that autonomous vehicles can improve travel safety by potentially reducing human errors [19], [20]. Moreover, by predicting the upcoming traffic signals and observing the movements of surrounding vehicles, autonomous vehicles can reduce fuel consumption and increase network sustainability [21], [22]. In addition, with cooperative strategies, autonomous vehicles can also increase the capacity of the local traffic [23], [24]. In particular, in this dissertation, we focus on two major features of autonomous vehicles (altruistic decision-making and controllable headway) and analyze the consequent impact on mixed autonomy transportation systems.

1.1 Selfish versus Altruistic Choice Behavior

Human drivers on the roads can be selfish, which implies that human drivers only care about their own costs and make decisions aiming to minimize their own costs. Lane-changing behavior is one typical potentially selfish behavior, and it is well known that vehicles' complex and unpredictable lane-change maneuvers can be a significant cause of congestion and safety concerns. Unfortunately, lane changes are notoriously difficult to model, both because it is difficult to predict when and why a driver might change lanes *and* how their maneuver will affect the movements of other vehicles [25].

A significant number of papers that analyze lane changes at the "microscopic level" focus on determining accurate yet simple driver behavior models that will be able to reproduce actual individual vehicle's lane changing behavior in a variety of scenarios. These lane-changing models can be categorized into four groups [26], among which rule-based models are widely explored. In [27], a typical rule-based model of a driver's lane-changing decision-making process is formulated, focusing on decisions that balance safety concerns with lane-changing incentives. These decisions require a series of evaluations concerning the velocity and proximity of the vehicles that surround the *ego vehicle* in the lane that it wishes to change to. Much work, both theoretical and simulation-based, has taken place on so-called "gap acceptance models", which model whether a driver will attempt to change lanes as a function of the inter-vehicle gaps that arise in their target lane (see [28]–[30], among others). Subsequently, researchers have endeavored to decipher people's decision-making process when performing a lane-changing maneuver via a variety of rule-based microscopic models. In [31], for example, a new lane-changing model, MOBIL, is proposed to minimize the overall braking induced by lane change. Microscopic-level research in vehicles' lane-changing behavior also considers the different characteristics that vehicles' lane–changing behaviors exhibit in various traffic scenarios and road configurations. For example, in [32], [33], the lane-changing behavior in a merging scenario is studied. Recently, a series of papers have been presented that study microscopic lane-changing behavior using game theory, such as [34], [35], which have brought new perspectives and insights to the field. Generally, microscopic modeling of human drivers' lane changing behavior can involve parameters sensitive to drivers' own characteristics, which need to be calibrated for distinct drivers to achieve accurate modeling. When a large number of vehicles are of interest, it is hard to attain or calibrate such a great number of parameters.

Another considerable part of related work addresses the "macroscopic" impact of vehicles' lane changing behavior, i.e., how lane changes affect other vehicles and the aggregate traffic conditions. In [36], [37], it is shown that the social delay may deteriorate under vehicles' selfish routing behavior. In [38], [39], researchers studied the macroscopic characteristics that affect vehicles' lane-changing behavior. Among all the traffic scenarios, highway on-ramps have gained considerable attention. In [40], lane-changing behaviors of vehicles entering a freeway on-ramp and how it affects the onset of congestion are examined. In [41], it is shown that lane-changing behaviors frequently cause the well-known "freeway capacity drop" phenomenon. Subsequently, [42], [43] analyzed the macroscopic impacts qualitatively
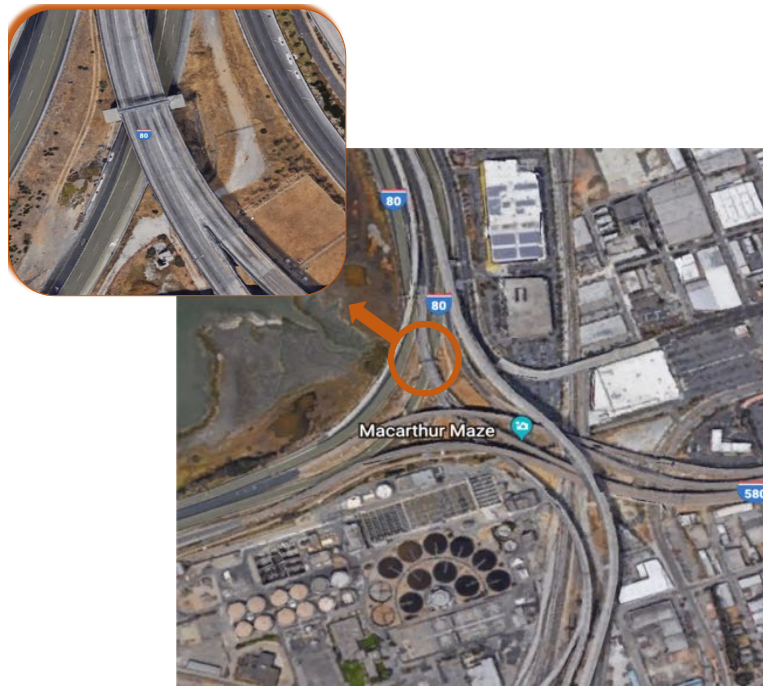
Figure 1.1: Satellite imagery from Google Earth of the MacArthur Maze with an enlarged
view of a typical diverge with a bifurcating lane.

and quantitatively of lane changing behaviors focusing on the section of lanes away from
freeway diverges, by modeling lane changing vehicles as particles linking interactive streams
on different lanes. In [44], a scenario where vehicles bypass at the end of the diverge is
studied, and the macroscopic choice behavior of vehicles of such a process is modeled as
a Wardrop equilibrium [45]. The resulting model shows impressive predictive power and
can be easily calibrated. Macroscopic modeling of human drivers' lane changing behavior
usually only require parameters that are more robust to drivers' own characteristics compared
to microscopic modeling. When a large number of vehicles' behavior or its impact are of
interest, macroscopic modeling can efficiently achieve the accuracy without considering a
single vehicle's characteristics.

In this dissertation, we approach and analyze the macroscopic lane changing or lane
choice behavior of selfish human-driven vehicles in various commonly encountered traffic
network scenarios. We assume that all human-driven vehicles act selfishly, i.e., they choose
a lane only when their own cost is minimized. We then aim to accurately model and predict
human-driven vehicles' selfish lane choice behavior and evaluate its impact on social traffic
conditions.

One typical scenario is a frequent cause of bottlenecks: *bifurcating* lanes at traffic diverges.
Bifurcating lanes are encountered in (poorly designed) complex distribution structures, such
as the four-freeway interchange in the San Francisco Bay Area known as the MacArthur

Maze (see Figure 1.1 for an aerial photograph of the MacArthur Maze), where consecutive
diverges with bifurcating lanes are employed to split the I-80 west/I-580 east (Eastshore
Freeway) traffic into 1) traffic going towards San Francisco via the I-80 west (Bay Bridge),
2) traffic going towards downtown Oakland, Walnut Creek, Hayward or Stockton via I-580
east (MacArthur Freeway) and I-980, and 3) traffic going towards San Jose via I-880 south
(Nimitz Freeway). The enlarged view in Figure 1.1 shows a typical diverge with a bifurcating
lane: one upstream lane in the middle target two exit directions (a bifurcating lane), whereas
each of the two upstream lanes on the sides only target one of the exit directions (feed-
through lanes). Vehicles face two choices at the diverge. One is to employ a feed-through
lane on the sides, while the other is to employ the bifurcating lane. Selfish drivers would
only employ the bifurcating lane in order to save time or effort, as compared to using one of
the feed–through lanes, and vice versa. Thus, in Chapter 3, we focus on the bifurcating lane
scenario and present a model that describes the decision-making process of selfish drivers at
such traffic diverges from a macroscopic view. The model is in a similar form of a Wardrop
Equilibrium [45] in the routing scenario, but it reveals the specific characteristics of vehicular
lane choice behavior at the bifurcating lane scenario, which to the best of our knowledge, has
not been previously addressed in the literature. Moreover, the model predicts selfish vehicles'
lance choice behavior at the diverge accurately but only requires traffic flow information at
the diverge, which is realistically attainable, in the calibration process of a small number of
parameters in the model.

Highway on–ramps are another typical bottlenecks which are severely affected by vehicles'
selfish lane–changing behaviors [46]. Vehicles' complex lane–changing behavior at on-ramp
areas can enormously contribute to the potential congestion propagating from the on-ramp
onto the highway mainline. However, it is hard to develop an expressive yet simple model to
accurately describe the underlying complex lane–changing behavior and meanwhile quantify
the potential resultant congestion. In Chapter 4, we focus on the selfish lane choice behavior
of mainline vehicles' facing on-ramps ahead. With the presence of an on-ramp, mainline
vehicles traveling on the outermost lane have two options: they either bypass the merging
area by switching to an inner lane, or they stay steadfast on the current lane and merge with
on-ramp vehicles later. We model and predict the macroscopic lane choice behavior of selfish
mainline vehicles facing on–ramps in a similar form to the Wardrop equilibrium while showing
unique characteristics of the behavior. We also show the model's promising predictive power
and ease of calibration, and further reveal that there is a gap between mainline vehicles' selfish
behavior and the socially optimal behavior, i.e., such selfish lane choice behavior degrades
social traffic conditions. The model analytically explains one underlying mechanism of how
the congestion forms at on-ramps and propagates onto the highway mainline.

Due to that vehicles' selfish behavior is one significant cause of severe bottlenecks, re-
searchers have resorted to various methods to constrain or guide vehicles' selfish behaviors to
improve social traffic conditions. In [11], [47]–[50], the impact of the toll pricing on vehicles
is studied in vehicles' selfish routing scenario. In [51], [52], a specific kind of toll called the
marginal cost is proved to be capable of optimizing the social delay when vehicles are selfish
routing. Recently, autonomous vehicles, which are more controllable than human-driven ve-

hicles, are also increasingly studied on transportation networks. In [53], autonomous vehicles are regarded as altruistic vehicles, which are willing to take routes with a longer delay than the quickest route when routing on a transportation network.

In Chapter 5, we propose to employ a proportion of altruistic vehicles among the selfish mainline vehicles to improve the social traffic conditions in the highway on-ramp scenarios studied in Chapter 4. *Selfish* mainline vehicles choose to stay steadfast or bypass to minimize their own travel delay, whereas *altruistic* vehicles make the decision to stay steadfast or bypass to minimize their own altruistic cost, which is a weighted average of the travel delay and the marginal cost [51], [52]. The weight configuration of the altruistic costs indicates how altruistic vehicles are. Altruistic vehicles are individual optimizers that require local delay and cost information but no centralized coordination. With the presence of autonomous vehicles, it is envisioned that connected and autonomous vehicles can be employed as altruistic vehicles perceiving and minimizing configured altruistic costs. To evaluate the effectiveness of the method, we first consider when the altruistic costs are perfectly measured by altruistic vehicles, and we find the conditions under which altruism helps to decrease or optimize the social delay. The conditions indicate altruism always improves social traffic conditions when altruistic vehicles are abundant, but to optimize social traffic conditions, the altruistic vehicles further need to be purely altruistic by not weighing their own travel delay at all. We also consider the scenarios when altruistic vehicles only have inaccurate estimates of altruistic costs, which are common in real-world applications. In the presence of measurement errors, the original optimal configurations of altruistic vehicles can be unexpectedly undermined. We then give the optimal weight configuration for altruistic vehicles that minimizes the worst-case social delay under such uncertainty.

1.2   Spontaneous versus Controllable Headway

Previous literature has also shown that under fine-tuned control, autonomous vehicles are capable of increasing lane capacities by forming platoons (a fleet of vehicles traveling with a predetermined headway) and preserving a shorter headway at a higher speed compared to human-driven vehicles [13], [23], [24]. Results in [13] have shown that the traffic throughput can be increased up to three-fold by platooning connected and autonomous vehicles. It is also shown that vehicle platoons are able to increase the capacity of intersections and decrease the total fuel consumption [54], [55]. Various research works also focused on the low-level effective control of vehicles in platoons [56]–[60].

The platooning ability of autonomous vehicles will also influence vehicle routing on transportation networks that are shared by both human-driven and autonomous vehicles. For a network with only human-driven vehicles, it is generally assumed that vehicles route selfishly, i.e., a vehicle never unilaterally changes to a route with a longer delay than its current route. Such selfish routing of vehicles to minimize their own travel cost with no consideration of the total traffic conditions may result in a tremendous waste of resources and even congested transportation networks [37], [61]. The selfish routing equilibria can be charac-

terized by Wardrop conditions and the selfish routing behavior of vehicles then converges
to the Wardrop equilibrium [45]. Such Wardrop equilibria may lead to higher total travel
costs compared to the scenario when all vehicles are altruistic, i.e, the goal of all vehicles is
to minimize the total travel costs [37], [61]. When autonomous vehicles are also present in
the transportation networks, considering that the delay of each roadway in the network is
related to the capacity of the roadway by functions such as Bureau of Public Roads (BPR)
delay functions [62], autonomous and connected vehicles can increase the capacity and de-
crease the delay of the roadways in the network [63]. Therefore, the presence of autonomous
vehicles will induce an impact on the overall traffic conditions of the transportation network.
However, such impact may be unexpectedly complex to model or predict due to vehicles'
competitive selfish routing behavior, for example, it was shown in [15] that increasing the
penetration rate of autonomous and connected vehicles in the network, may actually worsen
the traffic network's overall traffic conditions in certain scenarios.

In Chapter 6 and 7, we examine a routing game of mixed autonomy where both human–
driven and autonomous vehicles route selfishly on a transportation network shared by both
human-driven and autonomous vehicles. Compared to human-driven vehicles, autonomous
vehicles are able to increase road capacities by preserving a shorter headway. We utilize a
variable, capacity asymmetry degree [15] for each road in the network, which is the ratio
between the road capacity when all vehicles are human-driven and the road capacity when all
vehicles are autonomous, to mathematically characterize the impact of autonomous vehicles'
shorter headway on each road's capacity. The shorter the headway of autonomous vehicles
is, the smaller the capacity asymmetry degree is. We then innovate the traditional trans-
portation models to investigate the potential of autonomous vehicles in future transportation
systems.

In Chapter 6, we consider a selfish routing game of mixed autonomy on a transportation
network where all roads share a uniform penetration rate of autonomous vehicles and capacity
asymmetry degree. A central authority exists and is able to dictate a prescribed longitudi-
nal headway for platooning autonomous vehicles on each road. Therefore, the centralized
authority can adjust the headway of autonomous vehicles on each road in the network. We
then study the impact of varying the headway of autonomous vehicles on the social delay
of the network at the resulting Wardrop routing equilibrium [45]. We prove that, for net-
works with a single origin-destination (O/D) pair, we can always decrease the social delay by
decreasing the headway until the allowable minimum headway. For networks with parallel
links, we provide an estimate of the greatest impact of autonomous vehicles on decreasing
social delay. However, for networks with multiple O/D pairs, when we decrease the headway
for autonomous vehicle platoons, we may end up worsening the social traffic conditions. We
show an example for illustration and then find an upper bound for the potential negative
impact of autonomous vehicles on social delay.

The selfish routing model is non-linear even with affine travel costs, thus it is crucial
to determine the stability of the equilibria from a dynamic perspective. Only when the
equilibria are stable, the analysis of static equilibria such as the impact of mixed auton-
omy discussed in Chapter 6 can effectively reflect the true results. In [64], a continuous

day–to–day selfish routing model for homogeneous vehicles is proposed. In [65], a dynamic
selfish routing model for homogeneous human-driven vehicles which also considers queu-
ing dynamics and stabilizing responsive traffic signal controls, P_0 policy, is proposed and
studied. In Chapter 7, we innovate the selfish routing model to consider mixed autonomy
transportation networks. We also consider the effect of movement–wise vehicle queuing at
the intersections in the dynamic routing model and analyze the impact of both fixed-time
and traffic-responsive intersection signaling. For the fixed-time signaling case, we are able to
characterize the resulting Wardrop equilibria with queueing using an optimization problem
with boundary flow constraints. We then analyse the stability of the equilibria via the use
of dissipativity analysis tools for population games [66]–[68] and provide stability proofs of
the resulting model equilibria for both fixed-time and a movement–wise extension of the P_0
traffic responsive signalling policy introduced in [65].

However, the advantage of connected and autonomous vehicles that they can preserve
a shorter headway compared to human-driven vehicles, thus increasing road capacities, can
rely heavily on the organization of autonomous vehicles on the roads. Gathering autonomous
vehicles on the roads at a higher density will facilitate the platooning of autonomous vehicles
and also be safer due to the lack of disturbances from human-driven vehicles. Therefore, lane
policies for autonomous vehicles are of significant importance and can be decisive on the ef-
ficiency of employing autonomous vehicles. Currently, there are two major categories of lane
policies for autonomous vehicles. The first category is the integrated lane policy [15]. The
integrated lane policy indicates that autonomous vehicles travel along with human-driven
vehicles on the same group of lanes. Such policies are convenient but may compromise the
platooning ability and safety of autonomous vehicles. The second category of policies is
dedicated lane policies [69]–[71]. Under such policies, some lanes are reserved exclusively for
autonomous vehicles. Such policies are preferred considering the safety and easy organiza-
tion of autonomous vehicles. However, when the penetration rate of autonomous vehicles is
low, the employment of dedicated lanes shows adverse effects and compromises social mo-
bility [72], [73]. Further, in [74], autonomous vehicle toll lanes are studied, which admit
autonomous vehicles to travel freely but also allow human-driven vehicles to enter paying
a toll. As a result, when the penetration rate of autonomous vehicles is low, human-driven
vehicles can effectively use the toll lane and relieve congestion on regular lanes. However,
even when autonomous vehicles are prevalent and dedicated lanes are necessary in terms
of the safety and advantageous mobility, the implementation or construction of brand-new
lanes can be costly and time-consuming. Therefore, researchers have recently considered
converting other existing dedicated lanes such as high-occupancy vehicle lanes to dedicated
lanes for autonomous vehicles. For example, in [75], [76], simulations and experiments are
conducted to investigate the benefit of converting an existing high-occupancy vehicle lane to
a dedicated lane for autonomous vehicles. However, this would result in a loss of the benefits
of a dedicated high-occupancy vehicle lane, especially when a considerable proportion of
commuters choose to carpool.

Therefore, in Chapter 8, we try to capture the advantage of both dedicated high-occupancy
vehicle lanes and dedicated autonomous vehicle lanes. We consider the scenario where four

classes of vehicles are sharing a segment of highway: human-driven vehicles with low oc-
cupancy, human-driven vehicles with high occupancy, autonomous vehicles with low occu-
pancy and autonomous vehicles with high occupancy. Autonomous vehicles are capable of
increasing traffic throughput by preserving a shorter headway than human-driven vehicles.
High-occupancy vehicles carry multiple commuters per vehicle and low-occupancy vehicles
carry a single commuter per vehicle. We propose a toll lane framework, where on the high-
way, a toll lane is reserved freely for autonomous vehicles with high occupancy, and the
other three classes of vehicles can choose to enter the toll lane paying a toll or use the other
regular lanes freely. We consider all vehicles to be selfish and only interested in minimiz-
ing their own travel costs (the sum of travel delay and the toll cost). We then explore the
resulting lane choice equilibria and establish properties of the equilibria, which implicitly
compare high-occupancy vehicles with autonomous vehicles in terms of their capabilities to
increase social mobility. We further show the various potential applications of this toll lane
framework that unites high-occupancy vehicles and autonomous vehicles in the optimal toll
design, the optimal occupancy threshold design and the policy design problems. To the best
of our knowledge, this is the first work that systematically studies a toll lane framework that
unites autonomous vehicles and high-occupancy vehicles on the roads.

Chapter 2

Preview of the Thesis

2.1 Structure Overview

The dissertation is divided into four parts. Part I serves as the introduction. The main contents of the study are presented in Part II and Part III. Part IV includes final remarks.

Part I provides an introduction to the dissertation, serving as a comprehensive guide to the current state of mixed autonomy and the underlying logic that connects the various chapters in the dissertation. The introduction is structured in two parallel parts, mirroring the main contents of the dissertation: mixed autonomy's decision-making behavior and its headway in organizational contexts. The introduction sets the stage for the subsequent chapters, offering a clear and cohesive framework for the reader to navigate the research presented.

Part II consists of Chapter 3–5, proposes an approach to use autonomous vehicles as altruistic decision-makers to improve social traffic conditions compared to selfish human-
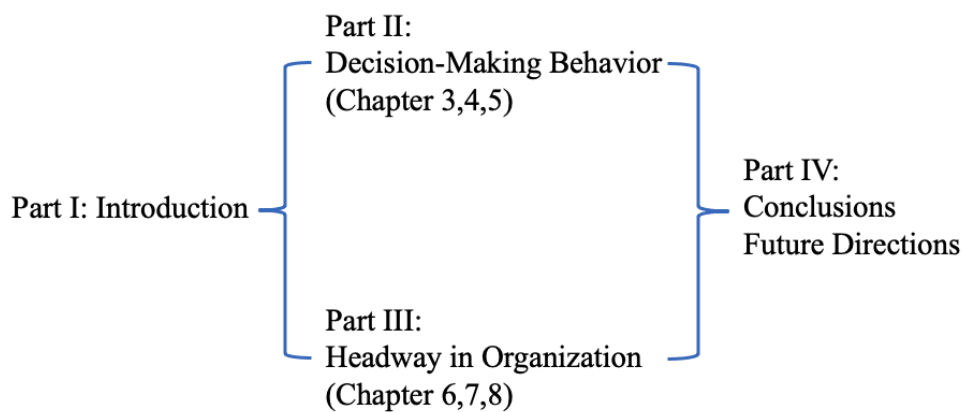
Figure 2.1: Structure of the dissertation. Part II and Part III are parallel.

driven vehicles by examining the decision-making of human-driven and autonomous vehicles in two typical scenarios: a diverge with a bifurcating lane and highway on-ramps. The approach involves a unified game-theoretic framework to model selfish vehicles' lane choices as a Wardrop equilibrium and a systematic approach to configure and control autonomous vehicles' perceived cost to improve social traffic conditions. Partial contents in this part are previously published in [77]–[79].

Part III containing Chapter 6–8 focuses on the headway of human-driven and autonomous vehicles in the organization. Autonomous vehicles are able to maintain a shorter longitudinal headway than human-driven vehicles' spontaneous headway under proper control. A routing scenario is first examined where vehicles selfishly choose the fastest path across a network. We show that reducing the headway of autonomous vehicles can decrease the overall network delay for networks with a single origin-destination pair and further provide an estimated bound of the best improvement which can serve as a crucial metric in policy design or evaluation. The stability of mixed autonomy's dynamic routing and queuing are further characterized using dissipativity tools. Moreover, a toll lane scenario is studied where mixed autonomy and high-occupancy vehicles coexist. A systematic toll lane framework that unites autonomous vehicles and high-occupancy vehicles is proposed and analyzed, and the framework shows power in multiple application scenarios such as policy design and regulation of autonomy. Partial results in this part are also included in [18], [80], [81].

Part IV serves as the concluding part of the dissertation. A summary of the contributions made in the previous parts of the dissertation is first presented, highlighting the main research goal and findings throughout the dissertation. Further, a path forward is discussed which briefly mentions potential topics for further research and development based on the implications and limitations of current findings.

2.2   Highlights of Contributions

The dissertation is situated in the context of the rapid development of autonomous driving technologies, while application scenarios remain limited due to safety concerns and high production costs. While the pursuit of "perfect" autonomy is a challenging goal, this dissertation aims to practically create the demand for autonomous vehicles by creating scenarios that highlight their societal benefits.

Specifically, the dissertation discusses two approaches for the application of autonomous vehicles:

- a systematic approach to employ and configure autonomous vehicles as altruistic decision-makers

- a comprehensive evaluation of the headway control for autonomous vehicles in mixed autonomy

Alternatively, the dissertation can be viewed as a collection of scenario-based studies that explore the impact of mixed autonomy on transportation systems, with a particular emphasis on typical transportation scenarios:

- diverges with a bifurcating lane in the middle

- highway on-ramps

- vehicles' routing on networks

- highway toll lanes

The ultimate goal of the dissertation is to address the following crucial challenges in integrating autonomous vehicles into human-dominated transportation systems:

- accurately yet concisely modeling human behavior

- modeling multi-agent systems that incorporate the key features of autonomous vehicles

- developing suitable control and optimization strategies for societal benefits

Finally, the dissertation demonstrates that autonomous vehicles have various potentials to serve for enhanced societal benefits while selfish drivers may exploit the benefits brought by autonomous vehicles. Therefore, effective control and optimization methods are necessary to assure the potential beneficial impact brought by vehicle autonomy and to pave the way for a safer, more efficient, and more sustainable future transportation system. We hope that the findings of this dissertation will stimulate further interest and exploration in the field of mixed autonomy and contribute to the development of more efficient, sustainable, and equitable transportation systems in the future.

Part II

Decision Making Behavior

Chapter 3

Selfish Lane Choice Behavior of Human-Driven Vehicles at a Diverge with a Bifurcating Lane in the Middle

3.1 Overview

As mentioned in the introduction (Section 1.1), considering the huge waste of resources produced by daily traffic congestion induced by vehicles' lane change maneuvers, it is crucial for the research community to find ways to accurately model and examine human-driven vehicles' lane changes.

In this Chapter, we focus on a specific traffic diverging scenario: *bifurcating* lanes at traffic diverges, which are commonly encountered in modern traffic networks and become a frequent cause of traffic bottlenecks. Figure 3.1 illustrates this diverge scenario, where the center lane "b" bifurcates such that vehicles in that lane must choose either to turn left or right.

Vehicles targeting one of the two exit links of the diverge face two options. One is to employ a feed-through lane lane (either lane "a" or lane "c" in Fig. 3.1), while the other is to employ the bifurcating lane. With the reasonable assumption that drivers choose their routes in a *selfish* manner in order to minimize their own travel time or effort, vehicles would only employ the bifurcating middle lane in order to save time or effort, as compared to using the exit's respective feed-through lane, and vice versa. In this Chapter, we derive a model that describes the decision making process encountered by drivers at such traffic diverges and then we obtain the macroscopic lane choices made by drivers by solving the model's corresponding Wardrop equilibrium. The model can accurately predict the aggregate lane choices of human-driven vehicles at the traffic diverges with a bifurcating lane in the middle and the calibration of our model only requires traffic flow information, which is realistically attainable.

The rest of the chapter is organized as follows. In Section 3.2, we first provide a detailed
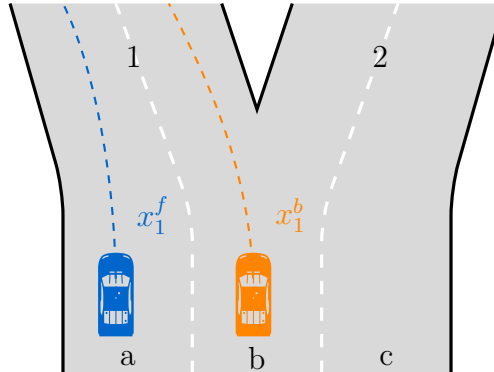
Figure 3.1: Problem setting: a traffic diverge with a bifurcating lane targeting two exit links.

description of the notation used throughout the chapter and subsequently derive a model that describes the decision making process of drivers at traffic diverges with middle bifurcating lanes. In Section 3.3, we establish the existence and uniqueness of the Wardrop equilibrium introduced by our model. In Section 3.4, we describe our model calibration and validation process using microscopic traffic simulation data. Finally, in Section 3.5, we summarize the chapter.

3.2   The Model

In this chapter, we consider a vehicular traffic diverge with a middle bifurcating lane. Such diverges are commonly used in a variety of modern transportation roadways, such as the well–known MacArthur Maze (see Figure 1.1), in the San Francisco Bay Area. A schematic of such a traffic diverge is shown in Figure 3.1. The diverge has two exit links, respectively denoted as link 1 and link 2, each consisting of two lanes, and a single entry link with three lanes respectively denoted by the letters a, b, and c. Vehicles traveling along feed-through lanes a and c respectively exit directly to links 1 and 2. However, vehicles traveling along the middle bifurcating lane b can exit to either link. Thus, drivers upstream of such a traffic diverge need to decide between two options. They can either use the feed–through lane that is designed to exclusively serve its corresponding destination link, or conversely they can use the middle bifurcating lane, which targets both exit links and is shared by vehicles targeting both exit links. For example, referring to Fig. 3.1, vehicles targeting link 1 may choose to utilize feed–through lane a or the bifurcating lane b. To model lane changing behavior upstream of this diverge, we consider 4 classes of vehicles. For either exit link, vehicles are either feed–through lane users or bifurcating lane users.

Here, some key points should be clarified. First, in this chapter we model the macroscopic lane changing behavior of a given vehicular flow, instead of attempting to model the decision making process of individual vehicles. Thus, features related to individual vehicles' choices

are not considered. Second, we will set the flow demands of both exit links within a feasible range, in order to exclude potential teleporting behavior of vehicles (i.e. vehicles disappear at the upstream link and then re–appear at a link downstream of the diverge), which is observed in several microscopic traffic models. Only bifurcating lane choice behavior will be studied in this work. Third, we assume that the capacity of either exit link is large enough to accommodate the corresponding demand. The impact of capacity drop downstream of the diverge is not considered in this work.

Let $I = \{1, 2\}$ be the index set of exit links at the diverge, and let $L = \{a, b, c\}$ be the index set of the entry link's lanes. At the diverge in Figure 3.1, lane a is the feed–through lane targeting exit link 1. Lane c is the feed–through lane targeting exit link 2. Lane b is the middle bifurcating lane targeting both link 1 and 2. We assume that the total demand for the diverge is fixed and given. For each exit link $i \in I$, let d_i be the demand of vehicles targeting exit link i, and let $q_i := \frac{d_i}{\sum_{i \in I} d_i}$ be the normalized demand of vehicles with destination link i. We collect the normalized demands and let $\mathbf{Q} := (q_i : i \in I)$ be the normalized demand configuration vector. For a diverge with the exit index set I and the normalized demand configuration vector $\mathbf{Q}$, we should have $\sum_{i \in I} q_i = 1$.

For each exit link $i \in I$, let n_i^f be the exact flow of feed–through lane users with destination link i and let n_i^b be the exact flow of bifurcating lane users with destination link i. For each $i \in I$, let $x_i^f := \frac{n_i^f}{\sum_{i \in I} d_i}$ be the proportion of feed–through lane users with destination link i. Likewise, for each $i \in I$, we let $x_i^b := \frac{n_i^b}{\sum_{i \in I} d_i}$ be the proportion of bifurcating lane users with destination link i. We then collect the proportions of the four classes of vehicles transiting through the diverge into the vector $\mathbf{x} := (x_i^f, x_i^b : i \in I)$. For a given normalized demand configuration vector $\mathbf{Q}$, we will use our model to predict the flow distribution vector $\mathbf{x}$. A flow vector $\mathbf{x}$ is feasible if it is non–negative and it satisfies flow conservation:

$$
\begin{aligned}
q_i &= x_i^f + x_i^b, \quad \forall i \in I, \\
x_i^f &\geq 0, x_i^b \geq 0, \quad \forall i \in I.
\end{aligned}
\tag{3.1}
$$

We assume all vehicles are *selfish* in that drivers will choose the route that minimizes their travel cost, which will be defined subsequently. That is to say, in this bifurcating lane scenario, vehicles would only choose the bifurcating lane when the cost experienced when traveling through the bifurcating lane is less than the cost experienced when traveling through the feed–through lane. We assume that vehicles of the same class, which are vehicles targeting the same destination link and utilizing the same entry lane, experience the same cost. We now model the cost experienced by each class of vehicles. For each exit link $i \in I$, let J_i^f denote the cost experienced by the feed–through lane users with destination link i, let J_i^b denote the cost experienced by the bifurcating lane users with destination link i. We now postulate that

$$
J_i^f(\mathbf{x}) = C_i^f x_i^f.
\tag{3.2}
$$

For each exit link $i \in I$, we let C_i^f represent the cost incurred by feed–through lane users targeting exit link i. For each exit link $i \in I$, we assume that $C_i^f > 0$ and it is a parameter related to the intrinsic features of the utilized feed–through lane, including the geometry, speed limits and other factors. To be specific in Figure 3.1, for exit link 1, C_1^f should be a parameter related to the intrinsic features of the feed–through lane a. For each exit link $i \in I$, since the feed–through lane is only shared by the feed–through lane users that exit through link i, the cost experienced by all users should be proportional to the proportion of the feed–through lane users that exit through link i. Thus, for each exit link $i \in I$, we let the cost, J_i^f, to be the product of C_i^f and x_i^f, as described by Eq. (3.2).

Let us now focus on the cost experienced by users of the middle bifurcating lane. For exit links $i \neq j \in I$, we model the cost experienced by the bifurcating lane users with destination link i as

$$J_i^b(\mathbf{x}) = C^b \left(\lambda_i x_i^b + \mu_i x_j^b \right) + \nu x_i^b x_j^b, \tag{3.3}$$

where C^b is a parameter characterizing the cost incurred by bifurcating lane users targeting either exit link. Likewise to feed–through lanes, we assume $C^b > 0$ and that it is a parameter related to the intrinsic features of the bifurcating lane. Since the bifurcating lane is shared by the bifurcating lane users for either exit link, the cost experienced by the users should be proportional to the sum of the proportions of the bifurcating lane users for either exit. Vehicles travelling along the bifurcating lane must take either of the two exit links at the end of the diverge, which might give rise to a sudden capacity increase for the bifurcating lane users targeting either exit link. This expected capacity increase would reduce the cost experienced by the bifurcating lane users. To account for this phenomenon, we define for each exit link i two positive parameters $\lambda_i \leq 1$ and $\mu_i \leq 1$. These parameters respectively characterize the possible capacity increase effect on bifurcating lane users targeting exit link i incurred by bifurcating lane users with the same destination link and the effect incurred by bifurcating lane users with a different destination link. If the effect is the same regardless of the inconsistency of the destination link, we should have $\lambda_i = \mu_i$; otherwise, $\lambda_i \neq \mu_i$. If either of the capacity increase effect is negligible, we will have $\lambda_i = 1$ or $\mu_i = 1$.

The second term in Eq. (3.3), which has the positive constant parameter ν is used to account for the detrimental effect on travel cost induced by the destination heterogeneity of the bifurcating lane users. This detrimental effect should increase when either of the two bifurcating lane vehicular flows increase. Therefore, we utilize the product between the two bifurcating lane proportions $\nu x_i^b x_j^b$, $i \neq j \in I$ in this term.

Thus, Eqs. (3.2) and (3.3) for $i \neq j \in I$, are used to describe the costs experienced by vehicles traveling through the diverge. We collect these cost parameters in these equations, and define $\mathbf{C} = (C_i^f, C^b, \lambda_i, \mu_i, \nu : i \in I)$ to be the cost coefficient vector characterizing the diverge.

Having modeled the costs (3.2) and (3.3), we will model vehicles' choice behavior on the macroscopic level. We assume that once a lane choice is made by the vehicle, it stays on its chosen lane. Since we have assumed that all vehicles are *selfish*, vehicles would only choose

the bifurcating lane when the cost experienced by traveling on the bifurcating lane is smaller than the cost experienced by traveling on the corresponding feed–through lane. Using the notations in our model, we can say, at the equilibrium of vehicles' choice behavior, if $x_i^b > 0$, then we must have $J_i^b(\mathbf{x}) \leq J_i^f(\mathbf{x})$; likewise, if $x_i^f > 0$, then we must have $J_i^f(\mathbf{x}) \leq J_i^b(\mathbf{x})$. Therefore, at an equilibrium of our model, if $J_i^f(\mathbf{x}) > J_i^b(\mathbf{x})$, then $x_i^f = 0$; if $J_i^f(\mathbf{x}) < J_i^b(\mathbf{x})$, then $x_i^b = 0$; only if $J_i^f(\mathbf{x}) = J_i^b(\mathbf{x})$, x_i^b and x_i^f may both be nonzero. These conditions can be formulated as a Wardrop equilibrium [45]. Now, let $\mathbf{C} = (C_i^f, C^b, \lambda_i, \mu_i, \nu : i \in I)$ be the cost coefficient vector and $\mathbf{Q} = (q_i : i \in I)$ be the normalized demand configuration vector. Let $G = (\mathbf{Q}, \mathbf{C})$ be a tuple configuring a traffic diverge in Figure 3.1, we interpret the above equilibrium conditions of our model and give the formal definition of the equilibrium of our model:

Definition 1. For a given $G = (\mathbf{Q}, \mathbf{C})$, a flow distribution vector $\mathbf{x}$ is an equilibrium if and only if for every $i \neq j \in I$, we have

$$
\begin{aligned}
x_i^f(J_i^f(\mathbf{x}) - J_i^b(\mathbf{x})) &\leq 0, \\
x_i^b(J_i^b(\mathbf{x}) - J_i^f(\mathbf{x})) &\leq 0.
\end{aligned}
\tag{3.4}
$$

Now that we have modeled the cost experienced by each class of vehicles and model the resulting choice equilibrium as a Wardrop equilibrium described in Definition 1, we can use this model to predict the proportion of bifurcating lane users and feed–through lane users for either exit link.

3.3 Equilibrium Properties

In this section, we will first establish the existence of the equilibrium induced by our model. Then, we will derive the sufficient conditions under which the existing equilibrium is guaranteed to be unique. Therefore, once the sufficient conditions are met, our model could be applied to the prediction of the proportions of bifurcating lane users and feed–through lane users.

Equilibrium Existence

We will first directly give a proposition based on the existence theorem stated and proved in [82].

Proposition 1. *Given a tuple $G = (\mathbf{Q}, \mathbf{C})$ configuring a traffic diverge in Figure 3.1, for each exit link $i \in I$, if each of the cost functions $J_i^f(\mathbf{x}), J_i^b(\mathbf{x})$ is continuous and monotone in $\mathbf{x}$, there exists at least one Wardrop equilibrium (as described in Definition 1) for G.*

From Equations (3.2) and (3.3), we observe that $J_i^b(\mathbf{x})$ and $J_i^b(\mathbf{x})$ are both continuous and monotone in the sense of non-decreasing in $\mathbf{x}$. Thus, by Proposition 1, we conclude the existence of the equilibrium described in Definition 1.

Equilibrium Uniqueness

As for the uniqueness of the induced equilibrium, we will use a similar method as what is stated in [44]. The basic idea is that we will first construct an equivalent Nash equilibrium of our equilibrium model. Then we will prove under certain conditions the uniqueness of the constructed Nash equilibrium. Therefore, the uniqueness of the Wardrop equilibrium induced by our model is concluded by equivalence.

For any tuple $G = (\mathbf{Q}, \mathbf{C})$ configuring a traffic diverge in Figure 3.1, we construct a two–player auxiliary game $\tilde{G} = \langle I, A, (\tilde{J}_i : i \in I) \rangle$. Here, $I = \{1, 2\}$ is the index set of our players. Let $A = A_1 \times A_2$ be the action space, $A_i = [0, q_i]$ be the action set of player i, and $\tilde{J}_i$ be the cost associated with each player $i \in I$. Let $\mathbf{y} = (y_i, i \in I)$ be the vector of actions taken by the players of the game $\tilde{G}$. To further build the correspondence, for each player $i \in I$, we let

$$y_i = x_i^b. \tag{3.5}$$

Then, for the cost associated with each player i, we define

$$\tilde{J}_i(\mathbf{y}) := \left(J_i^f(\mathbf{x}) - J_i^b(\mathbf{x}) \right)^2. \tag{3.6}$$

Next, we employ the definition of the constructed Nash equilibrium stated in [44]:

Definition 2. For the auxiliary game $\tilde{G}$, $\mathbf{y} = (y_i : i \in I)$ is a pure Nash equilibrium if and only if for every $i \neq j \in I$,

$$
\begin{aligned}
y_i &= B_i(y_j) \\
&= \operatorname{argmin}_{y_i \in [0, q_i]} \tilde{J}_i(\mathbf{y}),
\end{aligned} \tag{3.7}
$$

where B_i is the best response function of player i.

Now that we have constructed a Nash equilibrium, we will use the following lemma to establish the equivalence between the Wardrop equilibrium of G and the Nash equilibrium of $\tilde{G}$.

Lemma 1. *A flow distribution vector* $\mathbf{x} = (x_i^f, x_i^b : i \in I)$ *is a Wardrop equilibrium for G if and only if* $\mathbf{y} = (x_i^b, i \in I)$ *is a pure Nash equilibrium for $\tilde{G}$.*

Proof. First, using flow constraints (3.1), let us write $J_i^f(\mathbf{x})$ and $J_i^b(\mathbf{x})$ in terms of variables x_i^b. For each exit link $i \in I$, we have

$$J_i^f(\mathbf{x}) = C_i^f(q_i - x_i^b), \tag{3.8}$$
$$J_i^b(\mathbf{x}) = C^b \left(\lambda_i x_i^b + \mu_i x_j^b \right) + \nu x_i^b x_j^b. \tag{3.9}$$

Then, for each exit link $i \in I$, we calculate the derivatives of the costs with respect to x_i^b:

$$\frac{\partial J_i^f}{\partial x_i^b} = -C_i^f, \tag{3.10}$$

$$\frac{\partial J_i^b}{\partial x_i^b} = C^b \lambda_i + \nu x_j^b. \tag{3.11}$$

Notice that in Equation (3.10) and (3.11), given all coefficients are positive, for each exit link $i \in I$, $\frac{\partial J_i^f}{\partial x_i^b}$ is always negative and equals to a constant, i.e., $J_i^f(\mathbf{x})$ is a linear function of x_i^b with a negative slope. For each exit link $i \neq j \in I$, due to the flow constraints (3.1), x_j^b is always nonnegative, thus $\frac{\partial J_i^b}{\partial x_i^b}$ is always positive and increases as x_j^b increases.

We now will show sketches of $J_i^f(\mathbf{x})$ and $J_i^b(\mathbf{x})$ in the region of $x_i^b \in [0, q_i]$. There are 3 possible cases of the sketch and we draw each possibility in Figure 3.2. We then complete the proof of equivalence case by case.

- Case (a): In this scenario, for every $x_i^b \in [0, q_i]$, we have $J_i^f(x_i^b) > J_i^b(x_i^b)$. To minimize the cost associated with player i in Equation (3.6), we have $y_i = q_i$ at the constructed Nash equilibrium. Since we let $y_i = x_i^b$, we have $x_i^b = q_i$. Then due to flow constraints (3.1), we have $x_i^b = q_i, x_i^f = 0$, where $J_i^f(x_i^b) > J_i^b(x_i^b)$. This meets the conditions in Definition 1, thus the constructed Nash equilibrium leads to the Wardrop equilibrium. At a Wardrop equilibrium where $J_i^f(x_i^b) > J_i^b(x_i^b)$, we can conclude that $x_i^f = 0, x_i^b = q_i$. This leads to $y_i = q_i$. From plot (a), we can see that, the cost associated with player i is minimized. Therefore, the Wardrop equilibrium is also a constructed Nash equilibrium. In this case, the Wardrop equilibrium is equivalent to the constructed Nash equilibrium.

- Case (b): In this case, $J_i^f(x_i^b)$ and $J_i^b(x_i^b)$ have an intersection. Let us denote the x_i^b at the intersection as $\bar{x}_i^b$. Then we have $J_i^f(\bar{x}_i^b) = J_i^b(\bar{x}_i^b)$. At the Nash equilibrium, we let $y_i = \bar{x}_i^b$, therefore the minimum possible cost associated with player i is reached, which is 0. At this time, Wardrop conditions in Definition 1 are tight and met. Therefore, the constructed Nash equilibrium is also the Wardrop equilibrium. Reversely, when $J_i^f(x_i^b) = J_i^b(x_i^b)$ at the Wardrop equilibrium, from plot (b), x_i^b could only equal to $\bar{x}_i^b$. This results in a zero cost, which is the minimum possible value of the cost. Therefore, a Nash equilibrium is reached. The equivalence of Wardrop equilibrium and its constructed Nash equilibrium is established for this case.

- Case (c): This case is similar to case (a). For every $x_i^b \in [0, q_i]$, we have $J_i^f(x_i^b) < J_i^b(x_i^b)$. To minimize the cost associated with player i in Equation (3.6), we have $y_i = 0$ at the constructed Nash equilibrium. Since we let $y_i = x_i^b$, we have $x_i^b = 0$. Then due to flow constraints (3.1), we have $x_i^b = 0, x_i^f = q_i$, where $J_i^f(x_i^b) < J_i^b(x_i^b)$. This meets the conditions in Definition 1, thus the constructed Nash equilibrium leads to the Wardrop equilibrium. At a Wardrop equilibrium where $J_i^f(x_i^b) < J_i^b(x_i^b)$, we can conclude that
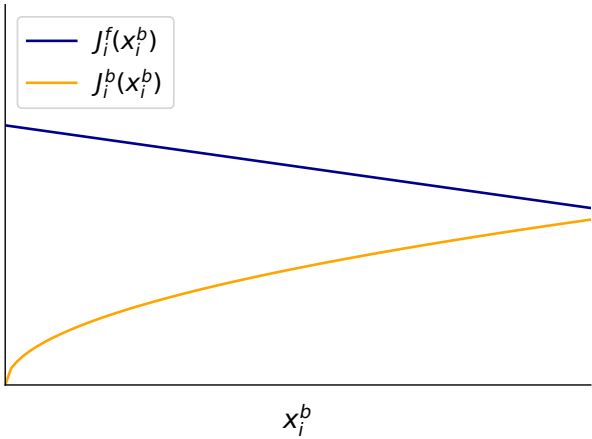
(a) $J_i^f(x_i^b) > J_i^b(x_i^b)$
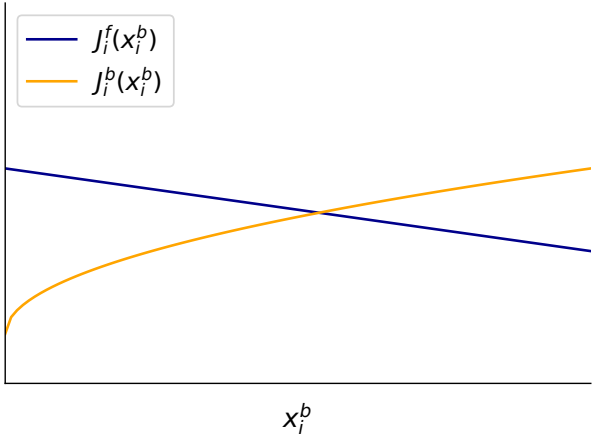
(b) $J_i^f(x_i^b)$ and $J_i^b(x_i^b)$ intersect
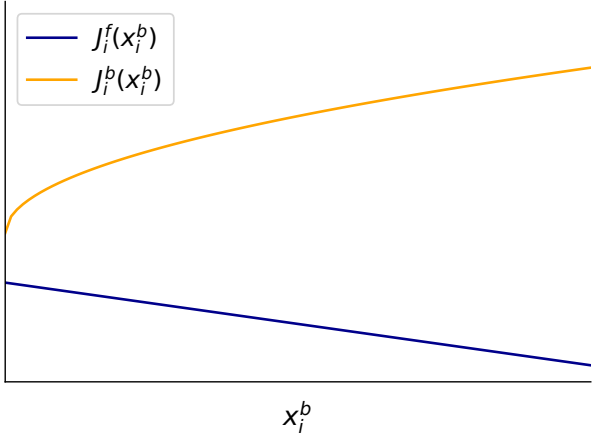
(c) $J_i^f(x_i^b) < J_i^b(x_i^b)$

Figure 3.2: Three possible sketches of $J_i^f(x_i^b)$ and $J_i^b(x_i^b)$ in the region of $x_i^b \in [0, q_i]$.

$x_i^f = q_i, x_i^b = 0$. This leads to $y_i = 0$. From plot (c), we can see that the cost associated with player i is minimized. Therefore, the Wardrop equilibrium is also a constructed Nash equilibrium. In this case, the Wardrop equilibrium is equivalent to the constructed Nash equilibrium.

□

Now in all cases, we have proved the equivalence between the Wardrop equilibrium and the constructed Nash equilibrium. Then, we use the following lemma to establish the uniqueness of the constructed Nash equilibrium.

Lemma 2. *For an auxiliary game $\tilde{G}$, the Nash equilibrium flow vector $\mathbf{y}$ in Definition 2 is unique if for each player $i \in I$:*

$$(\lambda_i - \mu_i)C^b \geq \nu - C_i^f. \tag{3.12}$$

Proof. At a Nash equilibrium, for each player $i \neq j \in I$, we have

$$y_i = B_i(y_j). \tag{3.13}$$

For each player $i \neq j \in I$, we can rewrite (3.13) as

$$y_i = B_i(B_j(y_i)). \tag{3.14}$$

Equation (3.14) indicates that $\mathbf{y}$ is an equilibrium if and only if for every $i \neq j \in I$, y_i is a fixed point for function $g(z) = B_i(B_j(z))$. Thereby, the number of the fixed points of function $g(z) = B_i(B_j(z))$ equals the number of equilibria. To guarantee the uniqueness of the equilibrium, we have to guarantee the uniqueness of the fixed point of function $g(z) = B_i(B_j(z))$. Notice that a fixed point z^* of function $g(z)$ must satisfy

$$g(z^*) = z^*. \tag{3.15}$$

Therefore, the fixed point z^* can be found by intersecting the identity function $h(z) = z$ and function $g(z)$. Thus, the basic idea of the following proof is to show that under (3.12), for every player $i \neq j \in I$, the slope of function $g(z) = B_i(B_j(z))$ is always non-negative and smaller than 1. Therefore, with $y_i \geq 0$, function $g(z) = B_i(B_j(z))$ can intersect the identity function at most once, which will establish the uniqueness of the fixed point of function $g(z) = B_i(B_j(z))$. Then we can conclude the uniqueness of the constructed Nash equilibrium.

First, for each player $i \neq j \in I$, we explore $\frac{dB_i(y_j)}{dy_j}$. Back to the three cases when we prove Lemma 1, for case (a) and case (c), $y_i = B_i(y_j)$ is always equal to q_i or 0 no matter how y_j changes, therefore, $\frac{dB_i}{dy_j} = 0$. Then the slope of function $g(z) = B_i(B_j(z))$ is always 0. Thus we only need to explore $\frac{dB_i(y_j)}{dy_j}$ in case (b), where $J_i^f(x_i^b)$ and $J_i^b(x_i^b)$ intersect in the region of $x_i^b \in [0, q_i]$. Remember that, we let $y_i = x_i^b$, for simplicity, we use x_i^b instead of y_i

in the following proof. Using the same notations as the proof of Lemma 1, in case (b), with a given x_j^b, let $J_i^f(x_i^b)$ and $J_i^b(x_i^b)$ intersect at $\bar{x}_i^b(x_j^b) \in [0, q_i]$. For $\bar{x}_i^b(x_j^b)$, we must have

$$J_i^f(\bar{x}_i^b, x_j^b) - J_i^b(\bar{x}_i^b, x_j^b) = 0. \tag{3.16}$$

Using implicit differentiation of $J_i^f(\bar{x}_i^b, x_j^b) - J_i^b(\bar{x}_i^b, x_j^b)$ with respect to x_j^b, we have

$$
\begin{aligned}
&\frac{\partial}{\partial \bar{x}_i^b} \left(J_i^f(\bar{x}_i^b, x_j^b) - J_i^b(\bar{x}_i^b, x_j^b) \right) \frac{d\bar{x}_i^b(x_j^b)}{dx_j^b} + \\
&\frac{\partial}{\partial x_j^b} \left(J_i^f(\bar{x}_i^b, x_j^b) - J_i^b(\bar{x}_i^b, x_j^b) \right) = 0.
\end{aligned} \tag{3.17}
$$

Using Equations (3.8) and (3.9), we have

$$\frac{\partial J_i^f}{\partial x_j^b} = 0, \tag{3.18}$$

$$\frac{\partial J_i^b}{\partial x_j^b} = C^b \mu_i + \nu x_i^b. \tag{3.19}$$

Since $x_i^b \geq 0$, we can conclude that for every $i \neq j \in I$, $\frac{\partial J_i^f}{\partial x_j^b}$ is always 0 and $\frac{\partial J_i^b}{\partial x_j^b}$ is always positive. Therefore, we have

$$\frac{\partial}{\partial x_j^b} \left(J_i^f(\bar{x}_i^b, x_j^b) - J_i^b(\bar{x}_i^b, x_j^b) \right) \leq 0. \tag{3.20}$$

From Equations (3.10) and (3.11) , we have

$$\frac{\partial}{\partial x_i^b} \left(J_i^f(\bar{x}_i^b, x_j^b) - J_i^b(\bar{x}_i^b, x_j^b) \right) \leq 0. \tag{3.21}$$

Thus, using Equation (3.17), we conclude that

$$\frac{d\bar{x}_i^b(x_j^b)}{dx_j^b} \leq 0. \tag{3.22}$$

Intuitively, from plot (b), when x_j^b increases, $J_i^f(\bar{x}_i^b, x_j^b)$ stays the same, whereas $J_i^b(\bar{x}_i^b, x_j^b)$ increases. The intersection climbs leftwards, therefore, $\bar{x}_i^b$ decreases.

To guarantee, for every player $i \neq j \in I$, that the slope of $g(z) = B_i(B_j(z))$ is always non-negative and smaller than 1, based on the chain rule, we have to guarantee that the slope of $B_i(y_j)$ is always non-positive and bigger than -1, i.e., $-1 \leq \frac{d\bar{x}_i^b(x_j^b)}{dx_j^b} \leq 0$. Now we plug Equations (3.10), (3.11), (3.18) and (3.19) into Equation (3.17), we have

$$
\begin{aligned}
&\left(-C_i^f - C^b \lambda_i - \nu x_j^b \right) \frac{d\bar{x}_i^b(x_j^b)}{dx_j^b} + \\
&\left(-C^b \mu_i - \nu x_i^b \right) = 0.
\end{aligned} \tag{3.23}
$$

For each player $i \neq j \in I$, to ensure $-1 \leq \frac{d\bar{x}_i^b(x_j^b)}{dx_j^b} \leq 0$, we need to guarantee

$$C_i^f + C^b \lambda_i + \nu x_j^b \geq C^b \mu_i + \nu x_i^b. \tag{3.24}$$

Let $M(x_i^b, x_j^b) = C_i^f + C^b \lambda_i + \nu x_j^b - C^b \mu_i - \nu x_i^b$, we need to guarantee that $\min M(x_i^b, x_j^b) \geq 0$. Since $M(x_i^b, x_j^b)$ is negatively linear in x_i^b and positively linear in x_j^b, the minimum possible value of $M(x_i^b, x_j^b)$ must be greater than the value of the extreme point, $M(1, 0) = C_i^f + C^b \lambda_i - C^b \mu_i - \nu$. Thus, we just need to guarantee that $M(1, 0) \geq 0$, which is as we stated in Lemma 2.

Thus, for every player $i \neq j \in I$, under condition (3.12), the slope of $g(z) = B_i(B_j(z))$ is always nonnegative and smaller than 1. Therefore, with $y_i \geq 0$, $g(z) = B_i(B_j(z))$ can intersect the identity line at most once, which establishes the uniqueness of the fixed point of function $g(z) = B_i(B_j(z))$. Thus, we can conclude the uniqueness of the constructed Nash equilibrium. □

We then give the following theorem to establish the uniqueness of the Wardrop equilibrium as described in Definition 1.

Theorem 1. *For a game* $G = (\mathbf{Q}, \mathbf{C})$, *the equilibrium flow vector* $\mathbf{x}$ *in Definition 1 is unique if for each exit link* $i \in I$:

$$(\lambda_i - \mu_i)C^b \geq \nu - C_i^f. \tag{3.25}$$

Proof. From Lemma 2, we know that the constructed Nash equilibrium in Definition 2 is unique under condition (3.25). By Lemma 1, we conclude that the constructed Nash equilibrium is equivalent to the Wardrop equilibrium in the sense of Definition 1. Thus, we can conclude that the Wardrop equilibrium as described in Definition 1 is unique. □

Notice that Theorem 1 only gives a sufficient but not necessary condition of the uniqueness of the equilibrium. This implies if condition (3.25) is met, we can guarantee the uniqueness of the equilibrium; however, if condition (3.25) is not met, it is also possible that the Wardrop equilibrium is unique.

3.4 Simulation Studies

Now that we have characterized the existence and uniqueness of the equilibrium induced by our model, we are going to test the performance of our model in terms of how it accurately describes steady state vehicular flow data generated by a micro-simulation flow model.

In this chapter, we generate vehicular steady state flow data for model calibration and validation using the traffic microscopic simulation software SUMO [83], which is commonly utilized by the transportation community. In the simulations, to ensure the reliability of the generated data, we set the SUMO car following model to be the default Krauss model,
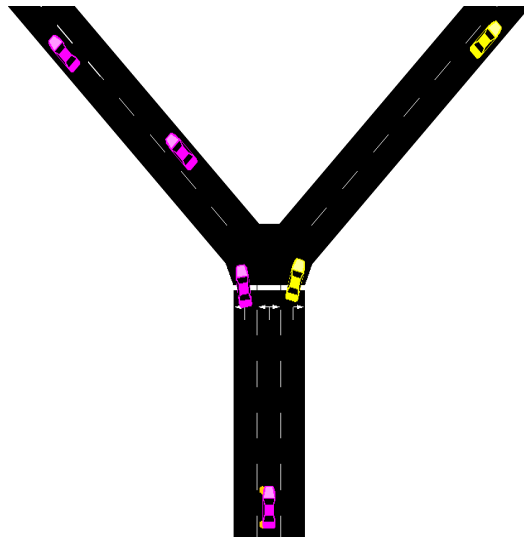
Figure 3.3: An enlarged view of the traffic diverge with a bifurcating lane in SUMO.

which is also known as the stochastic version of the Gipps' model. To be specific, the Krauss model supports stochastic driving behavior by setting an imperfection parameter *sigma*. The imperfection parameter *sigma*, which ranges from 0 to 1, represents the degree of randomness of vehicles' behavior. When *sigma* is set to nonzero, drivers will randomly vary their speed. In the simulations, we set *sigma* to a default value of 0.5, in order to realistically mimic vehicle randomness. An enlarged view of the established diverge in SUMO is shown in Figure 3.3. To ensure that the data we collect truly reveals the equilibrium state, we set the entry link to be sufficiently long and only recorded the proportions of different classes of vehicles ($\mathbf{x} := (x_i^f, x_i^b : i \in I)$), downstream of the diverge when the simulation has run for a sufficiently long time to reach the steady state.

Model Calibration

Notice that the cost coefficient vector $\mathbf{C} = (C_i^f, C^b, \lambda_i, \mu_i, \nu : i \in I)$ is related to the intrinsic features of a diverge. Thus, it is necessary to first calibrate the cost coefficient vector $\mathbf{C}$ in the model for a given diverge before we use the model for prediction. For the diverge shown in Figure 3.3, let the exit link index set be $I_{\text{exit}} = \{1, 2\}$. We define K to be the total number of data points that we need for calibration. For each data point, we run the simulation once, until it reaches an equilibrium state. We pick an appropriate total demand, D, of vehicles entering the diverge and fix it for all K simulations. For every simulation, we randomize the demand configuration for either exit link. In the kth simulation to generate the kth data point, we let d_1^k be the demand of vehicles targeting exit link 1 and similarly, let d_2^k be the demand of vehicles targeting exit link 2. For each $1 \le k \le K$, we should have $d_1^k + d_2^k = D$. Now, for each $1 \le k \le K$, we define $q_1^k := \frac{q_1^k}{D}$ and $q_2^k := \frac{q_2^k}{D}$ to be the normalized demand for

exit link 1 and exit link 2 and we should have $q_1^k + q_2^k = 1$. Then we let $\mathbf{Q}^k := \{q_1^k, q_2^k\}$ to be the kth flow configuration vector for the kth simulation. After the simulation has reached the equilibrium, for each exit link $i \in I_{\text{exit}}$, we record the proportions of the feed–through lane users $(x_i^f)^k$ and the bifurcating lane users $(x_i^b)^k$. For each $1 \le k \le K$, we collect the proportions in the flow distribution vector $\mathbf{x}^k = \{(x_i^f)^k, (x_i^b)^k : i \in I_{\text{exit}}\}$. Now, for each $1 \le k \le K$, we define a tuple $(\mathbf{Q}^k, x^k)$. Then using these K tuples, we employ the method developed in [44] for calibration, which we briefly describe below.

We want to find a cost coefficient vector $\mathbf{C} = (C_i^f, C^b, \lambda_i, \mu_i, \nu : i \in I_{\text{exit}})$ that can enable as many as possible of the K data points to meet the conditions in Definition 1. To deal with the variational inequalities when encoding the conditions in Definition 1 for each data point, for every $1 \le k \le K$ and $i \in I_{\text{exit}}$, we define binary variables $(e_i^f)^k$ and $(e_i^b)^k$ as

$$(x_i^f)^k(J_i^f(\mathbf{x}^k) - J_i^b(\mathbf{x}^k)) \le 0 \iff (e_i^f)^k = 0, \tag{3.26a}$$

$$(x_i^f)^k(J_i^f(\mathbf{x}^k) - J_i^b(\mathbf{x}^k)) > 0 \iff (e_i^f)^k = 1, \tag{3.26b}$$

$$(x_i^b)^k(J_i^b(\mathbf{x}^k) - J_i^f(\mathbf{x}^k)) \le 0 \iff (e_i^b)^k = 0, \tag{3.26c}$$

$$(x_i^b)^k(J_i^b(\mathbf{x}^k) - J_i^f(\mathbf{x}^k)) > 0 \iff (e_i^b)^k = 1. \tag{3.26d}$$

This way, we use the binary variables $(e_i^f)^k$ and $(e_i^b)^k$ to indicate for $(x_i^f)^k$ and $(x_i^b)^k$ in each data point whether the conditions in Definition 1 are violated. To optimize for $\mathbf{C}$, we will minimize the sum of binary variables $(e_i^f)^k$ and $(e_i^b)^k$ for all $i \in I_{\text{exit}}$ and $1 \le k \le K$. Moreover, to solve the optimization problem, we transfer the constraints in Equations (3.26) as in [84]. We set T as a large positive number, and we set ϵ as a small positive number close to zero. Then the constraints in Equations (3.26) can be transferred as below:

$$(x_i^f)^k(J_i^f(\mathbf{x}^k) - J_i^b(\mathbf{x}^k)) \le T(e_i^f)^k - \epsilon, \tag{3.27a}$$

$$-(x_i^f)^k(J_i^f(\mathbf{x}^k) - J_i^b(\mathbf{x}^k)) \le T(1 - (e_i^f)^k) - \epsilon, \tag{3.27b}$$

$$(x_i^b)^k(J_i^b(\mathbf{x}^k) - J_i^f(\mathbf{x}^k)) \le T(e_i^b)^k - \epsilon, \tag{3.27c}$$

$$-(x_i^b)^k(J_i^b(\mathbf{x}^k) - J_i^f(\mathbf{x}^k)) \le T(1 - (e_i^b)^k) - \epsilon. \tag{3.27d}$$

Then we can find the calibrated cost coefficient vector $\mathbf{C}$ by solving the mixed–integer linear program problem below:

$$\begin{aligned} \underset{\mathbf{C}}{\text{minimize}} \quad & \sum_{1 \le k \le K} \sum_{i \in I_{\text{exit}}} \left((e_i^f)^k + (e_i^b)^k \right) \\ \text{subject to} \quad & \text{Equations (3.27)}, \\ & \mathbf{C}_r \ge 1. \end{aligned} \tag{3.28}$$

In our simulation, the capacity per lane is 1100 vph (vehicles per hour). We pick the total demand D as 3000 vph. We vary the demand for exit link 1 from 1150 vph to 1850 vph. For each demand configuration, x_1^f, x_1^b, x_2^f, and x_2^b are recorded. In our simulation, we set

the intrinsic features of every entry lane to be uniform and the geometry of two exit links
to be symmetric. Thus we add the equality constraints below in our calibration process to
reflect the symmetry:

$$
\begin{aligned}
C_1^f = C_2^f = C^b, \\
\lambda_1 = \lambda_2, \\
\mu_1 = \mu_2.
\end{aligned}
\tag{3.29}
$$

After performing calibration process described above, we obtained the following cost coefficient vector $\mathbf{C}$:

$$
\begin{aligned}
C_1^f = C_2^f = C^b = 1.45, \\
\lambda_1 = \lambda_2 = 0.87, \\
\mu_1 = \mu_2 = 0.69, \\
\nu = 1.
\end{aligned}
\tag{3.30}
$$

Note that the obtained values of $\mathbf{C}$ satisfy (3.25), thus, with this $\mathbf{C}$, we can predict the
unique equilibrium $\mathbf{x}$ for each flow configuration $\mathbf{Q}$. Also, since for $i \in I_{\text{exit}}$, we have $\lambda_i < 1$
and $\mu_i < 1$, the capacity increase effect on bifurcating lane users is validated.

Model Validation

Having obtained the calibrated cost coefficient vector $\mathbf{C}$ in (3.30), we proceeded to validate our model using independently obtained simulation data from SUMO. We validate our
model under the total demand of 3200 *vph*. As Figure 3.4 shows, our model successfully
predicts the proportion of bifurcating lane users for either destination link. It is an obvious
linear relationship which is consistent with our intuition. When the normalized demand for
the same exit link increases, the proportion of bifurcating lane users increases due to the
increasing cost for taking the feed–through lane designed exclusively for the exit link. The
simulation results show an impressive accuracy of our model in the prediction of vehicles'
aggregate lane choice behavior. We also obtained similar results when the total demand was
varied.

3.5   Summary

This chapter examined human-driven vehicles' selfish lane choice behavior at a commonly
encountered traffic diverge scenario. A macroscopic model of vehicles' aggregating lane choice
behavior at diverges with a middle bifurcating lane is presented using Wardrop conditions.
We then proved the existence and uniqueness of the resulting Wardrop equilibrium. Next,
we used a microscopic traffic simulation software, SUMO, to generate data to calibrate and
validate our model. The calibration process is shown to be easy. In the end, the validation
results turned out to be promising and the model shows great potential in the application

(a) x_1^b

(b) x_2^b
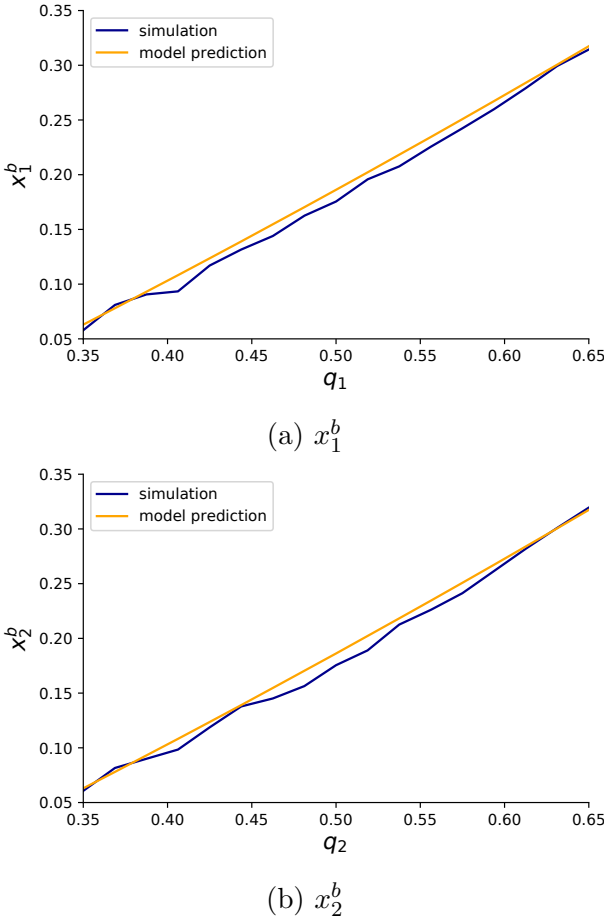
Figure 3.4: Model prediction of the proportion of bifurcating lane users, x_i^b is compared to simulation generated data.

to other similar traffic scenarios such as left-turning slots, and highway on-ramps, which are going to be discussed in the next chapter.

Chapter 4

Selfish Lane Choice Behavior of Human-Driven Vehicles at the Vicinity of Highway On-Ramps

4.1 Overview

Besides the traffic diverge scenario with a bifurcating lane in the middle discussed in the previous Chapter, another traffic scenario, which is significantly affected by vehicles' lane changes, is the highway on-ramp. Studies of the effects of lane changes at highway on-ramps include [40], [41], [46], [85], [86]. In [41], it is argued that the complex lane-changing behaviors in the on-ramp area contribute to the well-known "freeway capacity drop" phenomenon, and therefore, lead to severe congestion.

In this Chapter, we model the aggregate lane choice behavior of mainline through vehicles, particularly on the outermost lane (the lane closest to the on–ramp), while facing an on–ramp ahead. Knowing that a number of on–ramp vehicles are going to merge into the mainline traffic ahead, through vehicles on the outermost lane have two options. One is to stay steadfast, i.e., to remain on the current outermost lane and merge with on–ramp vehicles, while the other is to change to the adjacent lane away from the on–ramp and avoid the merging with on–ramp vehicles. We are interested in the proportion of the total through vehicles that choose to stay steadfast or to bypass the merging area facing an on–ramp ahead.

Similarly to the method employed in the previous chapter, we show that the aggregate lane choice behavior of mainline through vehicles at the vicinity of a highway on-ramp can be explained by a game-theoretic framework. We assume all vehicles are selfish so they only take the option which costs themselves the least. Then we model the resultant vehicles' aggregate lane choice equilibrium as a Wardrop equilibrium [45]. We then conduct a simulation study to illustrate the promising predictive power of our model.

U.S. right-of-way rules state that the vehicles already on the highway have absolute priority, and that they have no obligation to make room for vehicles entering through the
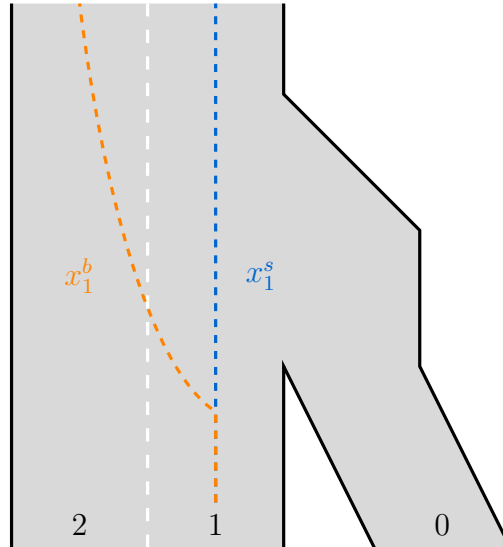
Figure 4.1: Problem setting: a proportion of mainline through vehicles bypass the on–ramp merging area.

on–ramp [87]. It is on–ramp vehicles' responsibility to find an acceptable gap between through vehicles and safely merge into the mainline traffic. However, should there be any advice for through vehicles' drivers so that the total traffic condition can be improved? To answer this question, we further model the socially optimal lane choice behavior of mainline through vehicles and we draw a conclusion that through vehicles, in order to improve the social traffic conditions, should be encouraged to bypass the merging area by steering to a neighboring lane instead of staying steadfast.

The chapter is organized as follows. In Section 4.2, we elaborate the mainline vehicles' lane choice model we build for a basic highway on-ramp setting. In Section 4.3, the existence and uniqueness of the resulting equilibrium of the lane choice model are concluded. In Section 4.4, we use microscopic traffic simulation (Aimsun) data to validate our model. Further, in Section 4.5, we model the socially optimal lane choice behavior of mainline vehicles and compare it with vehicles' user optimal behavior in reality. Finally, in Section 4.6, we summarize this chapter.

4.2   The Model

In this chapter, we consider a basic version of highway on–ramps with two lanes in the mainline as shown in Figure 4.1. We label the on–ramp lane as lane 0, the outermost lane (the lane closest to the on–ramp) in the mainline as lane 1 and the innermost lane (the lane furthest from the on–ramp) as lane 2. When on–ramp vehicles enter the highway through the on–ramp lane 0, they travel along a buffer zone and in the end merge into lane 1 to

join the highway mainline. Meanwhile, vehicles traveling on the outermost lane 1 have two
feasible actions facing this potential merge. On the one hand, they could stay on the current
outermost lane 1 and yet suffer the possible procrastination due to the merging with on–ramp
vehicles. We call the vehicles that choose to stay on the outermost lane 1 *steadfast* vehicles.
On the other hand, vehicles on lane 1 could dodge the merging with on–ramp vehicles by
changing to the neighboring lane further from the on–ramp, which is the innermost lane 2.
We call these vehicles that choose to steer to lane 2 *bypassing* vehicles. We assume that
all vehicles are selfish, i.e., a vehicle only chooses to be steadfast when staying steadfast is
less costly than performing bypassing behavior, and vice versa, without considering what
will benefit other vehicles. In this work, we focus on the aggregate lane choice behavior of
through vehicles on lane 1 instead of a single specific vehicle's lane choice. Therefore, in
our model, we do not predict individual vehicles' choices and instead predict proportions of
steadfast vehicles and bypassing vehicles among vehicles traveling along the outermost lane
1 as shown in Figure 4.1.

Let $I = \{0, 1, 2\}$ be the lane index set for the highway on–ramp in Figure 4.1. Lane
0 is the on–ramp lane and lane 1 is the outermost lane in the mainline. The outermost
lane 1 is where vehicles' bypassing behavior takes place, whereas lane 0 and lane 2 are two
neighboring lanes of lane 1. For every lane $i \in I$, let f_i be the traffic flow on lane i. For lane
$i \in \{0, 2\}$, we let $n_i := \frac{f_i}{\sum_{i \in \{0,2\}} f_i}$ be the normalized flow on lane i. For each lane $i \in \{0, 2\}$,
normalized flow n_i indicates the relative magnitude of flow on lane i among the neighboring
flows of lane 1. We should have $n_0 + n_2 = 1$. In our model, we consider n_0 and n_2 are known
and static. We collect them in the flow configuration vector $\mathbf{N} := (n_0, n_2)$. For lane 1, let
f_1^s represent the flow of vehicles travelling on lane 1 that choose to stay steadfast, and let
f_1^b represent the flow of vehicles travelling on lane 1 and yet bypass the merging area. Then
we let $x_1^s := \frac{f_1^s}{f_1}$ represent the proportion of steadfast vehicles on lane 1, and let $x_1^b := \frac{f_1^b}{f_1}$
represent the proportion of bypassing vehicles on lane 1. Now we collect the proportions of
steadfast and bypassing vehicles on lane 1 in the flow distribution vector $\mathbf{x} := (x_1^s, x_1^b)$. A
flow distribution vector is feasible if and only if

$$
\begin{aligned}
x_1^s + x_1^b &= 1, \\
x_1^s \geq 0, x_1^b &\geq 0.
\end{aligned}
\tag{4.1}
$$

As for vehicles' initiatives to bypass, we suppose all vehicles choose the option that costs
themselves the least. In other words, if being steadfast is less costly than bypassing, vehicles
would choose to be steadfast. On the contrary, if bypassing is less costly than being steadfast,
vehicles would bypass. Therefore, we model the cost vehicles experience under both options.
In this work, we consider the cost experienced by vehicles as the time delay, and thereby,
vehicles choosing the same option would experience the same cost. For lane 1, we let J_1^s
denote the cost experienced by steadfast vehicles, and we let J_1^b denote the cost experienced
by bypassing vehicles. For steadfast vehicles, we propose

$$
J_1^s(\mathbf{x}) = C_1^t \mu(x_1^s + n_0) + C_1^m x_1^s n_0.
\tag{4.2}
$$

The first term represents the traversing cost that steadfast vehicles on lane 1 would experience after the merging with on–ramp vehicles. For lane $i \in \{1, 2\}$ in the mainline, we define C_i^t to be a positive constant, denoting the unit cost for traversing lane i in the mainline. We let μ to be a positive constant to characterize the discomfort when vehicles travel across the on–ramp merging zone. If the discomfort is negligible, we should have $\mu = 1$, otherwise, $\mu > 1$. Since the outermost lane 1, after the merging area, is shared by steadfast vehicles travelling along lane 1 and on–ramp vehicles, the total traversing cost should be proportional to the total flow on lane 1, which is $x_1^s + n_0$. We then employ the product of $C_1^t \mu$ and $x_1^s + n_0$ as the first term of traversing cost. The second term indicates the merging cost for steadfast vehicles to merge with on–ramp vehicles on lane 1. For lane $i \in \{1, 2\}$ in the mainline, we let C_i^m to be a positive constant, denoting the unit cost incurred by the actual merging behavior on lane i. This merging cost should be proportional to the number of either of the merging parties. On lane 1, on–ramp vehicles are trying to merge with the steadfast vehicles along lane 1, thus we take the product of C_1^m and $x_1^s n_0$ as the second term of the merging cost.

Similarly, for bypassing vehicles on lane 1, we propose

$$J_1^b(\mathbf{x}) = C_2^t \left(\gamma x_1^b + n_2 \right) + C_2^m x_1^b n_2, \tag{4.3}$$

which also includes the first term of traversing cost and the second term of merging cost. The positive constant C_2^t, as described above, denotes the unit cost for traversing lane 2. Innermost lane 2, after the merging area, is shared by bypassing vehicles from lane 1 and vehicles traveling along lane 2, thus we multiply C_2^t by the total flow $x_1^b + n_2$ to be the traversing cost. The parameter γ is assumed to be a positive constant to characterize the discomfort for bypassing vehicles from lane 1 to perform an extra lane–changing maneuver than staying steadfast. If this discomfort is negligible, we should have $\gamma = 1$. Otherwise, we have $\gamma > 1$. The positive parameter C_2^m denotes the unit cost for merging on lane 2. On lane 2, bypassing vehicles from lane 1 have to merge with through vehicles on lane 2, thus we take the product of C_2^m and $x_1^b n_2$ to denote the merging cost. We now collect all the defined parameters in the cost coefficient vector $\mathbf{C} := (C_i^t, C_i^m, \mu, \gamma : i \in \{1, 2\})$.

As what we have discussed, vehicles only choose the option with their own minimized cost. With the costs we have modeled, at the equilibrium of through vehicles' lane choices, if bypassing is less costly, i.e., $J_1^s(\mathbf{x}) - J_1^b(\mathbf{x}) > 0$, all vehicles on lane 1 would choose to bypass, i.e., $x_1^s = 0$; if staying steadfast is less costly, i.e., $J_1^b(\mathbf{x}) - J_1^s(\mathbf{x}) > 0$, all vehicles on lane 1 would choose to stay steadfast, i.e., $x_1^b = 0$; if staying steadfast has the same cost as bypassing, i.e., $J_1^b(\mathbf{x}) - J_1^s(\mathbf{x}) = 0$, there may be both steadfast and bypassing vehicles, i.e., x_1^s and x_1^b may both be nonzero. Reversely, if there are no bypassing vehicles, i.e., $x_1^b = 0$, we can conclude that bypassing is more costly than staying steadfast, i.e., $J_1^b(\mathbf{x}) - J_1^s(\mathbf{x}) > 0$; if all vehicles bypass, i.e., $x_1^s = 0$, we can conclude that staying steadfast is more costly than bypassing, i.e., $J_1^s(\mathbf{x}) - J_1^b(\mathbf{x}) > 0$; if there are both steadfast and bypassing vehicles, we must have $J_1^b(\mathbf{x}) - J_1^s(\mathbf{x}) = 0$. These sufficient and necessary conditions can then be encoded as Wardrop conditions [45]. We thus give the formal equilibrium definition for our model. Let a tuple $G = (\mathbf{N}, \mathbf{C})$ be the full configuration of the highway on–ramp in Figure 4.1, where $\mathbf{N}$ is the static flow configuration vector and $\mathbf{C}$ is the cost coefficient vector.

Definition 3. For a given $G = (\mathbf{N}, \mathbf{C})$, a flow distribution vector $\mathbf{x}$ is an equilibrium if and only if we have

$$
\begin{aligned}
x_1^s(J_1^s(\mathbf{x}) - J_1^b(\mathbf{x})) \leq 0, \\
x_1^b(J_1^b(\mathbf{x}) - J_1^s(\mathbf{x})) \leq 0.
\end{aligned}
\tag{4.4}
$$

4.3 Equilibrium Properties

In this section, we prove the existence and uniqueness of the equilibrium described in Definition 3.

Equilibrium Existence

First, a proposition based on the existence theorem stated and proved in [82] is given as follows.

Proposition 2. *Given an on–ramp configuration $G = (\mathbf{N}, \mathbf{C})$, if both cost functions $J_1^s(\mathbf{x})$, $J_1^b(\mathbf{x})$ are continuous and monotone in $\mathbf{x}$, there is at least one Wardrop equilibrium (as described in Definition 10) for G.*

Based on Equations (4.2) and (4.3), it's obvious that $J_1^s(\mathbf{x})$ and $J_1^b(\mathbf{x})$ are both continuous and monotonically non-decreasing in $\mathbf{x}$. Thus, by Proposition 2, the equilibrium described in Definition 3 exists.

Equilibrium Uniqueness

Here we directly give the following uniqueness theorem and then elaborate its proof.

Theorem 2. *For an on–ramp configuration $G = (\mathbf{N}, \mathbf{C})$, the equilibrium flow vector $\mathbf{x}$ in Definition 3 is unique.*

Proof. First, using flow constraints (4.1), we have

$$
J_1^s(\mathbf{x}) = C_1^t \mu((1 - x_1^b) + n_0) + C_1^m(1 - x_1^b)n_0, \tag{4.5}
$$

$$
J_1^b(\mathbf{x}) = C_2^t \left(\gamma x_1^b + n_2\right) + C_2^m x_1^b n_2. \tag{4.6}
$$

Then we have the derivatives of the costs with respect to x_1^b:

$$
\frac{\partial J_1^s}{\partial x_1^b} = -C_1^t \mu - n_0 C_1^m, \tag{4.7}
$$

$$
\frac{\partial J_1^b}{\partial x_1^b} = C_2^t \gamma + n_2 C_2^m. \tag{4.8}
$$

Given all coefficients are positive, $\frac{\partial J_1^s}{\partial x_1^b}$ is a negative constant, i.e., $J_1^s(\mathbf{x})$ is a decreasing linear function of x_1^b. Likewise, $\frac{\partial J_1^b}{\partial x_1^b}$ is a positive constant, i.e., $J_1^b(\mathbf{x})$ is an increasing linear function of x_1^b.

Given a flow configuration (n_0, n_2) and a cost coefficient vector $\mathbf{C} := (C_i^t, C_i^m, \mu, \gamma : i \in \{1, 2\})$, $J_1^s(\mathbf{x})$ and $J_1^b(\mathbf{x})$ in the region of $x_1^b \in [0, 1]$ must conform to one of the three possibilities shown in Figure 4.2. The equilibrium uniqueness is then proved case by case.

- Case (a): For every $x_1^b \in [0, 1]$, $J_1^s(x_1^b) > J_1^b(x_1^b)$ holds in this case. At a Wardrop equilibrium defined by inequalities (4.4), for $J_1^s(x_1^b) > J_1^b(x_1^b)$, we conclude that $x_1^b = 1$, $x_1^s = 0$. Thus the equilibrium is unique.

- Case (b): In this case, $J_1^s(x_1^b)$ and $J_1^b(x_1^b)$ have an intersection. At the intersection, assuming $x_1^b = \bar{x}_1^b$, we have $J_1^s(\bar{x}_1^b) = J_1^b(\bar{x}_1^b)$. Only the flow distribution $x_1^b = \bar{x}_1^b$, $x_1^s = 1 - \bar{x}_1^b$ qualifies as a Wardrop equilibrium defined by inequalities (4.4). Thus, the equilibrium is unique.

- Case (c): Similar to case (a), for every $x_1^b \in [0, 1]$, we have $J_1^s(x_1^b) < J_1^b(x_1^b)$. At a Wardrop equilibrium defined by inequalities (4.4), for $J_1^s(x_1^b) < J_1^b(x_1^b)$, we conclude that $x_1^b = 0, x_1^s = 1$. The equilibrium is unique.

The unique equilibrium in each case is indicated by a green dot in the sketches. $\qquad\square$

Based on the proofs above, we conclude that the equilibrium in our model exists and is unique. We then evaluate the model performance using accessible simulation data.

4.4 Simulation Studies

In this chapter, we use the micro-scale traffic simulation software Aimsun to simulate a highway on–ramp in Figure 4.1 and then validate our model using simulation–generated data. The overview of the simulated highway on–ramp is shown in Figure 4.3. Lane 0 is the on–ramp lane and lane 1 is the outermost lane. The length of the simulated highway is set to be 1km to fully capture vehicles' lane–changing behavior caused by the on–ramp merging. The simulated highway segment consists of three zones, among which zone 2 is a 100-metre-long buffer zone as shown in Figure 4.3. In this buffer zone, on–ramp vehicles from lane 0 accelerate to a relatively high speed and wait for an acceptable gap to join the mainline traffic safely. In zone 1 and zone 2, lane–changing vehicles from lane 1 to lane 2 are considered to be bypassing vehicles that intend to avoid the on–ramp merging. In the simulation, the cooperation between vehicles is set high, which means for a lane–changing vehicle, the vehicles in its target lane would give it a large enough gap and allow it to merge. The capacity and the maximum speed of the highway mainline and the on–ramp are set according to [88], [89]. Detailed parameter values are shown in table 4.1.
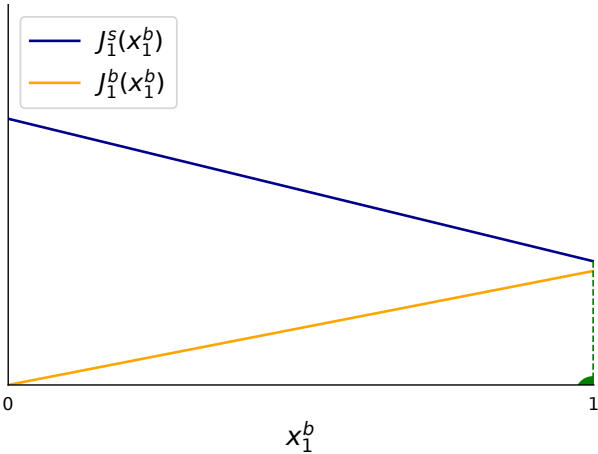
(a) $J_1^s(x_1^b) > J_1^b(x_1^b)$
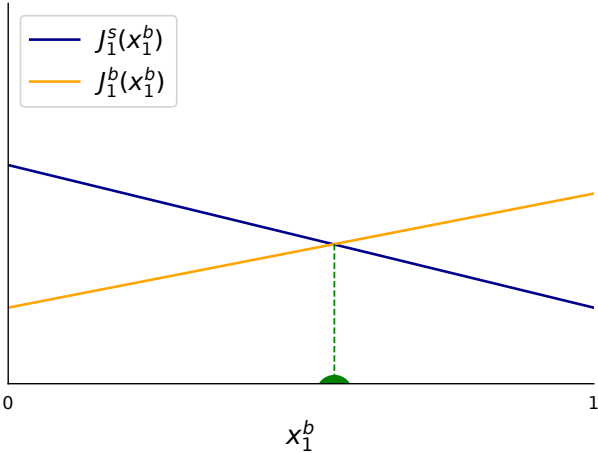
(b) $J_1^s(x_1^b)$ and $J_1^b(x_1^b)$ intersect
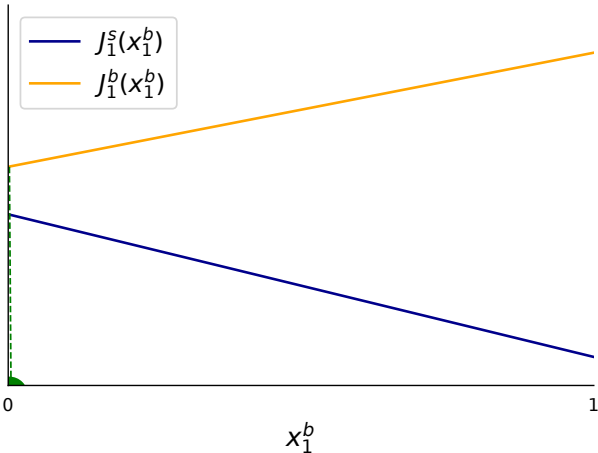
(c) $J_1^s(x_1^b) < J_1^b(x_1^b)$

Figure 4.2: Three possible sketches of $J_1^s(x_1^b)$ and $J_1^b(x_1^b)$ in the region of $x_1^b \in [0, 1]$.
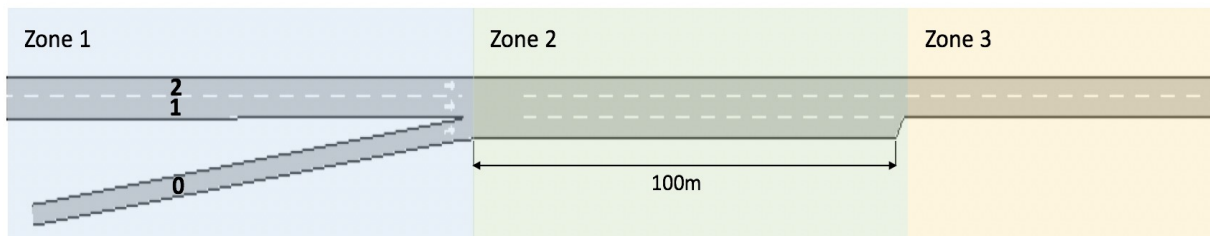
Figure 4.3: Enlarged view of the highway on–ramp in Aimsun.

	Mainline	On–ramp
Max Speed (km/h)	120	60
Capacity (veh/hr/lane)	1800	900

Table 4.1: Parameter settings in Aimsun.

To observe obvious lane–changing behaviors, the total demand of the outermost lane 1 and the on–ramp lane 0 should not be too small. If the total demand is too small, it's possible that the outermost lane 1 has enough vacant space that accommodates on–ramp vehicles easily so through vehicles on lane 1 would not be affected by on–ramp vehicles significantly. Moreover, the total demand of the highway should not greatly exceed the total capacity of the highway. If the total demand is too high, traffic will be jammed with a large density and it will be impossible for any vehicle to perform a lane–changing maneuver to any other lanes because there is no acceptable gap. Therefore, we set the total demand to around 3500 vehicles per hour in the simulation.

Model Calibration

To test the performance of our model, we first calibrate the cost coefficient vector $\mathbf{C}$. We employ the optimization method described in [44], [90]. We generate 20 data points from Aimsun. Each data point records the average equilibrium flow distribution vector $\mathbf{x} = (x_1^s, x_1^b)$ of 5 simulation replications with one distinct flow configuration $\mathbf{N}$. The duration of each simulation is long enough to make sure that the traffic operates in a stable state. With these data, we solve the optimization problem elaborated in [44], [90]. Since we assume symmetric properties for lane 1 and lane 2, we add an equality constraint in the calibration process:

$$C_1^t = C_2^t. \tag{4.9}$$

We then obtain the calibrated cost coefficients:

$$C_1^t = C_2^t = 1, \; C_1^m = 21.3, \; C_2^m = 1, \; \mu = 2.4, \; \gamma = 8.6. \tag{4.10}$$
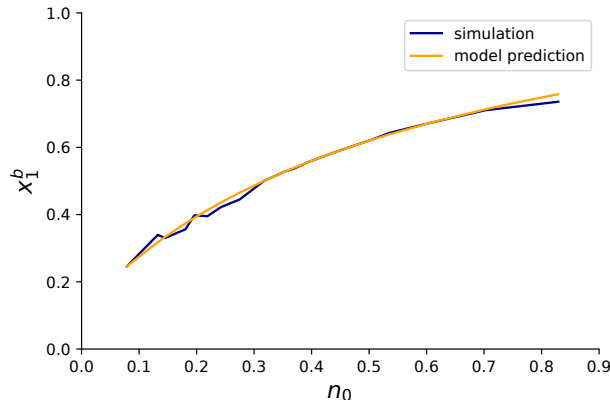
Figure 4.4: Model prediction of the proportion of bypassing vehicles is compared to simulation generated data.

Model Validation

To test the prediction accuracy of our model, we generate data points from Aimsun simulations with a different set of flow configurations and apply the calibrated model to this new test dataset. We then compare the model predicted proportions of bypassing and steadfast vehicles on lane 1 to the test simulation data. The test data are generated from simulations with all parameters the same as the calibration process.

Figure 4.4 shows the validation results. Our model prediction coheres with the simulation very well. The proportion of bypassing vehicles on lane 1 increases when the normalized on–ramp flow increases. This agrees with our intuition: the disturbance that on–ramp vehicles introduce increases with the on–ramp flow, therefore, more of through vehicles intend to gain a higher speed or run more smoothly by steering to lane 2. However, it is worth noticing that through vehicles become less sensitive to the disturbance introduced by on–ramp merging when the on–ramp flow increases.

4.5 Socially Optimal Behavior

In our model, we assume that vehicles are selfish so they only choose the option that minimizes their own cost. We call this behavior *user* optimal. However, this natural *user* optimal behavior in the reality may not be the optimal behavior considering the social cost for the total traffic. Should there be any advice or regulations for through vehicles' drivers so that the overall traffic condition can be improved? To answer this question, we first define a social cost for the total traffic flow.

The total traffic flow consists of four parties of vehicles. They are bypassing vehicles on lane 1, steadfast vehicles on lane 1, vehicles on lane 2 and on–ramp vehicles. We have defined the costs for steadfast vehicles and bypassing vehicles on lane 1 in Equations (4.2)
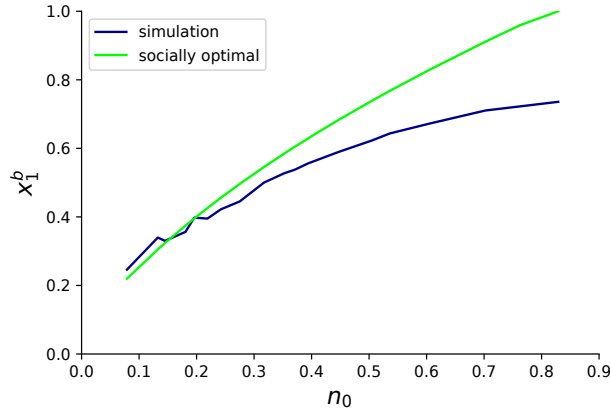
Figure 4.5: The socially optimal proportion of bypassing vehicles is compared to simulation generated data.

and (4.3), and now we specify costs for vehicles on lane 2 and on–ramp vehicles. For on–ramp vehicles, we let J_0 denote the cost on–ramp vehicles experience. The traversing cost and merging cost are both mutual and equal for on–ramp vehicles and steadfast vehicles, thus from Equation (4.2), we propose

$$J_0(\mathbf{x}) = C_1^t \mu (x_1^s + n_0) + C_1^m x_1^s n_0. \tag{4.11}$$

For vehicles on lane 2, we let J_2 denote the cost they experience. Similarly, it is reasonable to expect that the traversing cost and merging cost are both shared by bypassing vehicles and vehicles on lane 2, except that vehicles on lane 2 experience no discomfort for performing extra lane–changing behavior. We then propose

$$J_2(\mathbf{x}) = C_2^t (x_1^b + n_2) + C_2^m x_1^b n_2. \tag{4.12}$$

Thus we define the social cost of the total traffic flow to be

$$J_{soc}(\mathbf{x}) = x_1^s J_1^s(\mathbf{x}) + x_1^b J_1^b(\mathbf{x}) + n_0 J_0(\mathbf{x}) + n_2 J_2(\mathbf{x}). \tag{4.13}$$

To obtain the mainline vehicles' socially optimal lane choice behavior, we solve the following optimization problem with cost coefficients $\mathbf{C}$ calibrated in (4.10):

$$
\begin{aligned}
\underset{\mathbf{x}}{\text{minimize}} \quad & J_{soc}(\mathbf{x}) \\
\text{subject to} \quad & x_1^s + x_1^b = 1, \\
& x_1^s \geq 0, x_1^b \geq 0.
\end{aligned}
\tag{4.14}
$$

Figure 4.5 compares the mainline vehicles' user optimal lane choice behavior simulated in Section 4.4 and the socially optimal lane choice behavior under our model. Ideally, to improve the overall traffic condition, mainline through vehicles should be encouraged to bypass and give away more space to on–ramp vehicles.

4.6 Summary

In this chapter, we focused on mainline through vehicles' aggregate lane choice behavior facing a highway on–ramp ahead. We modeled vehicles' aggregate lane choice behavior as a Wardrop equilibrium and then validated our model using Aimsun data. The result shows the promising predictive power of our model. We further compared mainline vehicles' socially optimal and user optimal lane choice behavior. We concluded that through vehicles should be encouraged to bypass the on–ramp merging area instead of staying steadfast to improve overall traffic conditions.

Chapter 5

Employing Altruistic Vehicles at On-Ramps to Improve Social Traffic Conditions

5.1 Overview

Vehicles' selfish lane choice behavior on transportation networks is regarded as one important cause of traffic inefficiency. In the previous chapter, we discussed a highway on-ramp with two lanes in the mainline as shown in Figure 4.1. Vehicles traveling along the on-ramp lane 0 are trying to merge with mainline vehicles on lane 1. To minimize their own travel delay, selfish mainline vehicles along lane 1 choose between two options. The first option is to stay *steadfast* on the current lane 1 and merge with the on-ramp vehicles. The second option is to switch to the neighboring lane 2 and *bypass* the merging with on-ramp vehicles. We then modeled the aggregate choice behavior of selfish mainline vehicles as a Wardrop equilibrium [45]. The results from simulations show that the selfish lane choice behavior worsens the social delay and if properly more mainline vehicles bypass instead of staying steadfast on the current lane, then the social traffic conditions can be improved.

In this chapter, we employ a proportion of altruistic vehicles in addition to selfish mainline vehicles to improve the social traffic conditions of the highway on-ramp discussed in Chapter 4. *Selfish* mainline vehicles choose to stay steadfast or bypass to minimize their own travel delay, whereas *altruistic* vehicles make the decision to stay steadfast or bypass to minimize their own altruistic cost, which is a weighted average of the travel delay and the marginal cost [51], [52]. Altruistic vehicles are individual optimizers which require local delay and cost information but no centralized coordination. With the presence of autonomous vehicles, it is envisioned that connected and autonomous vehicles can be employed as altruistic vehicles perceiving and minimizing configured altruistic costs. The weight configuration of the altruistic costs indicates how altruistic vehicles are. Naturally, the first question arises: will altruism improve social traffic conditions in the on–ramp lane choice scenario? To an-
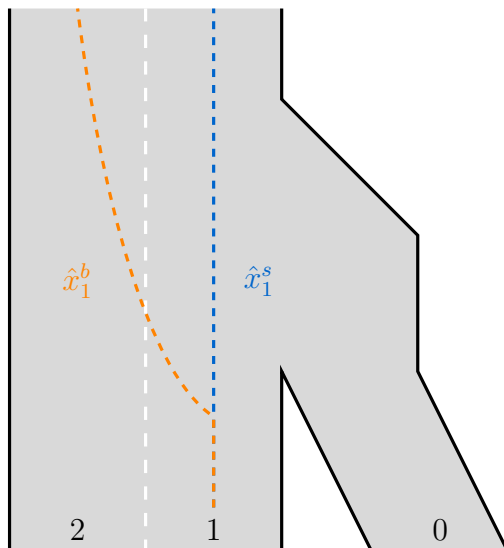
Figure 5.1: Problem setting: mainline vehicles on lane 1 (both selfish and altruistic) choose
to stay steadfast on lane 1 or bypass the merging with on–ramp vehicles.

swer this question, we first consider the case when the altruistic costs are perfectly measured
by altruistic vehicles, and we find the conditions under which altruism helps to decrease or
optimize the social delay. These conditions indicate that altruism always improves traffic
conditions when altruistic vehicles are abundant. However, for the scenarios when altruistic
vehicles only have inaccurate estimates of the altruistic costs, how altruistic should vehicles
be? In this scenario, we then give the optimal weight configuration for altruistic vehicles
that minimizes the worst case social delay under such uncertainty.

The chapter is organized as follows. In Section 5.2, we introduce selfish and altruistic
mainline vehicles' lane choice model. In Section 5.3, we give the conditions for altruistic
vehicles to improve or optimize the social delay when no uncertainty is present in the mea-
surements of costs. In Section 5.4, we consider inaccurate estimates of altruistic costs and
give the optimal configuration for altruistic vehicles to minimize the worst case social delay
under the uncertainty. Finally, in Section 5.5, we summarize the chapter.

5.2   The Model

Let $I = \{0, 1, 2\}$ be the lane index set for the highway on–ramp in Figure 5.1, where lane 0 is
the on–ramp lane, lane 1 is the outermost lane in the mainline and vehicles on lane 1 make
decisions to stay steadfast or bypass. For lane $i \in \{0, 2\}$, we let n_i be the normalized flow on
lane i, which indicates the relative magnitude of flow on lane i among the neighboring flows
of lane 1. Note that $n_0 + n_2 = 1$. We consider n_0 and n_2 to be known and static. We then
collect them in the neighboring flow configuration vector $\mathbf{N} := (n_0, n_2)$. For lane 1, let x_1^s

(resp., $\tilde{x}_1^s$) represent the proportion flow of selfish (resp., altruistic) steadfast vehicles on lane 1, and let x_1^b (resp., $\tilde{x}_1^b$) represent the proportion flow of selfish (resp., altruistic) bypassing vehicles on lane 1. Now we collect the proportion flows on lane 1 in the flow distribution vector $\mathbf{x} := (x_1^s, x_1^b, \tilde{x}_1^s, \tilde{x}_1^b)$. Let $\alpha \geq 0$ be the altruistic ratio, i.e., the proportion of altruistic vehicles among all the vehicles. A flow distribution vector is feasible if and only if

$$x_1^s + x_1^b = 1 - \alpha, \tag{5.1}$$

$$\tilde{x}_1^s + \tilde{x}_1^b = \alpha, \tag{5.2}$$

$$x_1^s \geq 0, x_1^b \geq 0, \tilde{x}_1^s \geq 0, \tilde{x}_1^b \geq 0. \tag{5.3}$$

Selfish vehicles will only choose the option that can minimize their own travel delay. For selfish vehicles, we employ the delay models that are calibrated and validated in our previous chapter 4. Notice that the selfish flow proportions in the original delay models have to be replaced by the total flow proportions including both selfish and altruistic vehicles choosing the same option. For simplicity of future reference, we let $\hat{x}_1^s := x_1^s + \tilde{x}_1^s$ and $\hat{x}_1^b := x_1^b + \tilde{x}_1^b$ be the total proportion of steadfast and bypassing vehicles. Note that

$$\hat{x}_1^s + \hat{x}_1^b = 1. \tag{5.4}$$

Let J_1^s denote the travel delay experienced by selfish steadfast vehicles, and J_1^b denote the delay experienced by selfish bypassing vehicles. We have

$$J_1^s(\mathbf{x}) = C_1^t \mu (\hat{x}_1^s + n_0) + C_1^m \hat{x}_1^s n_0, \tag{5.5}$$

$$J_1^b(\mathbf{x}) = C_2^t \left(\gamma \hat{x}_1^b + n_2 \right) + C_2^m \hat{x}_1^b n_2. \tag{5.6}$$

The cost coefficients are collected in the cost coefficient vector $\mathbf{C} := (C_i^t, C_i^m, \mu, \gamma : i \in \{1, 2\})$. The coefficients are all non–negative constants for an on–ramp, which need to be calibrated for each on–ramp. The detailed explanation of the coefficients can be seen in Section 4.2. For simplicity of reference, we rewrite the travel delay models for selfish vehicles:

$$J_1^s(\mathbf{x}) = K^s \hat{x}_1^s + B^s, \tag{5.7}$$

$$J_1^b(\mathbf{x}) = K^b \hat{x}_1^b + B^b, \tag{5.8}$$

where $K^s := C_1^t \mu + C_1^m n_0$, $B^s := C_1^t \mu n_0$, $K^b := C_2^t \gamma + C_2^m n_2$ and $B^b := C_2^t n_2$ are all non–negative constants for an on–ramp with a given neighboring flow configuration $\mathbf{N}$. Essentially, we care about the social traffic conditions, i.e., the social delay. We also employ the delay models proposed in Section 4.2 for vehicles on lane 2 and on–ramp vehicles. Let J_0 denote the delay experienced by on–ramp vehicles and J_2 denote the delay experienced by vehicles on lane 2. We have

$$J_0(\mathbf{x}) = K^s \hat{x}_1^s + B^s, \tag{5.9}$$

$$J_2(\mathbf{x}) = K_2 \hat{x}_1^b + B^b, \tag{5.10}$$

where $K_2 := C_2^{\mathrm{t}} + C_2^{\mathrm{m}} n_2$ is also a non–negative constant for an on–ramp with a given neighboring flow configuration. Notice that vehicles choosing the same option experience the same travel delay no matter whether they are selfish or altruistic. Therefore, the social delay can be expressed as

$$J_{\mathrm{soc}}(\mathbf{x}) = \hat{x}_1^{\mathrm{s}} J_1^{\mathrm{s}}(\mathbf{x}) + \hat{x}_1^{\mathrm{b}} J_1^{\mathrm{b}}(\mathbf{x}) + n_0 J_0(\mathbf{x}) + n_2 J_2(\mathbf{x}), \tag{5.11}$$

which is a convex function of $\mathbf{x}$ when $\mathbf{N}$ and $\mathbf{C}$ are given. Note that by Equation (5.4), we always have $\hat{x}_1^{\mathrm{s}} = 1 - \hat{x}_1^{\mathrm{b}}$. In the later proofs, we tend to use $\hat{x}_1^{\mathrm{b}}$ instead of $\mathbf{x}$ as the self–variable of the delay functions. Let $J_{\mathrm{opt}} := \min_{\hat{x}_1^{\mathrm{b}} \in [0,1]} J_{\mathrm{soc}}(\mathbf{x})$ denote the optimal social delay. Ideally, for an on–ramp with a given neighboring flow configuration, we aim to employ altruistic vehicles to decrease the social delay to its minimum.

Altruistic vehicles also choose to stay steadfast or bypass to minimize their own cost. However, to improve the social traffic conditions, they are configured to perceive an altruistic cost which is different from the travel delay. We propose the altruistic cost to be the weighted sum of the travel delay and the marginal cost (see [51], [52] for more details). Let $\tilde{J}_1^{\mathrm{s}}$ denote the altruistic cost for altruistic steadfast vehicles, and $\tilde{J}_1^{\mathrm{b}}$ denote the cost for altruistic bypassing vehicles. We have

$$\tilde{J}_1^{\mathrm{s}}(\mathbf{x}) = (1 - \beta) J_1^{\mathrm{s}}(\mathbf{x}) + \beta \frac{\partial J_{\mathrm{soc}}(\mathbf{x})}{\partial \hat{x}_1^{\mathrm{s}}} \tag{5.12}$$

$$= J_1^{\mathrm{s}}(\mathbf{x}) + \beta K^{\mathrm{s}}(\hat{x}_1^{\mathrm{s}} + n_0), \tag{5.13}$$

$$\tilde{J}_1^{\mathrm{b}}(\mathbf{x}) = (1 - \beta) J_1^{\mathrm{b}}(\mathbf{x}) + \beta \frac{\partial J_{\mathrm{soc}}(\mathbf{x})}{\partial \hat{x}_1^{\mathrm{b}}} \tag{5.14}$$

$$= J_1^{\mathrm{b}}(\mathbf{x}) + \beta (K^{\mathrm{b}} \hat{x}_1^{\mathrm{b}} + K_2 n_2), \tag{5.15}$$

where $0 \leq \beta \leq 1$ is the altruism level of the altruistic vehicles, which acts as the weight configuration of the altruistic costs. The altruism level is assigned to the altruistic vehicles by a central authority and can be interpreted as the propensity of altruistic vehicles to optimize the social delay. When $\beta = 0$, altruistic vehicles behave exactly like selfish vehicles; when the altruistic ratio $\alpha = 1$ and altruism level $\beta = 1$, the resulting social delay is minimized. In this work, we consider the altruism level to be the same for all altruistic vehicles at the on–ramp. Note that altruistic vehicles are not explicitly coordinated, but are still individual optimizers evaluating the altruistic cost instead of the travel delay. Therefore, just as the selfish vehicles in [78], the equilibrium of the choice behavior of altruistic vehicles can be formulated as a Wardrop equilibrium [45]. Let a tuple $G = (\mathbf{N}, \mathbf{C})$ be the full configuration of a highway on–ramp shown in Figure 5.1, where $\mathbf{N}$ is the static neighboring flow configuration and $\mathbf{C}$ is the cost coefficient vector. The resulting choice equilibrium of the mixed selfish and altruistic vehicles is then defined below.

Definition 4. For a given on–ramp configuration $G = (\mathbf{N}, \mathbf{C})$, a flow distribution vector $\mathbf{x}$ is a choice equilibrium if and only if

$$x_1^s(J_1^s(\mathbf{x}) - J_1^b(\mathbf{x})) \leq 0, \tag{5.16a}$$

$$x_1^b(J_1^b(\mathbf{x}) - J_1^s(\mathbf{x})) \leq 0, \tag{5.16b}$$

$$\tilde{x}_1^s(\tilde{J}_1^s(\mathbf{x}) - \tilde{J}_1^b(\mathbf{x})) \leq 0, \tag{5.16c}$$

$$\tilde{x}_1^b(\tilde{J}_1^b(\mathbf{x}) - \tilde{J}_1^s(\mathbf{x})) \leq 0. \tag{5.16d}$$

The definition mathematically expresses that selfish vehicles only choose the option with their own minimized travel delay, whereas altruistic vehicles choose the option with their own minimized altruistic cost.

5.3   When No Uncertainty Exists

In this section, we consider the scenarios when no uncertainty lies in the measurements of travel delay and altruistic costs. We aim to analyze the impact of the altruistic ratio α and the altruism level β on the resulting social delay.

In the rest of the chapter, we only discuss a certain meaningful set of on–ramp configurations. As discussed in Chapter 4, when all vehicles are selfish, properly encouraging the bypassing behavior of mainline vehicles can improve the social delay. Thus in this work, we only focus on the on–ramp configurations where selfish vehicles bypass less than the socially optimal scenario. Moreover, when all vehicles are selfish, at the choice equilibrium, if all the selfish vehicles are bypassing vehicles, we cannot decrease the social delay anymore by letting more vehicles bypass even with altruistic vehicles; if all the selfish vehicles choose to stay steadfast, as discussed in Chapter 4, for any $x_1^b \in (0, 1]$, we have $J_1^s(x_1^b) < J_1^b(x_1^b)$. Naturally, when there are altruistic vehicles, for any $\hat{x}_1^b \in (0, 1]$, we have $J_1^s(\hat{x}_1^b) < J_1^b(\hat{x}_1^b)$. Therefore, $x_1^b = 0$ for any altruistic ratio and any altruism level, and the choice equilibrium is only dependent on altruistic vehicles' choices. The choice equilibrium of a single class of vehicles is then much the same as discussed in Chapter 4. Furthermore, consider the scenario when all vehicles are bypassing vehicles at the socially optimal equilibrium, then to optimize the social delay, we have to make sure all altruistic vehicles always choose bypassing, i.e., $\tilde{J}_1^s(\hat{x}_1^b) > \tilde{J}_1^b(\hat{x}_1^b)$, for any $\hat{x}_1^b \in [0, 1)$, thus the problem totally depends on the selfish vehicles' choice, thus it becomes again very similar to what is discussed in Chapter 4.

Therefore, in the rest of the chapter, we only consider on–ramp configurations where we are able to employ altruistic vehicles to move the less efficient interior equilibrium when all vehicles are selfish to a socially optimal interior equilibrium with more bypassing vehicles.

Let Φ denote the bypassing flow at the interior equilibrium when all vehicles are selfish, which satisfies $J_1^s(\Phi) = J_1^b(\Phi)$. Solving the equation, we have

$$\Phi = \frac{K^s + B^s - B^b}{K^s + K^b}. \tag{5.17}$$
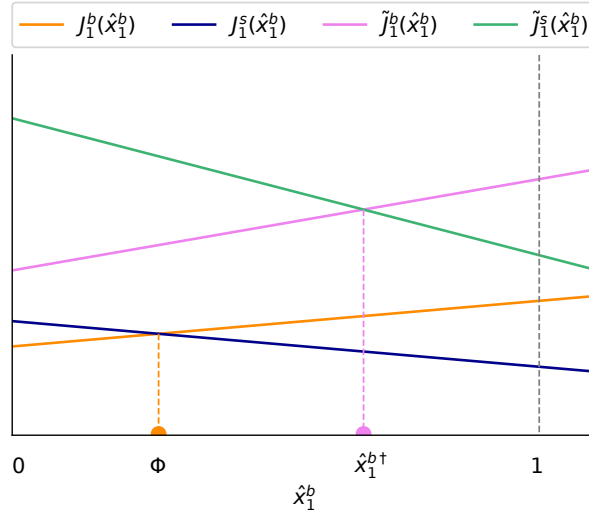
Figure 5.2: Sketch of the travel delay and altruistic cost functions, where Φ is indicated by the yellow dot and $\hat{x}_1^{b\dagger}$ is indicated by the pink dot.

Note that Φ is only dependent on the on–ramp configuration. For a specific on–ramp configuration, Φ is a constant. Moreover, recalling Equation (5.11), the social delay $J_{\text{soc}}(\hat{x}_1^b)$ is a convex quadratic function of $\hat{x}_1^b$. Let Δ be the unique global minimization point of the quadratic function, i.e., $J_{\text{soc}}(\Delta) = \min\limits_{\hat{x}_1^b \in \mathbb{R}} J_{\text{soc}}(\hat{x}_1^b)$. Note that Δ is only dependent on the on–ramp configuration. For a specific on–ramp configuration G, Δ is a constant regardless of any α or β and we always have $J_{\text{soc}}(\Delta) \leq J_{\text{opt}}$. If the social delay decreases when the bypassing proportion increases for some on–ramp configurations, we must have $\Phi < \Delta$. Also, to ensure at the social optimum, not all vehicles are bypassing vehicles, we must have $\Delta < 1$.

Let $\mathcal{G}$ be the meaningful set of on–ramp configurations, and we then have

$$\mathcal{G} = \{G : 0 < \Phi < \Delta < 1\}. \tag{5.18}$$

We then are ready to give the first core result in this work, which establishes the conditions for the altruistic vehicles' configurations to improve the social conditions or to reach the optimal social conditions.

Theorem 3. *For a given on–ramp configuration $G = (\mathbf{N}, \mathbf{C}) \in \mathcal{G}$ with altruistic ratio α and altruism level β.*

- *The social delay is decreased by altruistic vehicles , i.e., $J_{\text{soc}}(\hat{x}_1^b) < J_{\text{soc}}(\Phi)$, if and only if $\beta > 0$ and $\alpha \in \mathcal{A}_1$, where $\mathcal{A}_1 := (\Phi, 1]$.*

- *The social delay is optimized by altruistic vehicles, i.e., $J_{\text{soc}}(\hat{x}_1^b) = J_{\text{opt}}$, if and only if $\beta = 1$ and $\alpha \in \mathcal{A}_2$, where $\mathcal{A}_2 := [\Delta, 1]$.*

Proof. Let $\hat{x}_1^{\mathrm{b}\dagger}$ be the total bypassing proportion flow at the intersection of the altruistic
steadfast and bypassing costs, i.e., $\tilde{J}_1^{\mathrm{s}}(\hat{x}_1^{\mathrm{b}\dagger}) = \tilde{J}_1^{\mathrm{b}}(\hat{x}_1^{\mathrm{b}\dagger})$. Solving the equation, we have

$$\hat{x}_1^{\mathrm{b}\dagger} = \frac{1-\beta}{1+\beta}\Phi + \frac{2\beta}{1+\beta}\Delta. \tag{5.19}$$

Notice that $\hat{x}_1^{\mathrm{b}\dagger}$ is a function of the altruism level β for a certain on–ramp configuration.
When $\beta = 0$, the altruistic costs are exactly the same as the selfish delay. Therefore,
altruistic vehicles behave the same as selfish vehicles. Manipulating altruistic vehicles would
bring no change to the social delay. In the meaningful set $\mathcal{G}$, we always have $\Phi < \Delta$. When
$\beta > 0$, we have $\Phi < \hat{x}_1^{\mathrm{b}\dagger}$ and $\hat{x}_1^{\mathrm{b}\dagger}$ is always an increasing function of β. Note that $\hat{x}_1^{\mathrm{b}\dagger}$ can be
seen as a weighted average of Φ and Δ. We always have $\hat{x}_1^{\mathrm{b}\dagger} \le \Delta$ and when $\beta = 1$, we have
$\hat{x}_1^{\mathrm{b}\dagger} = \Delta$. We then enumerate all the possible cases of the resulting equilibria when altruistic
vehicles are involved, i.e., $\alpha > 0$ and the altruism level $\beta > 0$. See Figure 5.2 which sketches
the delays and altruistic costs, at the resulting equilibrium,

- Case (a): if $\hat{x}_1^{\mathrm{b}} \in [0, \Phi)$, since the bypassing delay is smaller than the steadfast delay
  and the bypassing altruistic cost is smaller than the steadfast altruistic cost, all vehicles
  will choose bypassing, i.e., $\hat{x}_1^{\mathrm{b}} = 1$. Since $\Phi < 1$, the conclusion $\hat{x}_1^{\mathrm{b}} = 1$ contradicts the
  assumption that $\hat{x}_1^{\mathrm{b}} < \Phi$. Therefore, the equilibrium cannot lie in this case.

- Case (b): if $\hat{x}_1^{\mathrm{b}} = \Phi$, the bypassing altruistic cost is smaller than the steadfast altruistic
  cost, thus all altruistic vehicles are bypassing vehicles, i.e., $\tilde{x}_1^{\mathrm{b}} = \alpha$. Therefore, we have
  $x_1^{\mathrm{b}} = \Phi - \alpha$. The requirement for this case to happen is $x_1^{\mathrm{b}} \ge 0$, i.e. $\alpha \le \Phi$.

- Case (c): if $\hat{x}_1^{\mathrm{b}} \in (\Phi, \hat{x}_1^{\mathrm{b}\dagger})$, the bypassing altruistic cost is smaller than the steadfast
  altruistic cost, thus all altruistic vehicles choose bypassing, i.e., $\tilde{x}_1^{\mathrm{b}} = \alpha$. However,
  the bypassing delay is larger than the steadfast delay, thus all selfish vehicles will stay
  steadfast, i.e., $x_1^{\mathrm{b}} = 0$. Therefore, we have $\hat{x}_1^{b} = \tilde{x}_1^{\mathrm{b}} = \alpha$. Thus, the requirement of this
  case is $\Phi < \alpha < \hat{x}_1^{\mathrm{b}\dagger}$.

- Case (d): if $\hat{x}_1^{\mathrm{b}} = \hat{x}_1^{\mathrm{b}\dagger}$, the bypassing delay is larger than the steadfast delay, thus all
  selfish vehicles will stay steadfast, i.e., $x_1^{\mathrm{b}} = 0$. Then we have $\hat{x}_1^{b} = \tilde{x}_1^{\mathrm{b}} = \hat{x}_1^{\mathrm{b}\dagger}$. The
  requirement for this case is $\tilde{x}_1^{\mathrm{b}} \le \alpha$, i.e., $\hat{x}_1^{\mathrm{b}\dagger} \le \alpha$.

- Case (e): if $\hat{x}_1^{\mathrm{b}} \in (\hat{x}_1^{\mathrm{b}\dagger}, 1]$, since bypassing delay is larger than the steadfast delay and
  the bypassing altruistic cost is larger than the steadfast altruistic cost, all vehicles must
  stay steadfast, i.e., $\hat{x}_1^{\mathrm{b}} = 0$. Since $\hat{x}_1^{\mathrm{b}\dagger} > \Phi > 0$, the equilibrium cannot lie in this case.

Consider the altruism level $\beta > 0$ as fixed, and consider the altruistic ratio α as a variable.
Recall that when $\alpha = 0$, all vehicles are selfish, and at the equilibrium, $\hat{x}_1^{\mathrm{b}} = \Phi$, we have the
social delay as $J_{\mathrm{soc}}(\Phi)$. We then only need to consider case (b), (c) and (d). In case (b), the
social delay remains the same as $J_{\mathrm{soc}}(\Phi)$, whereas in case (c) and (d), at the equilibrium, we
have $\Phi < \hat{x}_1^{\mathrm{b}} \le \Delta$. Recall that the social delay function (5.11) is a convex quadratic function

Figure 5.3: The social delay versus the altruistic ratio under different altruism levels. The on–ramp cost coefficients are $C_1^t = C_2^t = 1$, $C_1^m = 21.3$, $C_2^m = 1$, $\mu = 2.4$, $\gamma = 8.6$ (calibrated in Section 4.4) and the neighboring flow configuration is $n_0 = 0.37$. The on–ramp configuration lies in the meaningful set $\mathcal{G}$. As we can see, when altruistic vehicles are not abundant or the altruism level is less than 1, the social delay improvement is compromised.

of $\hat{x}_1^b$ with a minimization point Δ, thus we have $J_{\text{soc}}(\hat{x}_1^b) < J_{\text{soc}}(\Phi)$. Since $0 < \Delta < 1$, then $J_{\text{opt}} = J_{\text{soc}}(\Delta)$, and therefore, the optimal social delay is only reached when $\hat{x}_1^b = \hat{x}_1^{b\dagger} = \Delta$, i.e., $\beta = 1$ and the condition for case (c) is fulfilled.

In a nutshell, to decrease the social delay, we have to set $\beta > 0$ and $\alpha > \Phi$. Otherwise, when $\beta = 0$, altruistic vehicles act exactly like selfish vehicles, making no change; when $\alpha \leq \Phi$, the equilibrium is always in case (b) and we always have $\hat{x}_1^b = \Phi$. The social delay remains the same as $J_{\text{soc}}(\Phi)$. Since $0 < \Delta < 1$, we must have $J_{\text{opt}} = J_{\text{soc}}(\Delta)$. Therefore, to reach the optimal social delay, we have to let $\hat{x}_1^b = \Delta$, which is only possible in case (d) when $\hat{x}_1^{b\dagger} = \Delta$, i.e., $\beta = 1$. See Figure 5.3 as an example.

$\square$

Theorem 3 shows that with slightly altruistic vehicles, the social conditions can be improved as long as there are enough altruistic vehicles; however, to reach the optimal social traffic conditions, we have to employ enough purely altruistic vehicles. The altruism level of altruistic vehicles decides the best case of social delay we can do with abundant altruistic vehicles.

Theorem 3 provides valuable insights that can inform policy design by offering an estimate of potential expenses and benefits. It is worth noticing that it also demonstrates an underlying message that the benefit brought by altruistic vehicles can be exploited by selfish drivers. For instance, in a scenario where an altruistic vehicle altruistically changes lanes, a selfish human-driven vehicle following it may choose to stay in the current lane instead of originally intending to change lanes, taking advantage of the vacancy ahead.

5.4 When Uncertainty Exists

In reality, measuring the travel delay could be relatively easy whereas having an exact estimate of the altruistic part of the altruistic cost is hard. In this section, we assume that travel delay can be perfectly measured whereas some error $e \sim \mathcal{E}(e_{\mathrm{L}}, e_{\mathrm{U}})$ is embedded in the altruistic costs, where $\mathcal{E}(e_{\mathrm{L}}, e_{\mathrm{U}})$ is some probability distribution with a lower bound $e_{\mathrm{L}} > 0$ and an upper bound $e_{\mathrm{U}} > e_{\mathrm{L}}$. We assume all altruistic vehicles are affected by a homogeneous error, then the actual altruistic costs perceived by altruistic vehicles are

$$\tilde{J}_1^{\mathrm{s}}(\mathbf{x}) = J_1^{\mathrm{s}}(\mathbf{x}) + \beta e K^{\mathrm{s}}(\hat{x}_1^{\mathrm{s}} + n_0), \tag{5.20}$$

$$\tilde{J}_1^{\mathrm{b}}(\mathbf{x}) = J_1^{\mathrm{b}}(\mathbf{x}) + \beta e (K^{\mathrm{b}} \hat{x}_1^{\mathrm{b}} + K_2 n_2). \tag{5.21}$$

Without this uncertainty, we can easily use Theorem 3 to set $\beta = 1$ and when altruistic vehicles are abundant, i.e., $\alpha \in \mathcal{A}_2$, the social delay reaches optimal. However, with this uncertainty, we may not optimize the social delay as we expected. Thus, we are interested in the worst case social delay for different choice of altruism levels with the presence of the uncertainty. In the end, we aim to find an optimal altruism level to minimize the worst case social delay with respect to the cost uncertainty and level of on–ramp configuration uncertainty. We first give the following definition of the generalized price of anarchy to characterize the worst case social delay in our problem setting.

Definition 5. For a given on–ramp configuration $G = (\mathbf{N}, \mathbf{C}) \in \mathcal{G}$ with an altruism level β, the price of anarchy (PoA) is defined as

$$PoA(G, \beta, \mathcal{E}) := \sup_{e \sim \mathcal{E}(e_{\mathrm{L}}, e_{\mathrm{U}})} \sup_{\alpha \in \mathcal{A}_2} \frac{J_{\mathrm{soc}}(G, \beta, e, \alpha)}{J_{\mathrm{opt}}(G)}. \tag{5.22}$$

Note that the design goal is to optimize the social delay, therefore, the price of anarchy only focuses on the altruistic ratios in the $\mathcal{A}_2$ range. Then we define the optimal altruism level that we are trying to find.

Definition 6. For an on–ramp configuration $G \in \mathcal{G}$, the optimal altruism level β^* satisfies

$$\beta^* = \arg \min_{\beta \geq 0} PoA(G, \beta, \mathcal{E}). \tag{5.23}$$

Let $\Pi := \frac{1 - \Phi}{2\Delta - \Phi - 1}$. Note that in $\mathcal{G}$, we always have $1 - \Phi > 0$, thus Π is nonzero. Let $\mathcal{G}_1 := \left\{ G \in \mathcal{G} : 0 < \Pi < \sqrt{\frac{e_{\mathrm{U}}}{e_{\mathrm{L}}}} \right\}$ and $\mathcal{G}_2 := \{ G \in \mathcal{G} \setminus \mathcal{G}_1 \}$. We are ready to give the following theorem.

Theorem 4. *For an on–ramp configuration $G \in \mathcal{G}_1$, the optimal altruism level $\beta^* = \frac{1}{e_{\mathrm{L}} \Pi}$; for an on–ramp configuration $G \in \mathcal{G}_2$, the optimal altruism level $\beta^* = \frac{1}{\sqrt{e_{\mathrm{L}} e_{\mathrm{U}}}}$.*
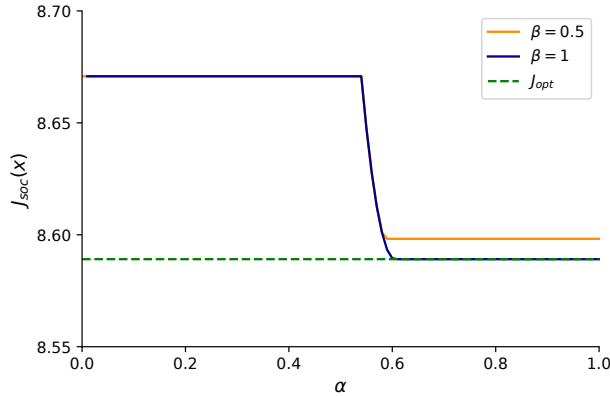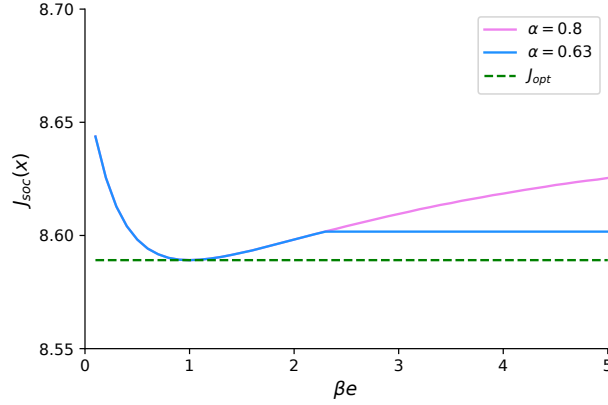
Figure 5.4: The social delay versus βe under different altruistic ratios. The on–ramp cost coefficients are $C_1^t = C_2^t = 1$, $C_1^m = 21.3$, $C_2^m = 1$, $\mu = 2.4$, $\gamma = 8.6$ (calibrated in Section 4.4) and the neighboring flow configuration is $n_0 = 0.37$. The on–ramp configuration lies in the set $\mathcal{G}_2$. The worst case social delay happens on the pink curve. The optimal altruism level satisfies $\beta^* = \frac{1}{\sqrt{e_L e_U}}$.

Proof. In the choice model considering the uncertainty, we see the product of e and β as the "effective" altruism level which corresponds to the altruism level in the cost models considering no uncertainty. The cases of equilibria are then enumerated in the proof of Theorem 3. Now consider the on–ramp configuration G, the altruistic ratio α and the error bounds e_L and e_U are fixed and see the product of βe as a variable. Since in the definition of PoA, $\alpha \in \mathcal{A}_2$, we must have $\alpha > \Phi$. Therefore, we only need to consider case (c) and (d). In a nutshell, when $\alpha \geq \hat{x}_1^{b\dagger}$, at the equilibrium, $\hat{x}_1^b = \hat{x}_1^{b\dagger}$, and the social delay is calculated as $J_{\text{soc}}(\hat{x}_1^{b\dagger})$; when $\alpha < \hat{x}_1^{b\dagger}$, at the equilibrium, $\hat{x}_1^b = \alpha$, and the social delay is calculated as $J_{\text{soc}}(\alpha)$. Recall that $\hat{x}_1^{b\dagger}$ is a function of βe (see Equation (5.19)), we then may use the notation $\hat{x}_1^{b\dagger}(\beta e)$. Now let us consider

- Case (A): $\Pi < 0$. In this case, the range $\mathcal{A}_2$ can be divided into two ranges.

  - Case (A.1): For any $\alpha \in [\Delta, 2\Delta - \Phi)$, the resulting equilibrium changes from case (d) to case (c) when $\hat{x}_1^{b\dagger}(\beta e) = \alpha$. Let $\tilde{\beta}$ denote the transition point, where $\hat{x}_1^{b\dagger}(\tilde{\beta}) = \alpha$. Solving the equation, we have $\tilde{\beta}(\alpha) = \frac{\alpha - \Phi}{2\Delta - \Phi - \alpha} \geq 1$, which is an increasing function of α. For $\beta e \leq \tilde{\beta}$, the equilibrium is at $\hat{x}_1^b = \hat{x}_1^{b\dagger}$, and the social delay can be calculated as $J_{\text{soc}}(\hat{x}_1^{b\dagger})$. Since the social delay function is a convex quadratic function of $\hat{x}_1^{b\dagger}$, $\hat{x}_1^{b\dagger}$ is an increasing function of βe, and $\hat{x}_1^{b\dagger}(\beta e = 1) = \Delta$, the social delay will first decrease, reaches optimal at $\beta e = 1$ and then increase to $J_{\text{soc}}(\alpha)$. For $\beta e > \tilde{\beta}$, the equilibrium remains at $\hat{x}_1^b = \alpha$, and the social delay remains the same at $J_{\text{soc}}(\alpha)$. Note that when α increases, since we have $\alpha \geq \Delta$, $J_{\text{soc}}(\alpha)$ increases.

For clarity, Figure 5.4 gives an example of an on–ramp configuration satisfying $\Pi < 0$. The blue curve ($\alpha = 0.63$) corresponds to case (A.1).

– Case (A.2): When $\alpha \in [2\Delta - \Phi, 1]$, for any $\beta e \geq 0$, the equilibrium is at $\hat{x}_1^{\mathrm{b}} = \hat{x}_1^{\mathrm{b}\dagger}$. The social delay can be calculated as $J_{\mathrm{soc}}(\hat{x}_1^{\mathrm{b}\dagger})$ and similarly to case (A.1), the social delay will first decrease, reaches optimal at $\beta e = 1$ and then increase with βe increasing.

The pink curve ($\alpha = 0.8$) in Figure 5.4 corresponds to case (A.2).

The shape of the social delay function in case (A.2) can be seen as a whole curve without the stage after $\tilde{\beta}$ in case (A.1). For the on–ramp configurations in case (A), considering all $\alpha \in \mathcal{A}_2$, the equilibrium with the worst case social delay happens at case (A.2). Notice that the function $J_{\mathrm{soc}}(\hat{x}_1^{\mathrm{b}\dagger})$ is a convex quadratic function of $\hat{x}_1^{\mathrm{b}\dagger}$ and $\hat{x}_1^{\mathrm{b}\dagger}$ is an increasing function of βe. Therefore, to minimize the PoA, we let

$$\hat{x}_1^{\mathrm{b}\dagger}(\beta^* e_{\mathrm{U}}) - \Delta = \Delta - \hat{x}_1^{\mathrm{b}\dagger}(\beta^* e_{\mathrm{L}}). \tag{5.24}$$

Thus, we have $\beta^* = \frac{1}{\sqrt{e_{\mathrm{L}} e_{\mathrm{U}}}}$, and $J_{\mathrm{soc}}(\hat{x}_1^{\mathrm{b}\dagger}(\beta^* e_{\mathrm{L}})) = J_{\mathrm{soc}}(\hat{x}_1^{\mathrm{b}\dagger}(\beta^* e_{\mathrm{U}}))$.

• case (B): $\Pi > 0$. In this case, for any $\alpha \in \mathcal{A}_2$, similar to case (A.1), the resulting equilibrium changes from case (d) to case (c) when $\hat{x}_1^{\mathrm{b}\dagger} = \alpha$. As discussed in case (A.1), for the on–ramp configurations in case (B), considering all $\alpha \in \mathcal{A}_2$, the equilibrium with the worst case social delay happens when $\alpha = 1$. Note that $\Pi = \tilde{\beta}(\alpha = 1)$, which is exactly the transition point when $\alpha = 1$. Due to $\Delta < 1$ in $\mathcal{G}$, we always have $\Pi > 1$. The worst social delay function with respect to βe is then a combination of the function $J_{\mathrm{soc}}(\hat{x}_1^{\mathrm{b}\dagger}(\beta e))$ and the constant stage $J_{\mathrm{soc}}(1)$ starting at $\beta e = \Pi$. We thus have to consider two scenarios. Letting $\beta_{gm} = \frac{1}{\sqrt{e_{\mathrm{L}} e_{\mathrm{U}}}}$, if $J_{\mathrm{soc}}(\hat{x}_1^{\mathrm{b}\dagger}(\beta_{gm} e_{\mathrm{L}})) = J_{\mathrm{soc}}(\hat{x}_1^{\mathrm{b}\dagger}(\beta_{gm} e_{\mathrm{U}}))$, then the same as case (A), we have $\beta^* = \beta_{gm}$; if $J_{\mathrm{soc}}(\hat{x}_1^{\mathrm{b}\dagger}(\beta_{gm} e_{\mathrm{L}})) > J_{\mathrm{soc}}(\hat{x}_1^{\mathrm{b}\dagger}(\beta_{gm} e_{\mathrm{U}}))$, then the constant stage has been reached at the upper bound of the error, i.e., $\beta_{gm} e_{\mathrm{U}} > \Pi$. Therefore, we could care less about the upper bound but more about the lower bound. To minimize the worst case social delay, instead of equalizing the social delay on the upper bound and the lower bound, we equalize the social delay of the lower bound and of the transition point Π. Therefore, we let

$$\hat{x}_1^{\mathrm{b}\dagger}(\Pi) - \Delta = \Delta - \hat{x}_1^{\mathrm{b}\dagger}(\beta^* e_{\mathrm{L}}). \tag{5.25}$$

Thus, we have $\beta^* = \frac{1}{e_{\mathrm{L}} \Pi}$.

Summarizing the cases, only when $\beta_{gm} e_{\mathrm{U}} > \Pi$ is satisfied in case (B), i.e., $0 < \Pi < \sqrt{\frac{e_{\mathrm{U}}}{e_{\mathrm{L}}}}$, we have $\beta^* = \frac{1}{e_{\mathrm{L}} \Pi}$; otherwise, we always have $\beta^* = \frac{1}{\sqrt{e_{\mathrm{L}} e_{\mathrm{U}}}}$.   □

According to Theorem 4, when measurements are imperfect, we can configure the altruistic vehicles with the optimal altruism level to minimize the worst case social delay under the uncertainty.

5.5 Summary

In this chapter, we proposed to employ autonomous vehicles as altruistic vehicles among the selfish mainline vehicles to improve the social traffic conditions of the on–ramps. We gave the conditions of the altruistic ratio and altruism level for altruistic vehicles to decrease or optimally decrease the social delay. Further, we assumed uncertainty in the altruistic cost measurements and we gave the optimal altruism level to configure altruistic vehicles which minimizes the worst case social delay under the uncertainty. It is worth noticing that altruism is not limited to autonomous vehicles and in practice, autonomous vehicles can serve as only one of the ways to achieve altruism.

Part III

Headway in Organization

Chapter 6

The Impact of Autonomous Vehicles' Headway on the Social Delay of Traffic Networks

6.1 Overview

Besides the altruistic decision-making discussed in Part II, another key advantage of autonomy is that connected and autonomous vehicles can form vehicle platoons (a fleet of vehicles traveling with a predetermined headway). With fine tuned control, autonomous vehicles in the platoon can preserve a shorter headway at a higher speed compared to human-driven vehicles, and therefore, are able to increase road traffic capacities. Starting from this chapter, we focus on the scenario where autonomous and human-driven vehicles are both selfishly routing on the transportation networks, whereas autonomous vehicles can preserve a shorter headway compared to human-driven vehicles.

In this chapter, we assume that a central authority will be able to dictate a prescribed longitudinal headway for platooning autonomous vehicles on each link(road). We utilize the concept of capacity asymmetry degree for each link, which is the ratio between the link capacity when all vehicles are human-driven and the link capacity when all vehicles are autonomous, to characterize and reflect the predetermined headway of autonomous vehicles on each link. We consider transportation networks where all links share a homogeneous capacity asymmetry degree, and we study the impact of varying the capacity asymmetry degree on the social(overall) delay of the network at the Wardrop routing equilibrium. We prove that, for networks with a single origin–destination (O/D) pair, we can always decrease the social delay by decreasing the capacity asymmetry degree. Specifically, for networks of parallel links with affine delay functions, we provide an upper bound of the social delay improvement brought by autonomous vehicles. However, for networks with multiple O/D pairs, when we decrease the capacity asymmetry degree, i.e., decrease the headway for autonomous vehicle platoons, we may end up worsening the social traffic conditions. We then give an upper

bound for the potential negative impact on social delay of networks with multiple O/D pairs brought by decreasing the headway for autonomous vehicles.

This chapter is organized as follows. In Section 6.2, we introduce the details of the models we employ. In Section 6.3, we study the impact of varying autonomous vehicles' headway on networks with a homogeneous capacity asymmetry degree and a single O/D pair, and deliver core results of this paper. In Section 6.4, we study the impact of varying autonomous vehicles' headway on networks with a homogeneous capacity asymmetry degree and multiple O/D pairs. Finally, in Section 6.5, we summarize the chapter.

6.2 Network, Delay and Routing Models

In this section, we introduce a transportation network model, a travel delay model that characterizes the delay experienced by human–driven and autonomous vehicles and a routing model characterizes the selfish routing of both human–driven and autonomous vehicles.

The Network Model

In this chapter, we use a directed graph $T = (N, L, D)$ to represent the topology of a transportation network, where N indicates the set of nodes and L indicates the set of links. Let D be the set of O/D pairs. For each O/D pair $d \in D$, we employ a set P_d to include all the feasible paths(routes) of the O/D pair. We then let $P = \cup_{d \in D} P_d$ to include all the feasible paths on the transportation network.

Throughout this chapter, we assume that human–driven vehicles (HV) and autonomous vehicles (AV) share the roads of the transportation network. Thus, for each O/D pair $d \in D$, we let R_d represent the total demand of the O/D pair and let $0 \leq \alpha_d \leq 1$ denote the autonomy ratio (the penetration rate of autonomous vehicles) for the O/D pair. Then, the demand of autonomous vehicles for the O/D pair $d \in D$ can be calculated as $R_d \alpha_d$, and the demand of human–driven vehicles for O/D pair d is $R_d(1 - \alpha_d)$. Throughout this chapter, we employ the superscript h to denote HV–related quantities and the superscript a to denote AV–related quantities. Meanwhile, we use lowercase letters to represent link–related quantities and uppercase letters for path–related quantities. To be specific, for each link $l \in L$, we specify f_l to be the total link flow, with f_l^h and f_l^a indicating the HV flow and AV flow on the link respectively. We then vectorize the HV flows on all links by the vector $\mathbf{f}^h$ and vectorize the AV flows on all links by the vector $\mathbf{f}^a$. For each path $p \in P$, we let F_p be the total path flow, with F_p^h and F_p^a indicating the HV flow and AV flow on the path respectively. We also include the HV flows on all paths on the network in the vector $\mathbf{F}^h$ and include the AV flows on all paths in the vector $\mathbf{F}^a$.

The flow of human–driven vehicles follow the flow conservation constraints introduced

by the topology of the transportation network. Thus, we have

$$\sum_{d \in D} \sum_{p \in P_d : l \in p} F_p^h = f_l^h, \ \forall l \in L, \tag{6.1}$$

$$\sum_{p \in P_d} F_p^h = R_d(1 - \alpha_d), \ \forall d \in D. \tag{6.2}$$

The flow conservation constraints also apply to autonomous vehicles:

$$\sum_{d \in D} \sum_{p \in P_d : l \in p} F_p^a = f_l^a, \ \forall l \in L, \tag{6.3}$$

$$\sum_{p \in P_d} F_p^a = R_d \alpha_d, \ \forall d \in D. \tag{6.4}$$

Obviously, the total flow on each link/path equals the sum of HV and AV flow on each link/path:

$$f_l^h + f_l^a = f_l, \quad \forall l \in L, \tag{6.5}$$

$$F_p^h + F_p^a = F_p, \ \forall p \in P. \tag{6.6}$$

Thus, combining Equations (6.2) and (6.4), we have

$$\sum_{p \in P_d} F_p = R_d, \ \forall d \in D. \tag{6.7}$$

The Delay Model

In this chapter, we use the Bureau of Public Roads (BPR) function [62] to quantify the travel delay experienced by vehicles. Let $\tilde{e}_l$ denote the travel delay on link $l \in L$ when all vehicles are human–driven, and then the BPR delay function is expressed as:

$$\tilde{e}_l(f_l^h) = \theta_l + \gamma_l \left(\frac{f_l^h}{m_l^h} \right)^{\beta_l}, \ \forall l \in L, \tag{6.8}$$

where m_l^h is the link capacity when all vehicles are human–driven. For any link $l \in L$, parameters θ_l, γ_l, β_l are non-negative. For link $l \in L$, when $\beta_l = 1$, the link delay function is affine in the link flow.

We assume autonomous vehicles can increase the capacity of the road by maintaining a shorter longitudinal headway compared to human–driven vehicles [63]. For each link $l \in L$, let m_l^a be the link capacity when all vehicles are autonomous. For link $l \in L$, the shorter the headway for autonomous vehicles is, the larger m_l^a is. Thus, for each link $l \in L$, we denote the variable $\mu_l := \frac{m_l^h}{m_l^a}$ to be the link capacity asymmetry degree, which reflects the headway of autonomous vehicles on the link. A centralized control authority can then dictate the

capacity asymmetry degree of the links by prescribing the desired headway for platooning autonomous vehicles on the links. For example, when the headway for human–driven vehicles is fixed, we can decrease the capacity asymmetry degree by commanding the autonomous vehicles maintain a shorter platoon headway. If autonomous vehicles are commanded to maintain the exact same headway as human–driven vehicles, then the capacity asymmetry degree will be exactly 1. In this chapter, we only consider the cases when autonomous vehicles maintain headway shorter than or equal to human–driven vehicles', i.e., we consider the capacity asymmetry degree within the following range:

$$0 < \mu_l \leq 1, \ \forall l \in L. \tag{6.9}$$

In practice, it is impossible to infinitely increase the road capacity considering the physical length of the vehicles and the safe headway. Thus, we normally define a feasible lower bound $\mu_{min} > 0$ for the capacity asymmetry degree. Then we have

$$\mu_{min} \leq \mu_l \leq 1, \ \forall l \in L. \tag{6.10}$$

To incorporate the influence of autonomous vehicles into the delay model, we refer to the results from [63] and [15]. Let e_l denote the travel delay in mixed traffic on link $l \in L$, then the delay of each link $l \in L$ can be calculated as

$$e_l(f_l^h, f_l^a) = \theta_l + \gamma_l \left(\frac{f_l^h}{m_l^h} + \frac{f_l^a}{m_l^a} \right)^{\beta_l}. \tag{6.11}$$

Let E_p denote the delay on path $p \in P$. Naturally, we have

$$\sum_{l \in L : l \in p} e_l = E_p, \ \forall l \in L, \ \forall p \in P. \tag{6.12}$$

In the networks, vehicles traveling along the same path experience the same delay, no matter whether they are human–driven or autonomous. We then define the social delay of the network as

$$J = \sum_{p \in P} F_p E_p. \tag{6.13}$$

The Routing Model

In this chapter, we assume that all vehicles act selfishly, i.e., vehicles only choose the path with the shortest delay among all feasible paths. When drivers select their paths selfishly, the network achieves the well-known Wardrop equilibrium as described in [45]. For two paths $p \in P, q \in P$, we define the notation $p \neq q$ to indicate that the two paths are distinct while joining the same O/D pair. Considering path $p \neq q \in P$, at a Wardrop equilibrium, if path p has longer delay than path q, then all of the vehicles, no matter whether they are

human–driven or autonomous, will take path q instead of path p. Reversely, if path p has shorter delay than path q, then all of the vehicles, no matter whether they are human–driven or autonomous, will take path p instead of path q. Only when path p and path q share the same delay, vehicles may take either of the paths. Thus, we formally define the Wardrop equilbrium for a transportation network with both human–driven and autonomous vehicles:

Definition 7. A path flow vector $(\mathbf{F}^h, \mathbf{F}^a)$ is a Wardrop equilibrium for a network $T = (N, L, D)$ in the mixed traffic, if and only if for any two paths $p \neq q \in P$, we have

$$F_p^h(E_p(\mathbf{F}^h, \mathbf{F}^a) - E_q(\mathbf{F}^h, \mathbf{F}^a)) \leq 0, \tag{6.14a}$$

$$F_p^a(E_p(\mathbf{F}^h, \mathbf{F}^a) - E_q(\mathbf{F}^h, \mathbf{F}^a)) \leq 0, \tag{6.14b}$$

$$F_q^h(E_q(\mathbf{F}^h, \mathbf{F}^a) - E_p(\mathbf{F}^h, \mathbf{F}^a)) \leq 0, \tag{6.14c}$$

$$F_q^a(E_q(\mathbf{F}^h, \mathbf{F}^a) - E_p(\mathbf{F}^h, \mathbf{F}^a)) \leq 0. \tag{6.14d}$$

From the Wardrop conditions (6.14), we easily conclude the following remark, which is helpful in the later derivation of the core results.

Remark 1. At a Wardrop routing equilibrium, for each O/D pair, the feasible paths with nonzero path flow share the same path delay, which is the smallest path delay among all feasible paths for the O/D pair.

In following sections, we investigate the networks where human–driven and autonomous vehicles are selfishly routing with inelastic demands and analyze the impact of reducing autonomous vehicles' headway on the social delay. According to [15], selfish routing of human–driven and autonomous vehicles on networks with heterogeneous capacity asymmetry degrees results in multiple equilibria with distinct equilibrium social delays. Relatively, for transportation networks with a homogeneous capacity asymmetry degree, there may also be multiple distinct equilibria, but all equilibrium states share the same social delay (see Theorem 1 in [15] for more details). Thus, it is reasonable to investigate the impact of capacity asymmetry degree on the social delay only for networks with a homogeneous capacity asymmetry degree. In the rest of this chapter, we discuss within only the category of networks with a homogeneous capacity asymmetry degree.

6.3   Networks with a Single O/D Pair

For the networks with a single O/D pair (with a homogeneous capacity asymmetry degree), the following theorem asserts that reducing the headway for the autonomous vehicles is always instrumental to the social traffic conditions.

Theorem 5. *Given a transportation network $T = (N,L,D)$ with a single O/D pair and a homogeneous capacity asymmetry degree μ, for any fixed demand R and autonomy ratio α, the equilibrium social delay $J(\mu)$ is a continuous and non-decreasing function of μ.*
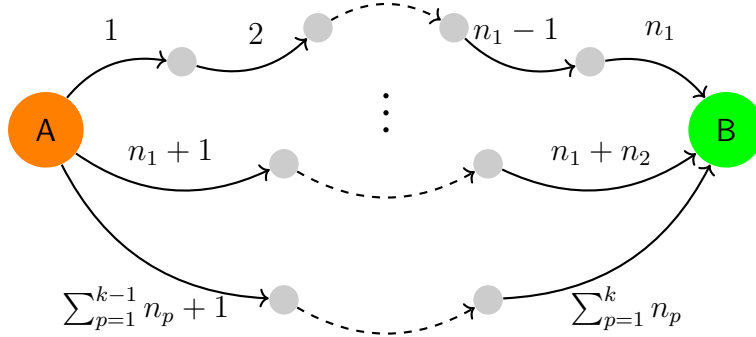
Figure 6.1: A network of parallel links with a single O/D pair from A to B. There are k feasible paths and path p ($p = 1, 2, ..., k$) has n_p links.

Proof. Theorem 5 is a straight forward extension of Theorem 1 in [15], if we regard the autonomy ratio α as fixed and the homogeneous capacity asymmetry degree μ as a variable. See [15] for further details. $\qquad\square$

Networks of parallel links with a single O/D pair

In this subsection, we investigate networks of parallel links with a single O/D pair. Let us consider a general network of parallel links with a single O/D pair shown in Figure 6.1. In the network, there are k feasible paths from the origin node A to the destination node B, thus we have $P = \{1, 2, ..., k\}$. Each path $p \in P$ is composed of n_p sequential links and each link is only used in one path. The link set can be expressed as $L = \{1, 2, ..., \sum_{p=1}^{k} n_p\}$. We also assume that the link delay functions in Equation (6.11) have affine configurations, i.e., $\beta_l = 1$, $\forall l \in L$. We then define some path–related parameters only for a network of parallel links. Let V_p be the freeflow delay on path $p \in P$, i.e.,

$$V_p = \sum_{l \in p} \theta_l, \ \forall p \in P. \tag{6.15}$$

Moreover, for path $p \in P$, we define the positive parameters:

$$W_p = \sum_{l \in p} \frac{\gamma_l}{m_l^h}, \ \forall p \in P. \tag{6.16}$$

Furthermore, to deliver the core result in this subsection, we need to first establish two lemmas of human–driven vehicles' routing on networks of parallel links. When only human–driven vehicles are routing on a network of parallel links, let $S(R)$ be the set of occupied paths at equilibrium when the demand is R. With the demand R known, $S(R)$ can be easily

calculated for networks of parallel links. Let $M(R) := \max\limits_{p \in S(R)} V_p$ to indicate the largest path freeflow cost among all the occupied paths at demand R. We give the following lemmas.

Lemma 3. *Consider a network of parallel links $T = (N, L, D)$ with a single O/D pair. When all vehicles are human–driven and selfishly routing at a demand R, if path $p \in S(R)$, then we have*

$$q \in S(R), \ \forall q : V_q \leq V_p. \tag{6.17}$$

Proof. We prove the lemma by contradiction. Suppose at the equilibrium, there is a path q which subjects to $V_q \leq V_p$, but does not belong to $S(R)$. Then the delay on path q, which is V_q, must be smaller than the delay on the occupied path p, which is larger than the freeflow cost V_p. This contradicts the Wardrop conditions (see Remark 1). $\square$

Lemma 4. *Consider a network of parallel links $T = (N, L, D)$ with a single O/D pair. When all vehicles are human–driven and selfishly routing at the demand R, then $M(R)$ is a non–decreasing function of R.*

Proof. We prove the lemma by contradiction. Suppose for the demand $\tilde{R} > R$, we have $M(\tilde{R}) < M(R)$. If we use path p to refer to the path that subjects to $V_p = M(R)$, then from our assumption and Lemma 3, we have

$$p \in S(R), \tag{6.18}$$

$$p \notin S(\tilde{R}). \tag{6.19}$$

When the demand is R, through Lemma 3, we conclude that $\{q, \ \forall q : V_q \leq V_p\} \subseteq S(R)$. Also we have the equilibrium path delay $\tilde{E}(R)$ that satisfies:

$$\tilde{E}(R) = V_q + W_q F_q^h(R) > V_p, \ \forall q \in S(R). \tag{6.20}$$

When the demand is $\tilde{R}$, through Lemma 3 and our assumption, we conclude that $S(\tilde{R}) \subseteq \{q, \ \forall q : V_q \leq V_p\} \subseteq S(R)$. Also we have the equilibrium delay $\tilde{E}(\tilde{R})$ satisfying:

$$\tilde{E}(\tilde{R}) = V_q + W_q F_q^h(\tilde{R}) \leq V_p, \ \forall q \in S(\tilde{R}). \tag{6.21}$$

Comparing Equation (6.20) and (6.21), we have:

$$V_q + W_q F_q^h(\tilde{R}) < V_q + W_q F_q^h(R), \ \forall q \in S(\tilde{R}). \tag{6.22}$$

Thus, we have

$$F_q^h(\tilde{R}) < F_q^h(R), \ \forall q \in S(\tilde{R}), \tag{6.23}$$

$$\tilde{R} = \sum_{q \in S(\tilde{R})} F_q^h(\tilde{R}) < \sum_{q \in S(\tilde{R})} F_q^h(R) < R. \tag{6.24}$$

Therefore, we have $\tilde{R} < R$, which violates our basic assumption. Note that even though in this proof, we assume delays are affine of the flow, the proof is easily validated for any increasing delay functions. $\square$

Combining Lemma 3 and Lemma 4, we have the following proposition:

Proposition 3. *Consider a network of parallel links $T = (N, L, D)$ with a single O/D pair. Assume all vehicles are human–driven and selfishly routing at a fixed demand. If the demand $\tilde{R} \le R$, we have $S(\tilde{R}) \subseteq S(R)$.*

With the lemmas ready, back to our mixed autonomy context, we consider autonomous vehicles and human–driven vehicles are both selfishly routing on the road network. In the later proofs, we frequently use the following proposition from [15] that gives an equivalent routing equilibrium of human–driven vehicles to the selfish routing equilibrium of the mixed autonomy (see the proof of Theorem 1 in [15] for further details).

Proposition 4. *Consider a transportation network $T = (N,L,D)$ with a single O/D pair and a homogeneous capacity asymmetry degree μ. When autonomous and human–driven vehicles route at a fixed demand R and autonomy ratio α, let $(\mathbf{F}^h, \mathbf{F}^a)$ be an equilibrium path flow vector of the network under the mixed autonomy, and let $E(\mathbf{F}^h, \mathbf{F}^a)$ be the equilibrium path delay under the mixed autonomy. Then $\tilde{\mathbf{F}} := \mathbf{F}^h + \mu\mathbf{F}^a$ is an equilibrium path flow vector of the network when all vehicles are human–driven and route at a demand of $\tilde{R} := R(1 - \alpha) + \mu R\alpha$. Further assuming $\tilde{E}(\tilde{\mathbf{F}})$ is the corresponding equilibrium path delay when all vehicles are human–driven, we have $\tilde{E}(\tilde{\mathbf{F}}) = E(\mathbf{F}^h, \mathbf{F}^a)$.*

Combining Proposition 3 and 4, we propose:

Proposition 5. *Consider that human–driven and autonomous vehicles are selfishly routing at a demand R on a network of parallel links $T = (N, L, D)$ with a single O/D pair and a homogeneous capacity asymmetry degree μ. For a fixed autonomy ratio α and any μ, we have $S(\tilde{R}) \subseteq S(R)$, where $\tilde{R} := R(1 - \alpha) + \mu R\alpha$.*

We then are ready to give the following theorem that bounds the social delay improvement on the network of parallel links by reducing autonomous vehicles' headway.

Theorem 6. *Consider that human–driven and autonomous vehicles are selfishly routing on a network of parallel links $T = (N, L, D)$ with a single O/D pair and a homogeneous capacity asymmetry degree μ. Assume for each link $l \in L$, the delay configuration is affine, i.e., $\beta_l = 1$. For a fixed demand R and an autonomy ratio $\alpha > 0$, with $\hat{J}$ denoting the equilibrium social delay when $\mu = 1$, we have*

$$J(\mu) = \tau(\alpha, \mu)\hat{J}, \tag{6.25}$$

where $1 - \alpha(1 - \mu) \le \tau(\alpha, \mu) \le 1$, if the demand R satisfies:

$$R \sum_{p \in S(R)\setminus\{q\}} \frac{W_q}{W_p} \le \sum_{p \in S(R)} \frac{V_p}{W_p}, \tag{6.26}$$

where $q := \underset{p \in P}{argmin}\ V_p$.

Proof. Assume path $q \in P$ is the path with the smallest freeflow cost. At an equilibrium, according to Lemma 3 and Lemma 4, path q is occupied at all demands. Therefore, recalling Remark 1 and Proposition 4, at a Wardrop equilibrium, for the fixed demand R and any μ, we have:

$$E_p(\mathbf{F}^h, \mathbf{F}^a, \mu) = E_q(\mathbf{F}^h, \mathbf{F}^a, \mu), \ \forall p \in S(\tilde{R}), \tag{6.27}$$

where $\tilde{R} := R(1-\alpha) + \mu R\alpha$. Considering the topology of the network in Figure 6.1, we have

$$\sum_{l \in p} e_l(F_p^h, F_p^a, \mu) = \sum_{l \in q} e_l(F_q^h, F_q^a, \mu), \ \forall p \in S(\tilde{R}). \tag{6.28}$$

From Proposition 4, we have

$$\sum_{l \in p} \tilde{e}_l(\tilde{F}_p) = \sum_{l \in q} \tilde{e}_l(\tilde{F}_q), \ \forall p \in S(\tilde{R}), \tag{6.29}$$

where $\tilde{F}_p := F_p^h + \mu F_p^a, \ \forall p \in P$. Assume an affine delay configuration for all links, together with Equations (6.2) and (6.4), the $k-1$ Equations (6.29) are easily solvable. We then have the solution:

$$\tilde{F}_q(\tilde{R}) = \frac{\tilde{R} - \sum_{p \in S(\tilde{R})\setminus\{q\}} \frac{V_q - V_p}{W_p}}{1 + \sum_{p \in S(\tilde{R})\setminus\{q\}} \frac{W_q}{W_p}}. \tag{6.30}$$

Since delays are affine of the flow, considering the topology of the network, we have

$$E_q(\mathbf{F}^h, \mathbf{F}^a, \mu) = V_q + W_q \tilde{F}_q(\tilde{R}). \tag{6.31}$$

Recalling Remark 1, we can then express the social delay as

$$J(\mu) = RE_q(\mathbf{F}^h, \mathbf{F}^a, \mu). \tag{6.32}$$

Therefore, we have

$$\frac{J(\mu)}{\hat{J}} = \frac{RE_q(\mathbf{F}^h, \mathbf{F}^a, \mu)}{RE_q(\mathbf{F}^h, \mathbf{F}^a, 1)} \tag{6.33}$$

$$= \frac{V_q + W_q \tilde{F}_q(\tilde{R})}{V_q + W_q \tilde{F}_q(R)} \tag{6.34}$$

$$= 1 - \frac{W_q(\tilde{F}_q(R) - \tilde{F}_q(\tilde{R}))}{V_q + W_q \tilde{F}_q(R)} \tag{6.35}$$

$$:= \tau(\alpha, \mu). \tag{6.36}$$

According to Theorem 3 in [91], easily we have that for any $p \in P$, $\tilde{F}_p(R)$ is a non-decreasing function of R. Thus, the increase of the flow on path q cannot exceed the increase of the total demand, and we then have

$$\tilde{F}_q(R) - \tilde{F}_q(\tilde{R}) \leq R - \tilde{R}. \tag{6.37}$$

Thus, we have

$$\tau(\alpha, \mu) \geq 1 - \frac{W_q(R - \tilde{R})}{V_q + W_q \tilde{F}_q(R)} \tag{6.38}$$

$$= 1 - \frac{W_q R}{V_q + W_q \tilde{F}_q(R)} \alpha(1 - \mu). \tag{6.39}$$

Plugging solution (6.30) back into Equation (6.39), as long as condition (6.26) holds, we have $\tau(\alpha, \mu) \geq 1 - \alpha(1 - \mu)$. Due to the positivity of W_p and V_p for any path $p \in P$, for any autonomy ratio $\alpha > 0$ and $0 < \mu \leq 1$, we then have

$$1 - \alpha(1 - \mu) \leq \tau(\alpha, \mu) \leq 1. \tag{6.40}$$

$\square$

Theorem 6 gives a bound of the improvement on the social delay by reducing autonomous vehicles' headway on a network of parallel links. The bound is dependent on both the capacity asymmetry degree and the autonomy ratio. We will discuss the bound in details.

When $\alpha > 0$, the bound $1 - \alpha(1 - \mu)$ is a strictly increasing function of μ and reaches 1 when $\mu = 1$. Therefore, we have $\tau(\alpha, 1) = 1$. Increasing the capacity asymmetry degree μ indicates that autonomous vehicles' headway increases. Therefore, the positive impact of autonomous vehicles on the social delay is compromised. Autonomous vehicles make no difference to the social delay if they increase no road capacity by maintaining the same headway as human–driven vehicles.

When μ is fixed, the bound $1 - \alpha(1 - \mu)$ is a strictly decreasing function of α. When μ approaches 0, the bound $1 - \alpha(1 - \mu)$ approaches $1 - \alpha$. For any $0 < \mu \leq 1$, we have $1 - \alpha < \tau(\alpha, \mu) \leq 1$. With the autonomy ratio increasing, we are able to manipulate more autonomous vehicles and therefore improve the social delay to a better level. In the most extreme scenario, we let all autonomous vehicles "vanish" by assigning them infinite capacity–increasing ability.

As for the sufficient condition (6.26), when only the path with the least freeflow cost is occupied at the demand R, condition (6.26) is always satisfied; for the other cases, the condition can be expressed as $R \leq \frac{\sum_{p \in S(R)} \frac{V_p}{W_p}}{\sum_{p \in S(R) \setminus \{q\}} \frac{W_q}{W_p}}$, the right hand side of which can then be intuitively seen as a weighted sum of *link* capacities when all vehicles are human–driven across the network. Thus, condition (6.26) can be mild considering the topology of networks of parallel links where the demand usually does not exceed the sum of the *path* capacities too
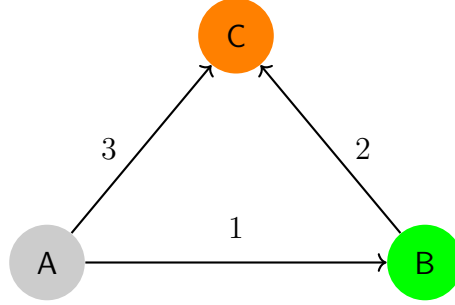
Figure 6.2: A simple network with multiple O/D pairs. Three O/D pairs are (A, C), (A, B) and (B, C). O/D pair (A, C) has two feasible paths, i.e., $P_{(A,C)} = \{\{1, 2\}, \{3\}\}$. The other two O/D pairs have one feasible path each, i.e., $P_{(A,B)} = \{\{1\}\}$ and $P_{(B,C)} = \{\{2\}\}$.

much. After all, Condition (6.26) is a sufficient but not necessary condition. For cases when condition (6.26) is not satisfied, the core result may still hold. As a specific example, we give the following proposition for networks of parallel links with equal freeflow path delays, where the core result holds without any conditions for the demand.

Proposition 6. *Consider a network of parallel links $T = (N, L, D)$ with a single O/D pair and a homogeneous capacity asymmetry degree μ. Assume for each link $l \in L$, the delay configuration is affine, i.e., $\beta_l = 1$ and the freeflow delay for all paths are equal, i.e., $V_p = V_q$, $\forall p, q \in P$. For a fixed demand R and an autonomy ratio $\alpha > 0$, with $\hat{J}$ denoting the equilibrium social delay when $\mu = 1$, we have*

$$J(\mu) = \tau(\alpha, \mu)\hat{J}, \tag{6.41}$$

where $1 - \alpha(1 - \mu) \leq \tau(\alpha, \mu) \leq 1$.

Proof. We simply follow the proof of Theorem 6, whereas we plug solution (6.30) directly into Equation (6.34). Since all path freeflow delays are equal, all paths are employed at any demand, therefore, we always have $S(\tilde{R}) = S(R)$. With slight algebraic transformation, we conclude the result under no conditions.   □

6.4 Networks with Multiple O/D Pairs

For transportation networks with multiple O/D pairs, Theorem 5 does not necessarily hold. Reducing the headway of autonomous vehicles may worsen the social delay for certain cases. A simplest possible example is the same as the example network in [15].

Example 1. Consider the example network in Figure 6.2 with three O/D pairs. Relevant delay parameters are set as $\{\theta_1 = \theta_2 = 0, \theta_3 = 10, \gamma_1 = \gamma_2 = \gamma_3 = \beta_1 = \beta_2 = \beta_3 = 1\}$. The capacity parameters are set as $\{m_1^h = m_2^h = m_3^h = 1\}$. The demands for each O/D pair
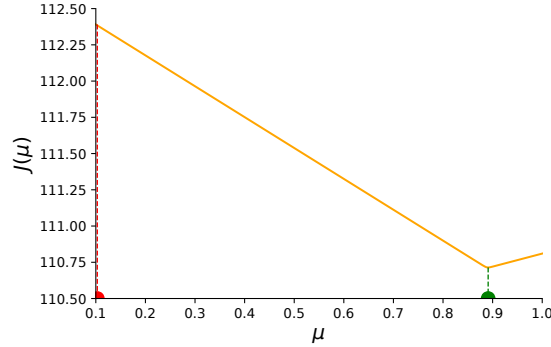
Figure 6.3: The equilibrium social delay $J(\mu)$ is not a monotone increasing function of the homogeneous capacity asymmetry degree μ as we may expect.

are set as $\{R_{(A,B)} = 1, R_{(B,C)} = 10, R_{(A,C)} = 0.9, \alpha_{(A,B)} = 0.9, \alpha_{(B,C)} = 0, \alpha_{(A,C)} = 0\}$. We specify the feasible region of μ in this example as $[0.1, 1]$. The resulting equilibrium social delay is not an increasing function of capacity asymmetry degree as shown in Figure 6.3. The social delay reaches minimum when $\mu = 0.89$ and reaches maximum at $\mu = 0.1$.

Intuitively, for a network with multiple O/D pairs that have shared roads, decreasing the homogeneous capacity asymmetry degree implies improving the capacity–increasing ability of individual autonomous vehicles on each link. However, the actual capacity increase effect on each link is also decided by the autonomous vehicle flow on the link (the number of autonomous vehicles we can manipulate). Considering the topology of the network, the configuration of demands and distinct autonomy ratios for O/D pairs, some links may gain a limited capacity increase effect due to the scarce autonomous flow on the link but receive more selfish vehicles due to the decreased capacity asymmetry degree. Therefore, vehicles traveling along such links would suffer a longer equilibrium delay and the social delay may deteriorate as shown in Example 1.

However, with rapidly developing technologies, the transportation networks will inevitably be shared by human–driven and autonomous vehicles in the near future. Thus we are intrigued to quantify or even bound the potential adverse effect on social delay induced by autonomous vehicles' ability to increase road capacity. We give the following theorem to bound the potential degradation on social delay induced by autonomous vehicles.

Theorem 7. *Consider a transportation network $T = (N, L, W)$ with a homogeneous capacity asymmetry degree. For each O/D pair $w \in W$, let R_w be the fixed demand and $\alpha_w \geq 0$ be the fixed autonomy ratio. (At least for one O/D pair w, $\alpha_w > 0$.) Let $\hat{J}$ be the equilibrium social delay when $\mu = 1$. For any capacity asymmetry degree $0 < \mu \leq 1$, we have*

$$J(\mu) \leq (1 - \lambda(\tilde{e}_l))^{-1} \hat{J}, \tag{6.42}$$

where $0 < \lambda(\tilde{e}_l) < 1$ is a parameter defined for delay functions (6.8).

Proof. The proof of Theorem 7 can be extended from the proof for Theorem 2 in [15].   □

6.5   Summary

In this chapter, we focused on transportation networks of mixed autonomy with a homogeneous capacity asymmetry degree. We have proved that for such networks with a single O/D pair, we can always improve the social traffic conditions by reducing the headway for autonomous vehicles. We also provided an upper bound for the social delay improvement brought by autonomous vehicles on networks of parallel links with affine delay functions. However, for networks with multiple O/D pairs, things become more complex and reducing the headway for autonomous vehicles may worsen social traffic conditions even in simple topology networks.

Chapter 7

Dynamic Routing and Queuing for Mixed Autonomy with Traffic Responsive Intersection Signaling

7.1   Overview

In the previous chapter, we have shown that in mixed autonomy transportation networks where roadways are shared by human–driven and autonomous vehicles, both of which are selfishly routing, it is always possible to decrease the overall or social network delay at equilibrium for series parallel networks with a single origin-destination pair and affine delay functions by reducing autonomous vehicle headway. In this chapter, we continue our discussion in a dynamic context. We also consider the effect of movement–wise vehicle queuing at the intersections in the dynamic routing model and analyze both fixed-time and traffic responsive intersection signalling. For the fixed-time signaling case, we are able to characterize the resulting Wardrop equilibria using an optimization problem with boundary flow constraints. We then analyse the stability of the equilibria via the use of dissipativity analysis tools for population games [66]–[68] and provide stability proofs of the resulting model equilibria for both fixed-time and a movement–wise extension of the P_0 traffic responsive signalling policy introduced in [65]. We also present a simple numerical example to illustrate the derived stability results and the advantage of using the P_0 traffic responsive signal policy over a fixed-time policy.

   The chapter is organized as follows. In Section 7.2, we give detailed descriptions of the routing model, the queuing delay model and the signaling controls we use for mixed autonomy. In Section 7.3, we characterize the resulting Wardrop equilibria under fixed-time signaling. In Section 7.4, we use dissipativity tools for population games to establish the stability of the resulting model equilibria under both fixed-time and responsive signal controls. In Section 7.5, we use a numerical example to testify the stability results. Finally, in Section 7.6, we conclude this chapter.

7.2 Dynamic Routing and Queuing Models

Let V be the origin–destination (O/D) pair set and for each O/D pair $v \in V$, we introduce a set P_v that includes all the feasible paths for the O/D pair. Combining we have $P := \bigcup_{v \in V} P_v$ including all the feasible paths across the network. Let L be the link set and $M \subseteq L \times L$ be the movement set for the network. A movement $(i,j) \in M$ refers to the movement of leaving link i and entering link j, where link $i, j \in L$ are two consecutive links. A path can be seen as a set of consecutive links or consecutive movements. For example, in Figure 7.1, the path containing link $1, 2, 4, 6, 7$ can also be seen as a set of movements $(1,2), (2,4), (4,6), (6,7)$. At the end of each link, there may be multiple movements targeting different downstream links.

Both human-driven and autonomous vehicles are routing under inelastic demands. For O/D pair $v \in V$, let Γ_v^h be the demand of human-driven vehicles for the O/D pair and Γ_v^a be the demand of autonomous vehicles. We then have the demand vector $\mathbf{\Gamma}^h := \left(\Gamma_v^h, v \in V \right)$ and $\mathbf{\Gamma}^a := (\Gamma_v^a, v \in V)$. For each path $i \in P$, we let F_i^h (resp., F_i^a) indicate the human–driven (resp., autonomous) vehicle flow on the path. We then have the path flow vector $\mathbf{F}^h := \left(F_i^h, i \in P \right)$ and $\mathbf{F}^a := (F_i^a, i \in P)$ for human–driven and autonomous vehicles respectively. For each link $i \in L$, we let f_i^h and f_i^a be the human–driven and autonomous vehicle flow on the link respectively. We then have the link flow vector $\mathbf{f}^h := \left(f_i^h, i \in P \right)$ and $\mathbf{f}^a := (f_i^a, i \in P)$ for human–driven and autonomous vehicles respectively. All the flows rates in this chapter are in the same unit of vehicles per unit time. Let $R \in \mathbb{R}^{|P| \times |L|}$ be the link–path transition matrix, where $R_{ij} = 1$ if path i contains link j, otherwise, $R_{ij} = 0$. Let matrix $O \in \mathbb{R}^{|V| \times |P|}$ be the path-O/D-pair transition matrix, where $O_{ij} = 1$ if path j joins OD-pair i and $O_{ij} = 0$ otherwise. According to the law of flow conservation, we have

$$\mathbf{f}^h = R^T \mathbf{F}^h, \qquad \mathbf{f}^a = R^T \mathbf{F}^a, \tag{7.1}$$

$$O\mathbf{F}^h = \mathbf{\Gamma}^h, \qquad O\mathbf{F}^a = \mathbf{\Gamma}^a. \tag{7.2}$$

Since queues may accumulate on certain movements, and not accumulate on others, the accuracy of the model can be much improved by differentiating the queuing effect on different movements. For each movement $(i,j) \in M$, we let $q_{(i,j)}$ be the queuing delay (in units of time) on the movement. We then define the queuing delay vector $\mathbf{q} := \left(q_{(i,j)}, (i,j) \in M \right)$ and an ordering $o : M \mapsto \mathbb{Z}^+$, so that $q_{(i,j)} = \mathbf{q}_l$, where $l = o((i,j))$. Let $Q \in \mathbb{R}^{|P| \times |M|}$ be the movement–path transition matrix, where $Q_{il} = 1$ if path i contains the lth element of the queuing delay vector $\mathbf{q}$, otherwise, $Q_{il} = 0$.

Usually vehicles at the intersections also follow certain signal control policies. Let K be the set of traffic intersections. In one cycle of the signaling at intersection $k \in K$, there are multiple stages, each assigned with a portion of green time. A stage is a set of simultaneous movements. Multiple movements belonging to the same stage share the same green time. For each intersection $k \in K$, we include all the stages at the intersection in the set T_k. Together we have $T := \bigcup_{k \in K} T_k$ including all the stages across the network. Assuming the cycle time
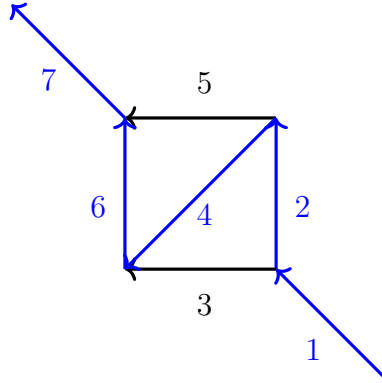
Figure 7.1: An illustration of paths, links and movements. The path containing link $1, 2, 4, 6, 7$ can also be seen as a set of movements $(1, 2), (2, 4), (4, 6), (6, 7)$.

is fixed, let g_i indicate the green ratio for each stage $i \in T$, which is the ratio between the green time allocated to the stage and the cycle time. We collect all the stage green ratios in the vector $\mathbf{g} := (g_i, i \in T)$. The green ratios should satisfy

$$\sum_{i \in T_k} g_i = 1, \ \forall k \in K. \tag{7.3}$$

Let $g_{(i,j)}$ be the green ratio for movement $(i, j) \in M$. If movement (j, m) belongs to stage i, we have

$$g_{(j,m)} = g_i. \tag{7.4}$$

In this section, we assume all intersections are under fixed-time signal controls, i.e., for any stage $i \in T$, the green ratio g_i is a constant. Evidently, for any movement $(i, j) \in M$, the green ratio $g_{(i,j)}$ is a constant.

The dynamic routing model

We consider transportation networks where human–driven vehicles and autonomous vehicles are selfishly routing, i.e., both human–driven and autonomous vehicles revise their paths only to shorten their own path delay. Vehicles traveling along the same path share the same delay no matter whether they are human–driven or autonomous vehicles. However, the participation of autonomous vehicles influences the path delay by increasing road capacities.

Let $\mu \in (0, 1]$ be the homogeneous capacity asymmetry degree, which is defined as the ratio of the link capacity when all vehicles are human–driven to the link capacity when all vehicles are autonomous across the network. When the headway of autonomous vehicles decreases, the capacity asymmetry degree μ decreases. To quantify the impact of autonomous

vehicles, we treat autonomous vehicles as human-driven vehicles with a shorter headway. For
path $i \in P$, we define the effective total vehicle flow on the path to be

$$\tilde{F}_i := F_i^h + \mu F_i^a. \tag{7.5}$$

Similarly, we define the effective total vehicle flow on the link to be

$$\tilde{f}_i := f_i^h + \mu f_i^a. \tag{7.6}$$

Collecting the flows in vectors, we have the effective path flow vector $\tilde{\mathbf{F}} := \left(\tilde{F}_i, i \in P \right)$ and
the effective link flow vector $\tilde{\mathbf{f}} := \left(\tilde{f}_i, i \in P \right)$. According to the flow conservation in (7.1),
we have

$$\tilde{\mathbf{f}} = R^T \tilde{\mathbf{F}}. \tag{7.7}$$

Throughout this chapter, we use the effective flows to explore the system equilibria and
dynamics. For $i \in I$, let $c_i(\cdot)$ be the traversing delay function among the class of volume
delay functions [92] (*e.g.* BPR functions [62]). We can express the traversing delay of link
i for both human–driven and autonomous vehicles as $c_i(\tilde{f}_i)$ in unit time. (see [15] for the
detailed derivation). For path $i \in P$, let d_i refer to the path delay. Aside from the traversing
delay on each link, vehicles traveling along the path may experience an additional queuing
delay on each movement. Thus for each path $i \in P$, we propose

$$d_i = \sum_{j \in L : j \in i} c_j(\tilde{f}_j) + \sum_{(j,m) \in M : (j,m) \in i} q_{(j,m)}. \tag{7.8}$$

where $q_{(i,j)}$ is the queuing delay of movement (i,j), which will be further discussed in section
7.2.

Dynamically within the same O/D pair, vehicles would always transfer to a feasible path
with a shorter delay until a Wardrop equilibrium [45] is reached. The dynamic routing model
for human–driven vehicles has been discussed from a macroscopic viewpoint in [64]. Here
we further explore the model in [64] for human–driven vehicles and extend it to account
for autonomous vehicles. Under inelastic demands, the effective total vehicle flow on each
feasible path satisfies:

$$\dot{\tilde{F}}_i(t) = \sum_{j \in P_v} \Big[\tilde{F}_j(t) \phi_j \left(d_j(t) - d_i(t) \right)$$
$$- \tilde{F}_i(t) \phi_i \left(d_i(t) - d_j(t) \right) \Big], \ i \in P_v, \ v \in V, \tag{7.9}$$

where, as previously defined, $\tilde{F}_i$ is the effective vehicle flow of the path i joining OD pair
$v \in V$, $i \in P_v \subset P$. P_v is the set of all paths joining joining OD pair v, while P is the
set of all feasible paths of the network. The functions ϕ_i for each path $i \in P_v$ are Lipschitz

continuous, non–negative, non–decreasing and satisfy $\phi_i(x) = 0$, when $x \leq 0$. Henceforth, we refer to functions with these properties as **class–$\mathcal{S}$** functions.

Note that according to (7.9), the effective total vehicle flow on the more costly path should decrease while the effective total vehicle flow on a less costly path should increase until the system reaches an equilibrium, if one exists. The magnitude of the flow exchange between two paths is related to the delay difference between the two paths and also the current flow on the path from which vehicles are switching and which is currently experiencing the longer delay. For simplicity and space saving, we omit the time argument t in subsequent equations.

The dynamic queuing model

From the dynamic perspective, the queuing delay in a movement increases when the input flow exceeds the output flow, and decreases when the output flow exceeds the input flow. At an equilibrium, the input flow remains equal to the output flow. For movement $(i, j) \in M$, let $f^h_{(i,j)}$ and $f^a_{(i,j)}$ be the human–driven and autonomous vehicle flow on the movement. Similarly, to quantify autonomous vehicles' impact, for movement $(i, j) \in M$, we define the effective movement flow as

$$\tilde{f}_{(i,j)} := f^h_{(i,j)} + \mu f^a_{(i,j)}. \tag{7.10}$$

Therefore, following [65], we define the variable queue pressure $p^q_{(i,j)}$ to represent the movement's effective input-output flow difference

$$p^q_{(i,j)} = \tilde{f}_{(i,j)} - s^h_{(i,j)} g_{(i,j)}, \ (i,j) \in M, \tag{7.11}$$

where $s^h_{(i,j)}$ is the human-driven vehicle saturation flow rate on movement (i, j) (in vehicles per unit time). Notice that, when $p^q_{(i,j)} > 0$ ($p^q_{(i,j)} < 0$), the movement's queue $q_{(1,j)}$ increases (decreases until it reaches 0), since $s^h_{(i,j)} g_{(i,j)}$ represents the maximum queue discharge rate. Consequently, we utilize the link–wise bottleneck model in [65] and adapt it to account for movement–wise queuing delays.

$$\dot{q}_{(i,j)} = \gamma_{(i,j)} \left(q_{(i,j)} \right) \phi^q_{(i,j)} \left(p^q_{(i,j)} - 0 \right)$$
$$- \psi_{(i,j)} \left(q_{(i,j)} \right) \phi^q_{(i,j)} \left(0 - p^q_{(i,j)} \right), \ \forall (i,j) \in M, \tag{7.12}$$

where for movement $(i, j) \in M$, the function $\phi^q_{(i,j)}$ belongs to **class–$\mathcal{S}$**. The functions $\psi_{(i,j)}$ for each movement $(i, j) \in M$ are Lipschitz continuous, increasing sigmoid functions that satisfy $\psi_{(i,j)}(0) = 0$ to ensure $q_{(i,j)}(t) \geq 0$ for any movement $(i, j) \in M$. The functions $\gamma_{(i,j)} \geq 0$ for each movement $(i, j) \in M$ are Lipschitz continuous, decreasing functions that satisfy $\gamma_{(i,j)}(\bar{q}_{(i,j)}) = 0$, where $\bar{q}_{(i,j)} > 0$ is some estimated maximum queuing delay for movement $(i, j) \in M$. The purpose of function $\gamma_{(i,j)}$ is to theoretically guarantee that $q_{(i,j)}(t) \leq \bar{q}_{(i,j)}$. In practice, $\bar{q}_{(i,j)} > 0$ can be set large enough to reflect the potential congestion scenarios.

7.3 Equilibrium Analysis

In this section, we analyze how the equilibria of mixed autonomy's routing and queuing under fixed-time signalling can be characterized from a static perspective, which facilitates our study of employing responsive signal controls in the dynamic routing and queuing of mixed autonomy.

As studied in [65], we give the following definition of the equilibria of the dynamic routing and queuing system.

Definition 8. A vector of effective flows and queuing delays is an equilibrium of the dynamic routing and queuing system if and only if the following conditions hold:

(a) for any two path $i, j \in P_v$ joining the same O/D pair $v \in V$, if $\tilde{F}_i > 0$, then

$$\sum_{l \in i} c_l(\tilde{f}_l) + \sum_{(l,m) \in i} q_{(l,m)} \leq \sum_{l \in j} c_l(\tilde{f}_l)) + \sum_{(l,m) \in j} q_{(l,m)}, \tag{7.13}$$

(b) for any movement $(l, m) \in M$,

$$q_{(l,m)} > 0 \Rightarrow \tilde{f}_{(l,m)} = s^h_{(l,m)} g_{(l,m)}, \tag{7.14}$$

$$\tilde{f}_{(l,m)} < s^h_{(l,m)} g_{(l,m)} \Rightarrow q_{(l,m)} = 0. \tag{7.15}$$

We define a vector $\tilde{\mathbf{s}} := \{s^h_{(i,j)} g_{(i,j)}, (i,j) \in M\}$, where the movements are listed in the same order o as in $\mathbf{q}$. Similar to the spirit in [93], where the authors considered the routing equilibrium of human-driven vehicles under bounding flow constraints, we present the following proposition:

Proposition 7. *Let $\tilde{\mathbf{F}}^*$ be the optimal solution and $\boldsymbol{\lambda}^+$ be the optimal dual variables for inequalities (7.17) of the following optimization problem:*

$$\min_{\tilde{\mathbf{F}}} \quad \sum_{i \in L} \int_0^{\tilde{f}_i} c_i(x) dx \quad \|_{\tilde{\mathbf{f}} = R^T \tilde{\mathbf{F}}} \tag{7.16}$$

$$s.t. \quad Q^T \tilde{\mathbf{F}} \leq \tilde{\mathbf{s}} \tag{7.17}$$

$$\tilde{\mathbf{F}} \geq \mathbf{0} \tag{7.18}$$

$$O\tilde{\mathbf{F}} = \boldsymbol{\Gamma}^h + \mu \boldsymbol{\Gamma}^a \tag{7.19}$$

Then $(\tilde{\mathbf{F}}^*, \boldsymbol{\lambda}^+)$ are equilibria defined in Definition 8 with $\boldsymbol{\lambda}^+$ regarded as the queuing delay vector.

Proof. Let $\boldsymbol{\lambda}^-$ be the optimal dual variables for inequalities (7.18), and let $\boldsymbol{\nu}$ be the optimal dual variables for equations (7.19). Since the objective function $\sum_{i \in L} \int_0^{\tilde{f}_i} c_i(x) dx \|_{\tilde{\mathbf{f}} = R^T \tilde{\mathbf{F}}}$ is

a convex function of $\tilde{\mathbf{F}}$ and Slater's condition holds, $(\tilde{\mathbf{F}}^*, \boldsymbol{\lambda}^+)$ should satisfy the following Karush–Kuhn–Tucker(KKT) conditions:

$$\lambda_{(l,m)}^+(\tilde{f}_{(l,m)}^* - s_{(l,m)}^h g_{(l,m)}) = 0, \ \forall (l,m) \in M, \tag{7.20}$$

$$\lambda_i^- \tilde{F}_i^* = 0, \ \forall i \in P, \tag{7.21}$$

$$R\mathbf{c}(\tilde{\mathbf{f}}^*) + Q\boldsymbol{\lambda}^+ - \boldsymbol{\lambda}^- + O^T \boldsymbol{\nu} = 0, \tag{7.22}$$

where $\mathbf{c}(\tilde{\mathbf{f}}^*) := (c_i(\tilde{f}_i^*), i \in L)$. Now KKT condition (7.20) is equivalent to conditions (7.14) and (7.15). We therefore need to demonstrate that KKT conditions (7.21) and (7.22) are sufficient for the Nash equilibrium condition (7.13) to complete the proof. For any path i joining O/D pair v, the KKT condition (7.22) yields

$$\sum_{l \in i} c_l(\tilde{f}_l^*) + \sum_{(l,m) \in i} \lambda_{(l,m)}^+ = \lambda_i^- - \nu_v. \tag{7.23}$$

If $\tilde{F}_i^* > 0$, then according to KKT condition (7.21), $\lambda_i^- = 0$. Consider any other path $j \in P_v$, $\lambda_j^- \geq 0$. Considering that

$$\sum_{l \in j} c_l(\tilde{f}_l^*) + \sum_{(l,m) \in j} \lambda_{(l,m)}^+ = \lambda_j^- - \nu_v, \tag{7.24}$$

we have

$$\sum_{l \in i} c_l(\tilde{f}_l^*) + \sum_{(l,m) \in i} \lambda_{(l,m)}^+ \leq \sum_{l \in j} c_l(\tilde{f}_l^*) + \sum_{(l,m) \in j} \lambda_{(l,m)}^+, \tag{7.25}$$

which is equivalent to condition (7.13). $\qquad \square$

7.4   Signaling and Stability Analysis

Fixed-time signalling policies

Consider the case when the signaling control is fixed-time. We now provide the following theorem that establishes the stability convergence of vehicles' routing and queuing under fixed-time signaling to the equilibria calculated in section 7.3.

Theorem 8. *The equilibria of the dynamic model specified by equations (7.9) and (7.12) are globally asymptotically stable.*

Proof. The proof of this theorem is a simplified case of the proof of Theorem 9, which will be presented in section and is omitted due to space constraints. $\qquad \square$

Traffic-responsive signaling policies

Traffic responsive signaling policies have been proposed and implemented as an alternative to fixed-time policies in order to improve mobility. In this section, we will present a traffic responsive policy similar to the ones presented in [7], [8], which balances the queuing of different movements at intersections. Such policies have been shown to reduce queuing delays and guarantee stability of the traffic management system under feasible inelastic demands.

Following [65], for stage $i \in T$, we define the stage's green ratio pressure, p_i^g as

$$p_i^g = \sum_{(j,m) \in M:(j,m) \in i} s_{(j,m)}^h q_{(j,m)}, \ \forall i \in T, \tag{7.26}$$

which indicates the how much increase in throughput can be achieved at the intersection by clearing this stage.

We now introduce the stage version of the P_0 signalling policy proposed in [65]:

$$\dot{g}_i = \sum_{j \in T_k} \left[g_j \phi_i^g \left(p_i^g - p_j^g \right) - g_i \phi_j^g \left(p_j^g - p_i^g \right) \right], \tag{7.27}$$

$$\forall i \in T_k, \ \forall k \in K,$$

where, as previously defined, g_i is the green ratio of the stage, $k \in K$ is the intersection where stage i belongs to and T_k is the set of all stages at intersection k. Thus, $i \in T_k \subset T$. Functions ϕ_i^g belong to **class**–$\mathcal{S}$.

Notice that this policy follows a game theoretic structure where the green ratios are treated as agents that aim to balance the green ratio pressures of all the movements at an intersection, so that no movement has an unduly large queuing delay.

We now analyze the stability of the traffic network equilibria consisting of vehicles' routing flows and intersection movement queues, under the P_0 signalling policy given in (7.27). To do so, we use dissipativity tools [66]–[68] for population games and first investigate the δ–dissipativity of the overall traffic flow and queuing dynamics.

We define the full state vector $\mathbf{y} := \left(\tilde{\mathbf{F}}, \mathbf{q}, \mathbf{g} \right)$ and show δ–dissipativity (defined below) for the subsystems for $\tilde{\mathbf{F}}, \mathbf{q}$ and $\mathbf{g}$ by treating as their inputs the negative path delays, the queue pressures and the green ratio pressures respectively. That is, the inputs are $\tilde{\mathbf{p}} := (-d_i, i \in P)$, $\mathbf{p}^q := \left(p_{(i,j)}^q, (i,j) \in M \right)$ and $\mathbf{p}^g := (p_i^g, i \in T)$, combined into the full input vector $\mathbf{p} := (\tilde{\mathbf{p}}, \mathbf{p}^q, \mathbf{p}^g)$. We rewrite the routing dynamics in equations (7.9) succinctly as $\dot{\tilde{F}}_i := \tilde{\eta}_i(\tilde{\mathbf{F}}, \tilde{\mathbf{p}})$, $i \in P$. Therefore, $\tilde{\eta}(\tilde{\mathbf{F}}, \tilde{\mathbf{p}}) = (\tilde{\eta}_i(\tilde{\mathbf{F}}, \tilde{\mathbf{p}}), \ i \in P)$. Recalling the queuing dynamics in equations (7.12), for $(i,j) \in M$, let $\dot{q}_{(i,j)} := \eta_{(i,j)}^q(\mathbf{q}, \mathbf{p}^q)$. Therefore, $\eta^q(\mathbf{q}, \mathbf{p}^q) = (\eta_{(i,j)}^q(\mathbf{q}, \mathbf{p}^q), \ (i,j) \in M)$. Recalling the signaling dynamics in equations (7.27), for $i \in T$, let $\dot{g}_i := \eta_i^g(\mathbf{g}, \mathbf{p}^g)$. Thus we have $\eta^g(\mathbf{g}, \mathbf{p}^g) = (\eta_i^g(\mathbf{g}, \mathbf{p}^g), \ i \in T)$. We then give the following definition of the δ–dissipativity from [68].

Definition 9. A dynamic model $\dot{\mathbf{x}} = \eta(\mathbf{x}, \mathbf{u})$, with state $\mathbf{x} \in \mathbb{X} \subseteq \mathbb{R}^n$, and input $\mathbf{u} \in \mathbb{R}^n$ is δ–dissipative characterized by $\Pi = \Pi^T \in \mathbb{R}^{2n \times 2n}$ if there exists a continuously differentiable nonnegative storage function $S : \mathbb{X} \times \mathbb{R}^n \mapsto \mathbb{R}_{\geq 0}$ and a nonnegative function $\sigma : \mathbb{X} \times \mathbb{R}^n \mapsto \mathbb{R}_{\geq 0}$ that satisfy the following inequality for all $\mathbf{x} \in \mathbb{X}, \mathbf{u} \in \mathbb{R}^n, \mathbf{r} \in \mathbb{R}^n$:

$$\frac{\partial S(\mathbf{x}, \mathbf{u})}{\partial \mathbf{x}} \eta(\mathbf{x}, \mathbf{u}) + \frac{\partial S(\mathbf{x}, \mathbf{u})}{\partial \mathbf{u}} \mathbf{r} \leq$$
$$- \sigma(\mathbf{x}, \mathbf{u}) + \begin{bmatrix} \eta(\mathbf{x}, \mathbf{u}) \\ \mathbf{r} \end{bmatrix}^T \Pi \begin{bmatrix} \eta(\mathbf{x}, \mathbf{u}) \\ \mathbf{r} \end{bmatrix}, \tag{7.28}$$

where S and σ must satisfy:

$$S(\mathbf{x}, \mathbf{u}) = 0 \iff \eta(\mathbf{x}, \mathbf{u}) = 0, \tag{7.29}$$
$$\sigma(\mathbf{x}, \mathbf{u}) = 0 \iff \eta(\mathbf{x}, \mathbf{u}) = 0. \tag{7.30}$$

With Definition 9, we give the following lemmas to establish the δ–dissipativity of the routing, queuing and signaling dynamics.

Lemma 5. *The dynamic routing model of mixed autonomy specified by equations* (7.9) *is δ–dissipative characterized by* $\tilde{\Pi} = \begin{bmatrix} 0 & \frac{1}{2} I^{|P|} \\ \frac{1}{2} I^{|P|} & 0 \end{bmatrix}$*, with the choice of the functions:*

$$\tilde{S}(\tilde{\mathbf{F}}, \tilde{\mathbf{p}}) := \sum_{v \in V} \sum_{i \in P_v} \sum_{j \in P_v} \tilde{F}_i \int_0^{d_i - d_j} \phi_i(z) d(z), \tag{7.31}$$

$$\tilde{\sigma}(\tilde{\mathbf{F}}, \tilde{\mathbf{p}}) := - \sum_{v \in V} \sum_{i \in P_v} \sum_{j \in P_v} \tilde{\eta}_i(\tilde{\mathbf{F}}, \tilde{\mathbf{p}}) \int_0^{d_i - d_j} \phi_i(z) d(z). \tag{7.32}$$

Proof. For path $i \in P$, let $\tilde{r}_i = \dot{\tilde{p}}_i$. Thus, we have $\tilde{\mathbf{r}} = (\dot{\tilde{p}}_i, i \in P)$. Also note that for any path $i \in P$, we have

$$\left(\frac{\partial \tilde{S}(\tilde{\mathbf{F}}, \tilde{\mathbf{p}})}{\partial \tilde{\mathbf{p}}} \right)_i$$
$$= \sum_{j \in P_v} \left[\tilde{F}_j \phi_j^h (d_j - d_i) - \tilde{F}_i \phi_i (d_i - d_j) \right] \tag{7.33}$$
$$= \tilde{\eta}_i(\tilde{\mathbf{F}}, \tilde{\mathbf{p}}). \tag{7.34}$$

Thus, we have

$$
\frac{\partial \tilde{S}(\tilde{\mathbf{F}}, \tilde{\mathbf{p}})}{\partial \tilde{\mathbf{F}}} \tilde{\eta}(\tilde{\mathbf{F}}, \tilde{\mathbf{p}}) + \frac{\partial \tilde{S}(\tilde{\mathbf{F}}, \tilde{\mathbf{p}})}{\partial \tilde{\mathbf{p}}} \tilde{\mathbf{r}}
$$

$$
= \sum_{v \in V} \sum_{i \in P_v} \sum_{j \in P_v} \tilde{\eta}_i(\tilde{\mathbf{F}}, \tilde{\mathbf{p}}) \int_0^{d_i - d_j} \phi_i(z) d(z)
$$

$$
+ \sum_{v \in V} \sum_{i \in P_v} \tilde{\eta}_i(\tilde{\mathbf{F}}, \tilde{\mathbf{p}}) \tilde{r}_i \tag{7.35}
$$

$$
= -\tilde{\sigma}\left(\tilde{\mathbf{F}}, \tilde{\mathbf{p}}\right) + \begin{bmatrix} \tilde{\eta}(\tilde{\mathbf{F}}, \tilde{\mathbf{p}}) \\ \tilde{\mathbf{r}} \end{bmatrix}^T \tilde{\Pi} \begin{bmatrix} \tilde{\eta}(\tilde{\mathbf{F}}, \tilde{\mathbf{p}}) \\ \tilde{\mathbf{r}} \end{bmatrix}. \tag{7.36}
$$

The nonnegativity of the functions and conditions (7.29) and (7.30) can then be shown. See Remark 4 in [68] for more details. □

Lemma 6. *The dynamic queuing delay model of mixed autonomy specified by equations* (7.12) *is* $\delta-$*dissipative characterized by* $\Pi^q = \begin{bmatrix} 0 & \frac{1}{2} I^{|M|} \\ \frac{1}{2} I^{|M|} & 0 \end{bmatrix}$*, with the choice of the functions:*

$$
S^q(\mathbf{q}, \mathbf{p}^q) := \sum_{(i,j) \in M} \left[\gamma_{(i,j)}\left(q_{(i,j)}\right) \int_0^{p_{(i,j)}^q - 0} \phi_{(i,j)}^q(z) d(z) \right.
$$

$$
\left. + \psi_{(i,j)}\left(q_{(i,j)}\right) \int_0^{0 - p_{(i,j)}^q} \phi_{(i,j)}^q(z) d(z) \right], \tag{7.37}
$$

$$
\sigma^q(\mathbf{q}, \mathbf{p}^q) := - \sum_{(i,j) \in M} \left[\eta_{(i,j)}^q(\mathbf{q}, \mathbf{p}^q) \left(\psi_{(i,j)}'\left(q_{(i,j)}\right) \right. \right.
$$

$$
\int_0^{0 - p_{(i,j)}^q} \phi_{(i,j)}^q(z) d(z)
$$

$$
\left. \left. + \gamma_{(i,j)}'\left(q_{(i,j)}\right) \int_0^{p_{(i,j)}^q - 0} \phi_{(i,j)}^q(z) d(z) \right) \right]. \tag{7.38}
$$

Proof. For movement $(i,j) \in M$, let $r_{(i,j)}^q = \dot{p}_{(i,j)}^q$. Thus, we have $\mathbf{r}^q = (\dot{p}_{(i,j)}^q, (i,j) \in M)$.

Therefore, we have

$$
\frac{\partial S^q(\mathbf{q}, \mathbf{p}^q)}{\partial \mathbf{q}} \eta^q(\mathbf{q}, \mathbf{p}^q) + \frac{\partial S^q(\mathbf{q}, \mathbf{p}^q)}{\partial \mathbf{p}^q} \mathbf{r}^q
$$

$$
= \sum_{(i,j) \in M} \eta^q_{(i,j)}(\mathbf{q}, \mathbf{p}^q) \left(\psi'_{(i,j)}\left(q_{(i,j)}\right) \int_0^{0 - p^q_{(i,j)}} \phi^q_{(i,j)}(z) d(z) \right.
$$

$$
\left. + \gamma'_{(i,j)}\left(q_{(i,j)}\right) \int_0^{p^q_{(i,j)} - 0} \phi^q_{(i,j)}(z) d(z) \right) \tag{7.39}
$$

$$
+ \sum_{(i,j) \in M} r^q_{(i,j)} \left[\gamma_{(i,j)}\left(q_{(i,j)}\right) \phi^q_{(i,j)}\left(p^q_{(i,j)} - 0\right) \right.
$$

$$
\left. - \psi_{(i,j)}\left(q_{(i,j)}\right) \phi^q_{(i,j)}\left(0 - p^q_{(i,j)}\right) \right] \tag{7.40}
$$

$$
= -\sigma^q\left(\mathbf{q}, \mathbf{p}^q\right) + \begin{bmatrix} \eta^q(\mathbf{q}, \mathbf{p}^q) \\ \mathbf{r}^q \end{bmatrix}^T \Pi^q \begin{bmatrix} \eta^q(\mathbf{q}, \mathbf{p}^q) \\ \mathbf{r}^q \end{bmatrix}. \tag{7.41}
$$

Since for any movement $(i, j) \in M$, $\psi_{(i,j)}(\cdot)$ is a sigmoid function, thus we have $\psi'_{(i,j)}(\cdot) > 0$. Also, we have $\gamma'_{(i,j)}(\cdot) < 0$. We can then easily verify the nonnegativity of the functions and that conditions (7.29) and (7.30) hold. $\qquad \square$

Lemma 7. *The dynamic signaling model specified by equations* (7.27) *is* $\delta-$*dissipative characterized by* $\Pi^g = \begin{bmatrix} 0 & \frac{1}{2}I^{|M|} \\ \frac{1}{2}I^{|M|} & 0 \end{bmatrix}$, *with the choice of the functions:*

$$
S^g(\mathbf{g}, \mathbf{p}^g) = \sum_{k \in K} \sum_{i \in T_k} \sum_{j \in T_k} g_i \int_0^{p^g_j - p^g_i} \phi^g_j(z) d(z), \tag{7.42}
$$

$$
\sigma^g(\mathbf{g}, \mathbf{p}^g) := - \sum_{k \in K} \sum_{i \in T_k} \sum_{j \in T_k} \eta^g_i(\mathbf{g}, \mathbf{p}^g) \int_0^{p^g_j - p^g_i} \phi^g_j(z) d(z). \tag{7.43}
$$

The proof for Lemma 7 is analogous to the proof for Lemma 5, thus omitted here. We then are ready to investigate the stability of the model equilibria via dissipativity tools.

Recall equations (7.8), (7.11) and (7.26). The input vectors are functions of the full state vector. We let

$$
\mathbf{p} = \begin{bmatrix} \tilde{\mathbf{p}} \\ \mathbf{p}^q \\ \mathbf{p}^g \end{bmatrix} = \begin{bmatrix} \tilde{H}(\mathbf{y}) \\ H^q(\mathbf{y}) \\ H^g(\mathbf{y}) \end{bmatrix} := H(\mathbf{y}). \tag{7.44}
$$

Generalizing Corollary 1 in [68], we give the following proposition for the global convergence in our setting.

Proposition 8. *The equilibria of the dynamical model described by equations* (7.9), (7.12), (7.27) *is globally asymptotically stable if the following condition holds:*

$$W \frac{\partial H(\mathbf{y})}{\partial \mathbf{y}} + \left(\frac{\partial H(\mathbf{y})}{\partial \mathbf{y}} \right)^T W \leq 0, \ \forall \mathbf{y}, \tag{7.45}$$

where $W = \begin{bmatrix} I^{|P|} & 0 & 0 \\ 0 & w^q I^{|M|} & 0 \\ 0 & 0 & w^g I^{|T|} \end{bmatrix}$, *for some positive scalars* w^q *and* w^g.

We thus give the following theorem:

Theorem 9. *The set of the equilibria of the dynamic model specified by Equations* (7.9), (7.12) *and* (7.27) *is globally asymptotically stable.*

Proof. For the simplicity of future reference, we first define the following matrices.

- Let $G \in \mathbb{R}^{|T| \times |M|}$ be the movement–stage transition matrix, where $G_{ij} = 1$ if stage i contains the jth movement in $\mathbf{q}$, otherwise, $G_{ij} = 0$.

- Let $C \in \mathbb{R}^{|L| \times |L|}$ be a diagonal matrix, where $C_{ii} := \frac{\partial c_i(x)}{\partial x} \geq 0, i \in L$.

- Let $Z \in \mathbb{R}^{|M| \times |M|}$ be a diagonal matrix, on the diagonal of which are the human–driven vehicle saturation rates on each movement in the same order o as in $\mathbf{q}$.

We thus have

$$\frac{\partial \tilde{H}(\mathbf{y})}{\partial \mathbf{y}} = \begin{bmatrix} -RCR^T & -Q & 0 \end{bmatrix}, \tag{7.46}$$

$$\frac{\partial H^q(\mathbf{y})}{\partial \mathbf{y}} = \begin{bmatrix} Q^T & 0 & -ZG^T \end{bmatrix}, \tag{7.47}$$

$$\frac{\partial H^g(\mathbf{y})}{\partial \mathbf{y}} = \begin{bmatrix} 0 & GZ & 0 \end{bmatrix}. \tag{7.48}$$

Combining we then have

$$\frac{\partial H(\mathbf{y})}{\partial \mathbf{y}} = \begin{bmatrix} -RCR^T & -Q & 0 \\ Q^T & 0 & -ZG^T \\ 0 & GZ & 0 \end{bmatrix}. \tag{7.49}$$

Choosing $W = \begin{bmatrix} I^{|P|} & 0 & 0 \\ 0 & I^{|M|} & 0 \\ 0 & 0 & I^{|T|} \end{bmatrix}$, we have

$$W \frac{\partial H(\mathbf{y})}{\partial \mathbf{y}} + \left(\frac{\partial H(\mathbf{y})}{\partial \mathbf{y}} \right)^T W \leq 0. \tag{7.50}$$

According to Proposition 8, we conclude the global asymptotic stability of the resulting equilibria of the model.   □

Theorem 8 and 9 justifies the stability of the model equilibrium points and therefore, the significance to study the properties of the model equilibria from a static perspective as in Section 7.3.

7.5   A Simple Numerical Example

To illustrate the efficacy of the P_0 traffic responsive signaling policy and the overall convergence, we employ a numerical example shown in Figure 7.2.
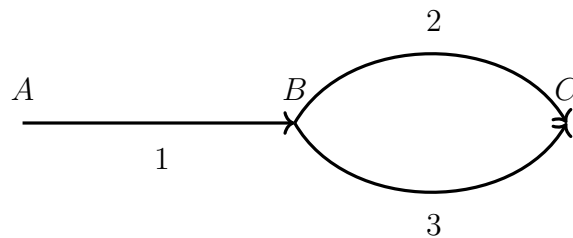
Figure 7.2: A numerical example. All vehicles travel from A to C through one of the two paths. At intersection B, there is a either a fixed-time or a P_0 traffic responsive signalling policy implemented.

In this example, all vehicles including human-driven and autonomous vehicles are traveling from node A to node C. They can travel either on the path containing link 1 and 2 (i.e. movement $(1,2)$) or the path containing link 1 and 3 (i.e. movement $(1,3)$). At intersection B, vehicle flow is regulated by a signalling policy with two stages. The fist stage is for movement $(1,2)$ while the second is for movement $(1,3)$. Therefore, in this example, the movement green ratios are regulated directly.

Since the only O/D pair is from A to C, we omit the subscript for O/D pairs. The relevant model parameters are $\{\Gamma^h = 3, \Gamma^a = 4, \mu = 0.25, s^h_{(1,2)} = 4, s^h_{(1,3)} = 6\}$, and for link $i \in \{1,2,3\}$, we let the traversing delay functions be $c_i(\tilde{f}_i) = \tilde{f}_i$.

We first simulate a fixed-time signalling policy and arbitrarily assign the green time ratios to be $\{g_{(1,2)} = 0.25, g_{(1,3)} = 0.75\}$ (as shown in Figure 7.3). From the simulation, we have that, at the equilibrium, $\{\tilde{f}_{(1,2)} = 1, \tilde{f}_{(1,3)} = 3\}$ and $\{q_{(1,2)} = 2, q_{(1,3)} = 0\}$ (as shown in Figure 7.5). The equilibrium flows and queuing delays can also be obtained by solving the optimization problem in section 7.3, and the solutions are equivalent to the simulation results. Under this fixed-time signalling policy, vehicles queue up on movement $(1,2)$ and induce a considerable queuing delay. At the equilibrium, each vehicle experiences a path delay of 7, and therefore the total network delay is 49.

Secondly, the P_0 traffic responsive signalling policy described by (7.27) is simulated, with initial green time ratios equal to the previously selected fixed time policy ratios. As shown in Figure 7.3), the green ratio for movement $(1,2)$ converges to a larger value, while the green
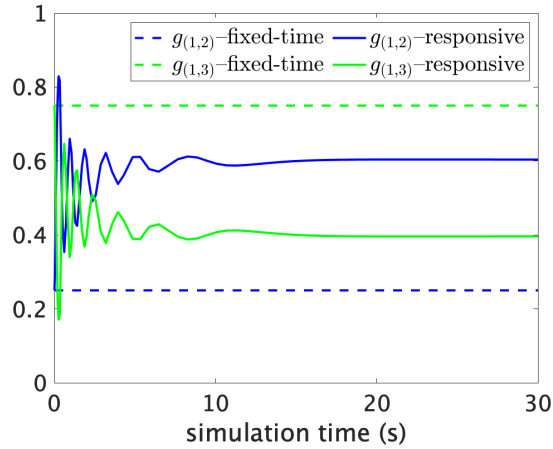
Figure 7.3: Green signalling ratios under fixed-time and traffic responsive signalling policies.

ratio for movement $(1,3)$ decreases correspondingly ($\{g_{(1,2)} = 0.6, g_{(2,3)} = 0.4\}$ to balance out the green pressures at the intersection. As a result, at the equilibrium the previously existing queue is dissipated $\{q_{(1,2)} = 0, q_{(1,3)} = 0\}$ (as shown in Figure 7.5) and the flows converge to $\{\tilde{f}_{(1,2)} = 2, \tilde{f}_{(1,3)} = 2\}$. As a consequence at the equilibrium, each vehicle experiences a path delay of 6, and therefore the total network delay is 42, which is lower than the total network delay under the fixed-time signalling policy. This is a typical example in which the P_0 traffic-responsive signalling policy can tune the allocation of the green time ratios of the different movements to balance the queuing delay of the movements and therefore effectively improve traffic mobility.
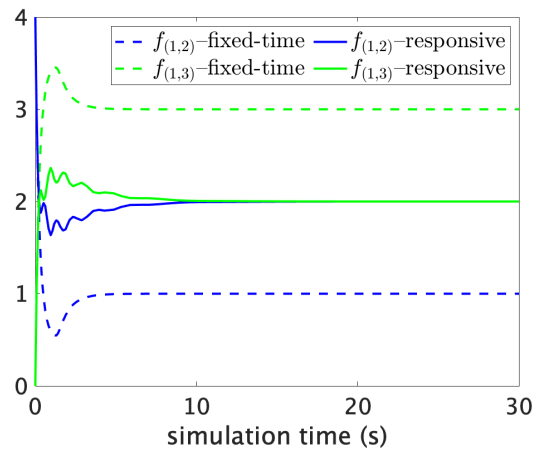
Figure 7.4: Traffic flow responses under fixed-time and traffic responsive signalling policies.
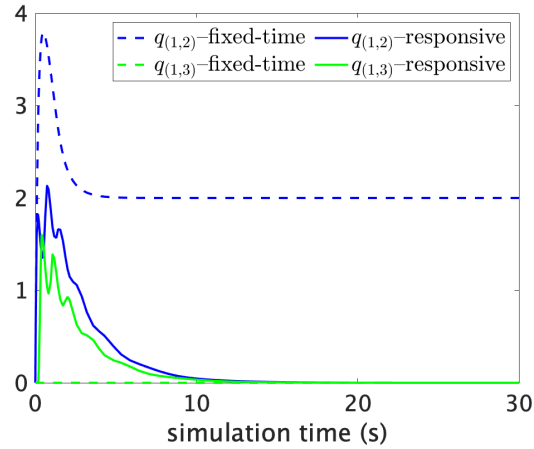
Figure 7.5: Queuing responses under fixed-time and traffic responsive signalling policies.

7.6   Summary

In this chapter, we proposed a continuous–time dynamic routing and queuing model of mixed autonomy (human-driven/autonomous vehicles) with stabilizing signal controls. In the models, autonomous vehicles are configured with a shorter headway compared to human–driven vehicles and therefore, increase the road capacities. We accounted for the capacity–increasing effect of autonomous vehicles on the selfish routing and movement–wise queuing dynamics. We examined the equilibria under fixed-time signal controls from a static perspective and then established the global asymptotic stability of the resulting model equilibria under fixed-time and responsive signal controls via dissipativity tools for population games.

Chapter 8

A Unified Framework for Designing Tolls on Freeways with Autonomous and High-Occupancy Vehicles

8.1 Introduction

As we have discussed in the previous chapters, connected and autonomous vehicles can be formed into platoons with a shorter headway compared to human-driven vehicles, and therefore, increase the traffic throughput. Thus, the corresponding advantages of connected and autonomous vehicles rely heavily on the organization of autonomous vehicles on the roads, such as whether there are dedicated lanes for autonomous vehicle lanes, just as existing dedicated lanes for high-occupancy vehicles. In this chapter, we try to capture the advantage of both dedicated high-occupancy vehicle lanes and dedicated autonomous vehicle lanes. We consider the scenario where four classes of vehicles are sharing a segment of highway: human-driven vehicles with low occupancy, human-driven vehicles with high occupancy, autonomous vehicles with low occupancy and autonomous vehicles with high occupancy. Autonomous vehicles are capable of increasing traffic throughput by preserving a shorter headway than human-driven vehicles. High-occupancy vehicles carry multiple commuters per vehicle and low-occupancy vehicles carry a single commuter per vehicle. We propose a toll lane framework, where on the highway, a toll lane is reserved freely for autonomous vehicles with high occupancy and the other three classes of vehicles can choose to enter the toll lane paying a toll or use the other regular lanes freely. We consider all vehicles to be selfish and only interested in minimizing their own travel costs (the sum of travel delay and the toll cost). We then explore the resulting lane choice equilibria and establish properties of the equilibria, which implicitly compare high-occupancy vehicles with autonomous vehicles in terms of their capabilities to increase the social mobility. We further use numerical examples to clarify the various potential applications of this toll lane framework that unites high-occupancy vehicles and autonomous vehicles in the optimal toll design, the optimal occupancy threshold design
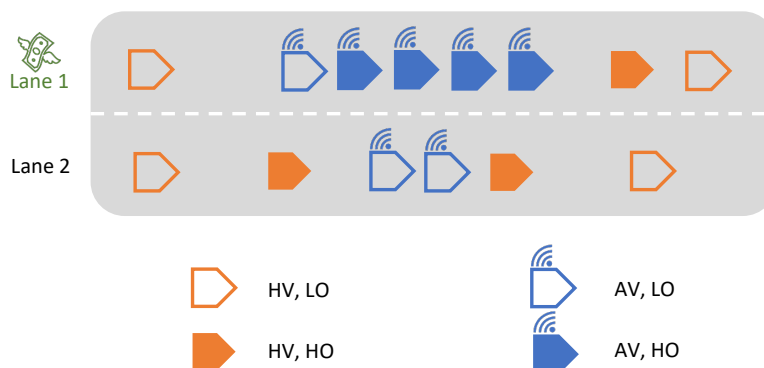
Figure 8.1: Problem setting: all autonomous vehicles with high occupancy travel freely on lane 1, whereas the other three classes of vehicles either pay a toll to travel on lane 1 or travel on lane 2 freely.

and the policy design problems. In order to effectively decrease the total commuter delay, we propose an algorithm that configures various classes of vehicles with differentiated tolls and we examine the potential misbehavior of various classes of vehicles, i.e, vehicles use the toll lane paying a smaller toll than the designed toll, and counter-intuitively find out that lane delays can remain robust to vehicles' misbehavior under certain conditions. To the best of our knowledge, this is the first work that systematically studies a toll lane framework that unites autonomous vehicles and high-occupancy vehicles on the roads.

The chapter is organized as follows. In Section 8.2, we give detailed descriptions of the toll lane framework and vehicles' lane choice model. In Section 8.3, we establish the properties of the resulting lane choice equilibria. In Section 8.4, we clarify how the toll lane framework can be used to find the optimal toll/occupancy threshold/lane policy that minimizes the total commuter delay. In Section 8.5, we propose an efficient method to decrease the total commuter delay by differentiating the tolls. In Section 8.6, we examine the potential misbehavior of vehicles and discuss the impact of vehicles' misbehavior on the total delay of all commuters. Finally, in Section 8.7, we summarize this chapter.

8.2   The Model

Let $\mathcal{I} = \{1, 2\}$ be the lane index set for a segment of highway shown in Figure 8.1, where lane 1 is the reserved toll lane (or toll lanes), and lane 2 is a regular lane (or regular lanes) that can be used by any class of vehicles freely. We consider that four classes of vehicles are sharing the roads: human-driven vehicles with low occupancy (HV,LO), human-driven vehicles with high occupancy (HV,HO), autonomous vehicles with low occupancy (AV,LO) and autonomous vehicles with high occupancy (AV,HO). We denote $\mathcal{P} := \{HV, LO; HV, HO; AV, LO; AV, HO\}$ to be the set of all classes of vehicles. We assume high-occupancy vehicles have $n \geq 2$

commuters per vehicle and low-occupancy vehicles have only one commuter per vehicle.
Throughout this work, we assume the commuter demands are inelastic. Let $d^p \geq 0$, be the
fixed demand of commuters who either individually drive, use or commute in a vehicle of
class $p \in \mathcal{P}$. We collect the **commuter demands** in the vector $\mathbf{d} \in \mathbb{R}_+^4$:

$$\mathbf{d} := \left(d^{\mathrm{HV,LO}},\ d^{\mathrm{HV,HO}},\ d^{\mathrm{AV,LO}},\ d^{\mathrm{AV,HO}} \right). \tag{8.1}$$

Therefore, on the segment of highway, we have $d^{\mathrm{HV,LO}}$ human-driven vehicles with low occu-
pancy, $\frac{d^{\mathrm{HV,HO}}}{n}$ human-driven vehicles with high occupancy, $d^{\mathrm{AV,LO}}$ autonomous vehicles with
low occupancy, and $\frac{d^{\mathrm{AV,HO}}}{n}$ autonomous vehicles with high occupancy.

We also assume in this chapter that autonomous vehicles can preserve a shorter headway
than human-driven vehicles and can therefore increase the commuter capacity of the lanes
that they transit on. To quantify such capability of autonomous vehicles, we will employ the
concept introduced and studied in [15] and [78], the capacity symmetry degree $\mu \in (0,1)$,
which is the ratio between the maximum vehicle density of a lane, when it is only transited
by human-driven vehicles, and the maximum vehicle density of the same lane, when it is only
transited by autonomous vehicles. Thus, the smaller μ, the larger the lane capacity increase
effect in a lane due to autonomous vehicles and, as μ approaches 1, autonomous vehicles will
have almost the same headway as human-driven vehicles and will barely increase the lane
capacity.

In this chapter, we will also use volume-capacity delay models, such as BPR functions [62],
in which the travel delay is a continuous and increasing function of the flow-capacity ratio
and will assume that autonomous vehicles share a uniform and fixed capacity asymmetry
degree μ on both lanes on the highway. Based on these assumptions, we can define δ^p to be
the effective demand for vehicles of class $p \in \mathcal{P}$ and collect them in the **effective vehicle
demands** vector $\boldsymbol{\delta} \in \mathbb{R}_+^4$:

$$\begin{aligned}
\boldsymbol{\delta} &:= (\delta^{\mathrm{HV,LO}}, \delta^{\mathrm{HV,HO}}, \delta^{\mathrm{AV,LO}}, \delta^{\mathrm{AV,HO}}) \\
&= \left(d^{\mathrm{HV,LO}}, \frac{d^{\mathrm{HV,HO}}}{n}, \mu d^{\mathrm{AV,LO}}, \mu \frac{d^{\mathrm{AV,HO}}}{n} \right).
\end{aligned} \tag{8.2}$$

Notice that δ^p describes the substantive impact of the demand of class p vehicles on the traffic
delay at the segment of highway. The ratio between the commuter and the effective vehicle
demand $\nu^p := \frac{d^p}{\delta^p}$ for each class of vehicles $p \in \mathcal{P}$ will be denoted as the **mobility degree**. It
indicates the benefit that high-occupancy, autonomous driving and the combination of both
have in mitigating traffic congestion and enhancing mobility. Consequentially, we have

$$\nu^{\mathrm{HV,LO}} = 1 < \left\{ \nu^{\mathrm{HV,HO}} = n,\ \nu^{\mathrm{AV,LO}} = \frac{1}{\mu} \right\} < \nu^{\mathrm{AV,HO}} = \frac{n}{\mu}. \tag{8.3}$$

Notice that we do not make an a-priori assumption regarding whether the mobility degree of
human driven, high occupancy vehicles is larger than that of autonomous vehicles with low
occupancy (i.e. $\nu^{\mathrm{HV,HO}} > \nu^{\mathrm{AV,LO}}$), or vice-versa, and will consider both cases individually.

Autonomous vehicles with high occupancy (AV,HO) have the largest increased mobility degree and, as a consequence, the best capability to increase the overall capacity of the freeway segment among all four classes of vehicles because they carry multiple commuters per vehicle and maintain a shorter headway than human-driven vehicles. Therefore, we will allow autonomous vehicles with high occupancy (AV,HO) to transit freely (without paying a toll) on lane 1. Moreover, since the concentration of autonomous vehicles increases safety and makes it easier for them to form platoons, we will assume in this chapter that ***all autonomous vehicles with high occupancy (AV,HO) will be exclusively routed on lane 1***. (We will discuss this assumption again in the next section and show that it is a reasonable assumption.) The other three classes of vehicles can then choose to either pay a toll and enter lane 1, or travel freely on lane 2. We therefore will denote

$$\bar{\mathcal{P}} := \{\text{HV}, \text{LO}; \text{HV}, \text{HO}; \text{AV}, \text{LO}\} \subset \mathcal{P} \tag{8.4}$$

to be the set of ***decision making vehicles***, which can either choose to travel freely in lane 2, or pay a toll to travel on lane 1. Notice that we are excluding autonomous vehicles with high occupancy, (AV,HO), from this set, since we assume that they will always travel in lane 1.

Given lane $i \in \mathcal{I}$, we denote f_i^p as the flow of vehicles of class $p \in \bar{\mathcal{P}}$ on that lane. We then define the flow distribution vector $\mathbf{f}$ of decision making vehicles as follows:

$$\begin{aligned}
\mathbf{f} &:= (\mathbf{f}_1, \mathbf{f}_2) \in \mathbb{R}_+^6, \\
\mathbf{f}_1 &:= \left(f_1^{\text{HV,LO}}, \ f_1^{\text{HV,HO}}, \ f_1^{\text{AV,LO}} \right) \in \mathbb{R}_+^3, \\
\mathbf{f}_2 &:= \left(f_2^{\text{HV,LO}}, \ f_2^{\text{HV,HO}}, \ f_2^{\text{AV,LO}} \right) \in \mathbb{R}_+^3.
\end{aligned} \tag{8.5}$$

The elements of the flow distribution vector $\mathbf{f}$ must satisfy:

$$\begin{aligned}
\sum_{i \in \mathcal{I}} f_i^{\text{HV,LO}} &= d^{\text{HV,LO}}, \\
\sum_{i \in \mathcal{I}} f_i^{\text{HV,HO}} &= \frac{d^{\text{HV,HO}}}{n}, \\
\sum_{i \in \mathcal{I}} f_i^{\text{AV,LO}} &= d^{\text{AV,LO}},
\end{aligned} \tag{8.6}$$

$$f_i^{\text{HV,LO}} \geq 0, \ f_i^{\text{HV,HO}} \geq 0, \ f_i^{\text{AV,LO}} \geq 0, \ \forall i \in \mathcal{I}.$$

Notice that we do not treat the flow of autonomous vehicles with high occupancy as a variable, since we are assuming that $f_1^{\text{AV,HO}} = d^{\text{AV,HO}}/n$ always. We now consider the ***effective vehicle flow*** in each lane to account for the substantive impact of autonomous vehicles maintaining a smaller headway than human driven vehicles on the travel delay. For lane $i \in \mathcal{I}$, we denote ϕ_i to be the effective vehicle flow on that lane, specifically, we have

$$\begin{aligned}
\phi_1 &:= f_1^{\text{HV,LO}} + f_1^{\text{HV,HO}} + \mu f_1^{\text{AV,LO}} + \delta^{\text{AV,HO}}, \\
\phi_2 &:= f_2^{\text{HV,LO}} + f_2^{\text{HV,HO}} + \mu f_2^{\text{AV,LO}}.
\end{aligned} \tag{8.7}$$

Naturally, we have

$$\phi_1 + \phi_2 = \sum_{p \in \mathcal{P}} \delta^p. \tag{8.8}$$

Also, the effective flows are bounded as follows:

$$\phi_1 \in \left[\delta^{\text{AV,HO}}, \sum_{p \in \mathcal{P}} \delta^p\right] \quad \text{and} \quad \phi_2 \in \left[0, \sum_{p \in \mathcal{P}} \delta^p - \delta^{\text{AV,HO}}\right], \tag{8.9}$$

where the effective vehicle demand vector $\boldsymbol{\delta}$ and its components were defined in Eq.(8.2).

   We assume that all vehicles behave selfishly by always choosing the lane that minimizes their travel cost (except for autonomous high occupancy vehicles, which are all exclusively routed on lane 1). The travel cost takes into account the travel delay and any toll expense that exists. We first assume that a uniform toll price $\tau > 0$ is charged to low occupancy autonomous vehicles and all human driven vehicles that choose to travel on lane 1, while no toll is assigned to vehicles traveling on lane 2. Thus, for lane 1, the travel cost equals the sum of the travel delay in that lane and the toll, whereas for lane 2, the travel cost is equal to the travel delay. For lane $i \in \mathcal{I}$, we denote C_i as the travel cost, and D_i as the travel delay. Recall that in this chapter, we use volume-capacity delay models, such as BPR functions [62], in which the travel delay on lane i, D_i is a continuous and increasing function of the effective vehicle flow ϕ_i. We then have

$$C_1(\mathbf{f}) = D_1(\phi_1) + \tau,$$
$$C_2(\mathbf{f}) = D_2(\phi_2). \tag{8.10}$$

   Let the tuple $G = (\mathbf{D}, \mathbf{d}, \tau, n, \mu)$ represent a segment of highway shown in Figure 8.1 with the delay models $\mathbf{D} := (D_i, i \in \mathcal{I} = \{1, 2\})$, commuter demands $\mathbf{d}$, a uniform toll price τ, an occupancy threshold n for high-occupancy vehicles and a capacity asymmetry degree μ for autonomous vehicles. The selfish lane choice equilibrium of the three classes of vehicles can then be modeled as a Wardrop equilibrium [45] as shown below.

Definition 10. For a segment of highway $G = (\mathbf{D}, \mathbf{d}, \tau, n, \mu)$, a feasible flow distribution vector $\mathbf{f}$ is a lane choice equilibrium if and only if for any vehicle class $p \in \bar{\mathcal{P}}$, we have

$$f_1^p(C_1(\mathbf{f}) - C_2(\mathbf{f})) \leq 0, \tag{8.11a}$$
$$f_2^p(C_2(\mathbf{f}) - C_1(\mathbf{f})) \leq 0. \tag{8.11b}$$

The definition presents sufficient and necessary conditions for the choice equilibrium. Specifically, at the choice equilibrium, if the travel cost of lane 1 is higher than the travel cost of lane 2, then all of the three classes of vehicles would travel on lane 2; if the travel cost of lane 1 is lower than the travel cost of lane 2, then all of the three classes of vehicles would choose to pay the toll and travel on lane 1; if the travel cost of lane 1 is equal to the travel

cost of lane 2, then any vehicle of the three classes of vehicles could travel either on lane 1 or on lane 2. Reasoning reversely, if any of the three classes of vehicles are on lane 1, then the travel cost of lane 1 cannot be higher than the cost of lane 2; if any of the three classes of vehicles are on lane 2, then the travel cost of lane 2 cannot be higher than the cost of lane 1; if the any class of vehicles use both lane 1 and lane 2, then the travel cost of lane 1 and lane 2 must be equal.

A selfish lane choice equilibrium described in Definition 10 is usually not socially optimal. The metric we use in this framework to evaluate the social mobility is the total delay of all commuters, which can be calculated as follows:

$$
J(\mathbf{f}) = \left[f_1^{\mathrm{HV,LO}} + f_1^{\mathrm{AV,LO}} + n \left(f_1^{\mathrm{HV,HO}} + \frac{d^{\mathrm{AV,HO}}}{n} \right) \right] D_1(\phi_1)
$$
$$
+ \left(f_2^{\mathrm{HV,LO}} + f_2^{\mathrm{AV,LO}} + n f_2^{\mathrm{HV,HO}} \right) D_2(\phi_2). \tag{8.12}
$$

8.3   Equilibrium Properties

In this section, we establish crucial properties of the resulting lane choice equilibria under the framework described in Definition 10. According to the core theorem in [82], we give the following proposition without proof.

Proposition 9. *For a segment of highway $G = (\mathbf{D}, \mathbf{d}, \tau, n, \mu)$, there always exists at least one lane choice equilibrium as described in Definition 10.*

The next theorem states that the resulting lane choice equilibrium is generally only unique if at the equilibrium, all of the three classes of vehicles simultaneously choose to travel on the same lane or there is simply one homogeneous class of vehicles making the lane choices.

Theorem 10. *For a segment of highway $G = (\mathbf{D}, \mathbf{d}, \tau, n, \mu)$, the lane choice equilibrium as described in Definition 10 is unique if and only if at least one of the following conditions hold:*

1) $\tau \geq D_2 \left(\sum_{p \in \mathcal{P}} \delta^p - \delta^{\mathrm{AV,HO}} \right) - D_1 \left(\delta^{\mathrm{AV,HO}} \right),$

2) $\tau \leq D_2 (0) - D_1 \left(\sum_{p \in \mathcal{P}} \delta^p \right).$

3) *At most one class of vehicles $p \in \bar{\mathcal{P}}$ has a positive commuter demand, i.e., $d^p > 0$.*

Proof. The travel cost on lane 1, $C_1(\mathbf{f})$ is a continuous, increasing function of ϕ_1, and therefore can be written as a function of the lane 1's effective flow ϕ_1, $C_1(\phi_1)$. Similarly, $C_2(\mathbf{f})$ is a continuous, increasing function of ϕ_2. According to Equation (8.8), with slight abuse of notation, we can also treat the travel cost on lane 2, $C_2(\mathbf{f})$ as a continuous, decreasing function of the lane 1's effective flow ϕ_1, written as $C_2(\phi_1)$. Three possible sketches of $C_1(\phi_1)$ and $C_2(\phi_1)$ for $\phi_1 \in [\delta^{\mathrm{AV,HO}}, \sum_{p \in \mathcal{P}} \delta^p]$ are shown in Figure 8.2. In case (a), $C_1(\phi_1) \geq C_2(\phi_1)$
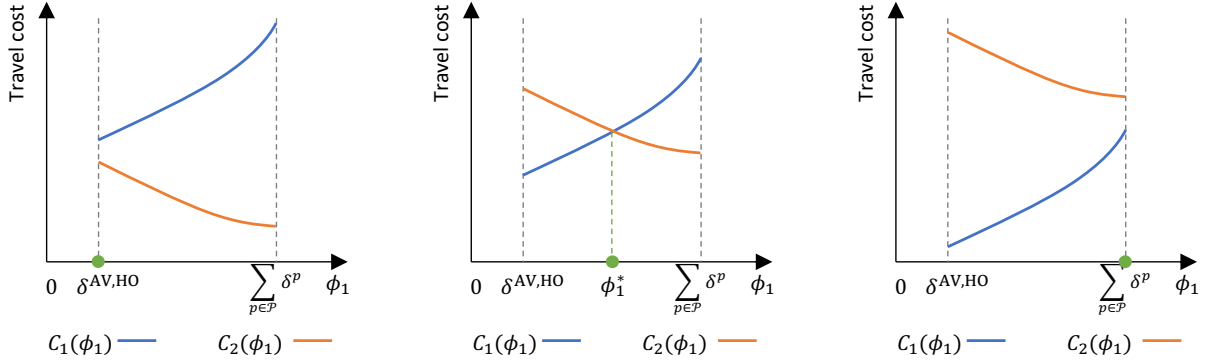
(a) $C_1(\phi_1) \geq C_2(\phi_1)$, $\forall \phi_1 \in [\delta^{\text{AV,HO}}, \sum_{p \in \mathcal{P}} \delta^p]$.

(b) $C_1(\phi_1)$ and $C_2(\phi_1)$ intersect at $\phi_1^* \in (\delta^{\text{AV,HO}}, \sum_{p \in \mathcal{P}} \delta^p)$.

(c) $C_1(\phi_1) \leq C_2(\phi_1)$, $\forall \phi_1 \in [\delta^{\text{AV,HO}}, \sum_{p \in \mathcal{P}} \delta^p]$.

Figure 8.2: Possible sketches of the travel cost on both lanes. Resulting lane choice equilibria are indicated by the green dots. Non-unique equilibria only exist in case (b).

for any possible $\phi_1 \in [\delta^{\text{AV,HO}}, \sum_{p \in \mathcal{P}} \delta^p]$, thus all of the three classes of vehicles would use lane 2, and the lane choice equilibrium is unique at $\mathbf{f}_1 = (0, 0, 0)$. In case (c), $C_1(\phi_1) \leq C_2(\phi_1)$ for any possible $\phi_1 \in [\delta^{\text{AV,HO}}, \sum_{p \in \mathcal{P}} \delta^p]$, thus all of the three classes of vehicles would use lane 1, and the lane choice equilibrium is unique at $\mathbf{f}_1 = \left(d^{\text{HV,LO}}, \frac{d^{\text{HV,HO}}}{n}, d^{\text{AV,LO}}\right)$.

In case (b), the resulting lane choice equilibria are in general not unique. Possible lane choice equilibria in case (b) that satisfy Definition 10 must satisfy

$$C_1(\phi_1^*) = C_2(\phi_1^*), \tag{8.13}$$

where $\phi_1^* \in (\delta^{\text{AV,HO}}, \sum_{p \in \mathcal{P}} \delta^p)$ is the value of ϕ_1 at the equilibria, which can be solved by a golden-section search algorithm given the highway tuple G. Thus according to Equation (8.7), the resulting equilibria must satisfy

$$
\begin{aligned}
f_1^{\text{HV,LO}} + f_1^{\text{HV,HO}} + \mu f_1^{\text{AV,LO}} &= \phi_1^* - \delta^{\text{AV,HO}}, \\
f_2^{\text{HV,LO}} + f_2^{\text{HV,HO}} + \mu f_2^{\text{AV,LO}} &= \sum_{p \in \mathcal{P}} \delta^p - \phi_1^*.
\end{aligned}
\tag{8.14}
$$

All resulting equilibria should also satisfy the feasibility conditions. Therefore, the resulting equilibria lie in a simplex $\mathcal{S} \subset \mathbb{R}_+^6$ which can be characterized as

$$\mathcal{S} := \{\mathbf{f} \in \mathbb{R}_+^6 : \mathbf{f} \text{ satisfies } (8.14) \text{ and } (8.6)\}. \tag{8.15}$$

If there are at least two classes of vehicles $p \in \bar{\mathcal{P}}$ that possess a positive commuter demand, i.e., $d^p > 0$, $\mathcal{S}$ contains at least two distinct equilibria.   □

As described in the proof of Theorem 10, for a segment of highway $G = (\mathbf{D}, \mathbf{d}, \tau, n, \mu)$, the resulting lane choice equilibrium is generally only unique if the toll is either too large or too small so that all three classes of vehicles (HV,LO/HV,HO/AV,LO) choose the same lane. Otherwise, we can characterize the lane choice equilibria by the simplex $\mathcal{S}$ in Equation (8.15), and notice that the simplex $\mathcal{S}$ can be fully characterized by the highway segment tuple G.

However, the total commuter delay at the equilibrium can be ambiguous if there are multiple equilibria. Therefore, in this chapter, we mainly study the multiple equilibria in the simplex $\mathcal{S}$ and in the following theorem we will characterize the multiple equilibria in the simplex $\mathcal{S}$ that respectively yield the *largest* and *lowest* total commuter delays. This will be helpful for future analysis. Also notice that, at the equilibria in the simplex $\mathcal{S}$, according to Equation (8.13), where $\tau > 0$, the travel delay on lane 1 is strictly smaller than the travel delay on lane 2. Therefore, all AV,HOs will naturally accumulate on lane 1 even if we don't deliberately route them.

Theorem 11. *For a segment of highway $G = (\mathbf{D}, \mathbf{d}, \tau, n, \mu)$ with non-unique lane choice equilibria as described in Definition 10, let $\mathbf{f}^+ \in \mathcal{S}$ be the worst-case equilibrium with the highest total commuter delay, i.e.,*

$$J(\mathbf{f}) \leq J(\mathbf{f}^+), \ \forall \mathbf{f} \in \mathcal{S}, \tag{8.16}$$

and let $\mathbf{f}^- \in \mathcal{S}$ be the best-case equilibrium with the lowest total commuter delay, i.e.,

$$J(\mathbf{f}) \geq J(\mathbf{f}^-), \ \forall \mathbf{f} \in \mathcal{S}, \tag{8.17}$$

where $\mathbf{f}$, as defined in Eq. (8.5), is any equilibrium flow, $J(\mathbf{f})$ is given by Eq. (8.12) and the simplex $\mathcal{S}$ is defined in Eq. (8.15).

1) *If $n > \frac{1}{\mu}$, i.e., the required number of passengers for a vehicle to qualify as high-occupancy is larger than the inverse of the capacity asymmetry degree of autonomous vehicles and, as a consequence, human-driven vehicles with high-occupancy (HV,HO) have a larger mobility degree than autonomous vehicles with low occupancy (AV,LO), i.e., $\nu^{\mathrm{HV,HO}} > \nu^{\mathrm{AV,LO}}$, we have*

$$\mathbf{f}_1^+ = \left(\max_{\mathbf{f} \in \mathcal{S}} f_1^{\mathrm{HV,LO}}, \ \min_{\mathbf{f} \in \mathcal{S}} f_1^{\mathrm{HV,HO}}, \ * \right), \tag{8.18a}$$

$$\mathbf{f}_1^- = \left(\min_{\mathbf{f} \in \mathcal{S}} f_1^{\mathrm{HV,LO}}, \ \max_{\mathbf{f} \in \mathcal{S}} f_1^{\mathrm{HV,HO}}, \ * \right). \tag{8.18b}$$

2) *Conversely, if $n < \frac{1}{\mu}$ and, as a consequence, $\nu^{\mathrm{HV,HO}} < \nu^{\mathrm{AV,LO}}$, we have*

$$\mathbf{f}_1^+ = \left(\max_{\mathbf{f} \in \mathcal{S}} f_1^{\mathrm{HV,LO}}, \ *, \ \min_{\mathbf{f} \in \mathcal{S}} f_1^{\mathrm{AV,LO}} \right), \tag{8.19a}$$

$$\mathbf{f}_1^- = \left(\min_{\mathbf{f} \in \mathcal{S}} f_1^{\mathrm{HV,LO}}, \ *, \ \max_{\mathbf{f} \in \mathcal{S}} f_1^{\mathrm{AV,LO}} \right). \tag{8.19b}$$

3) *Finally, if* $n = \frac{1}{\mu}$ *and, as a consequence,* $\nu^{HV,HO} = \nu^{AV,LO}$, *we have*

$$\mathbf{f}_1^+ = \left(\max_{\mathbf{f} \in \mathcal{S}} f_1^{HV,LO}, \; *, \; * \right), \tag{8.20a}$$

$$\mathbf{f}_1^- = \left(\min_{\mathbf{f} \in \mathcal{S}} f_1^{HV,LO}, \; *, \; * \right). \tag{8.20b}$$

Notice that $*$ *in the above equations indicates that the quantity can be any value that fulfills that* $\mathbf{f}^+ \in \mathcal{S}$ *and* $\mathbf{f}^- \in \mathcal{S}$, *where* $\mathcal{S}$ *is defined in Eq.* (8.15).

Theorem 11 explicitly compares the capabilities of AV,LO and HV,HO to decrease the total commuter delay. When $\nu^{HV,HO} > \nu^{AV,LO}$, HV,HO are more capable than AV,LO in decreasing total commuter delay. Therefore, among the multiple equilibria, the best-case equilibrium that minimizes the total commuter delay happens when we prioritize high-occupancy vehicles instead of autonomous vehicles on the toll lane 1. Conversely, when $\nu^{HV,HO} < \nu^{AV,LO}$, HV,HO are less capable than AV,LO in decreasing total commuter delay, and therefore, among the multiple equilibria, the best-case equilibrium that minimizes total commuter delay happens when we prioritize autonomous vehicles with low occupancy instead of high-occupancy vehicles on the toll lane 1. In all cases, the vehicles that take the most space per commuter are HV,LO, whch have the smallest mobility degree $\nu^{HV,LO} = 1$. Thus the worst-case equilibria that maximize total commuter delay happen when we prioritize HV,LO on toll lane 1.

Proof. We will only provide a detailed derivation for $\mathbf{f}^+$ in Eq. (8.18a), when $n > \frac{1}{\mu}$. Similar calculations can be used to prove the other results in the theorem, and are omitted due to space constraints.

Assume that $n > \frac{1}{\mu}$, $\mathbf{f} = (\mathbf{f}_1, \mathbf{f}_2) \in \mathcal{S}$, $\mathbf{f}^+ = \left(\mathbf{f}_1^+, \mathbf{f}_2^+ \right) \in \mathcal{S}$ and $\mathbf{f} \neq \mathbf{f}^+$. Let

$$\mathbf{f}_1^+ = \left(\max_{\mathbf{f} \in \mathcal{S}} f_1^{HV,LO}, \; \min_{\mathbf{f} \in \mathcal{S}} f_1^{HV,HO}, \; f_1^{+AV,LO} \right) \text{ and } \mathbf{f}_2^+ = \left(f_2^{+HV,LO}, \; f_2^{+HV,HO}, \; f_2^{+AV,LO} \right).$$

From Eq. (8.12) we have

$$
\begin{aligned}
J(\mathbf{f}) - J(\mathbf{f}^+) \;=\; & \left[f_1^{HV,LO} + f_1^{AV,LO} + n f_1^{HV,HO} \right] D_1(\phi_1^*) + \left(f_2^{HV,LO} + f_2^{AV,LO} + n f_2^{HV,HO} \right) D_2(\phi_2^*) \\
& - \left[\max_{\mathbf{f} \in \mathcal{S}} f_1^{HV,LO} + f_1^{+AV,LO} + n \min_{\mathbf{f} \in \mathcal{S}} f_1^{HV,HO} \right] D_1(\phi_1^*) \\
& - \left(f_2^{+HV,LO} + f_2^{+AV,LO} + n f_2^{+HV,HO} \right) D_2(\phi_2^*).
\end{aligned}
\tag{8.21}
$$

Since both $\mathbf{f}$ and $\mathbf{f}^+$ satisfy Equation (8.14), we have

$$
\begin{aligned}
f_1^{AV,LO} - f_1^{+AV,LO} \;&=\; \frac{1}{\mu} \left[\left(\max_{\mathbf{f} \in \mathcal{S}} f_1^{HV,LO} - f_1^{HV,LO} \right) + \left(\min_{\mathbf{f} \in \mathcal{S}} f_1^{HV,HO} - f_1^{HV,HO} \right) \right], \\
f_2^{AV,LO} - f_2^{+AV,LO} \;&=\; \frac{1}{\mu} \left[\left(f_2^{+HV,LO} - f_2^{HV,LO} \right) + \left(f_2^{+HV,HO} - f_2^{HV,HO} \right) \right].
\end{aligned}
$$

Furthermore, from Eqs. (8.6), we have

$$
\begin{aligned}
f_2^{\text{HV,LO}} - f_2^{+\text{HV,LO}} &= \max_{\mathbf{f} \in \mathcal{S}} f_1^{\text{HV,LO}} - f_1^{\text{HV,LO}}, \\
f_2^{\text{HV,HO}} - f_2^{+\text{HV,HO}} &= \min_{\mathbf{f} \in \mathcal{S}} f_1^{\text{HV,HO}} - f_1^{\text{HV,HO}}.
\end{aligned}
$$

Therefore,

$$
\begin{aligned}
&J\left(\mathbf{f}\right) - J\left(\mathbf{f}^+\right) \\
&= \left[f_1^{\text{HV,LO}} - \max_{\mathbf{f} \in \mathcal{S}} f_1^{\text{HV,LO}} - \frac{1}{\mu}\left(f_1^{\text{HV,LO}} - \max_{\mathbf{f} \in \mathcal{S}} f_1^{\text{HV,LO}} + f_1^{\text{HV,HO}} - \min_{\mathbf{f} \in \mathcal{S}} f_1^{\text{HV,HO}} \right) \right.\\
&\quad \left. + n\left(f_1^{\text{HV,HO}} - \min_{\mathbf{f} \in \mathcal{S}} f_1^{\text{HV,HO}} \right) \right] D_1\left(\phi_1^*\right) \\
&\quad - \left[f_1^{\text{HV,LO}} - \max_{\mathbf{f} \in \mathcal{S}} f_1^{\text{HV,LO}} - \frac{1}{\mu}\left(f_1^{\text{HV,LO}} - \max_{\mathbf{f} \in \mathcal{S}} f_1^{\text{HV,LO}} + f_1^{\text{HV,HO}} - \min_{\mathbf{f} \in \mathcal{S}} f_1^{\text{HV,HO}} \right) \right.\\
&\quad \left. + n\left(f_1^{\text{HV,HO}} - \min_{\mathbf{f} \in \mathcal{S}} f_1^{\text{HV,HO}} \right) \right] D_2\left(\sum_{p \in \mathcal{P}} \delta^p - \phi_1^* \right) \qquad (8.22) \\
&= \left[f_1^{\text{HV,LO}} - \max_{\mathbf{f} \in \mathcal{S}} f_1^{\text{HV,LO}} - \frac{1}{\mu}\left(f_1^{\text{HV,LO}} - \max_{\mathbf{f} \in \mathcal{S}} f_1^{\text{HV,LO}} + f_1^{\text{HV,HO}} - \min_{\mathbf{f} \in \mathcal{S}} f_1^{\text{HV,HO}} \right) \right.\\
&\quad \left. + n\left(f_1^{\text{HV,HO}} - \min_{\mathbf{f} \in \mathcal{S}} f_1^{\text{HV,HO}} \right) \right] \left(D_1\left(\phi_1^*\right) - D_2\left(\sum_{p \in \mathcal{P}} \delta^p - \phi_1^* \right) \right) \qquad (8.23) \\
&= \left[\left(1 - \frac{1}{\mu}\right)\left(f_1^{\text{HV,LO}} - \max_{\mathbf{f} \in \mathcal{S}} f_1^{\text{HV,LO}} \right) \right.\\
&\quad \left. + \left(n - \frac{1}{\mu}\right)\left(f_1^{\text{HV,HO}} - \min_{\mathbf{f} \in \mathcal{S}} f_1^{\text{HV,HO}} \right) \right] \left(D_1\left(\phi_1^*\right) - D_2\left(\sum_{p \in \mathcal{P}} \delta^p - \phi_1^* \right) \right). \qquad (8.24)
\end{aligned}
$$

According to Equation (8.13), we have

$$
D_1\left(\phi_1^*\right) + \tau = D_2\left(\sum_{p \in \mathcal{P}} \delta^p - \phi_1^* \right).
$$

Since $\tau > 0$, we have

$$
D_1\left(\phi_1^*\right) - D_2\left(\sum_{p \in \mathcal{P}} \delta^p - \phi_1^* \right) < 0. \qquad (8.25)
$$

Also, according to the conditions of the theorem, we have $1 - \frac{1}{\mu} < 0$, $n - \frac{1}{\mu} > 0$, $f_1^{\text{HV,LO}} - \max_{\mathbf{f} \in \mathcal{S}} f_1^{\text{HV,LO}} \leq 0$ and $f_1^{\text{HV,HO}} - \min_{\mathbf{f} \in \mathcal{S}} f_1^{\text{HV,HO}} \geq 0$. Therefore, we can conclude that

$$
J\left(\mathbf{f}\right) - J\left(\mathbf{f}^+\right) \leq 0.
$$

To complete the proof, we have to also show that $\mathbf{f}^+ \in \mathcal{S}$ exists. To show this, we prove that there exists some flow $f_1^{+\text{AV,LO}}$ that both satisfies condition (8.14) and (8.6), i.e., there exists some flow $f_1^{+\text{AV,LO}}$ that satisfies

$$\max_{\mathbf{f}\in\mathcal{S}} f_1^{\text{HV,LO}} + \min_{\mathbf{f}\in\mathcal{S}} f_1^{\text{HV,HO}} + \mu f_1^{+\text{AV,LO}} = \phi_1^* - \delta^{\text{AV,HO}}, \tag{8.26}$$

$$0 \le f_1^{+\text{AV,LO}} \le d^{\text{AV,LO}}. \tag{8.27}$$

Equivalently, we want to show that

$$0 \le \phi_1^* - \delta^{\text{AV,HO}} - \max_{\mathbf{f}\in\mathcal{S}} f_1^{\text{HV,LO}} - \min_{\mathbf{f}\in\mathcal{S}} f_1^{\text{HV,HO}} \le \mu d^{\text{AV,LO}}. \tag{8.28}$$

We first prove the left-side inequality of Eq. (8.28). Let $\tilde{f}_1^{\text{HV,HO}}$ be any flow of human-driven vehicles with high occupancy on lane 1 at any $\mathbf{f} \in \mathcal{S}$ given that the flow of human-driven vehicles with low occupancy on lane 1 equals $\max_{\mathbf{f}\in\mathcal{S}} f_1^{\text{HV,LO}}$. According to Equation (8.14), we must have

$$\tilde{f}_1^{\text{HV,HO}} \le \phi_1^* - \delta^{\text{AV,HO}} - \max_{\mathbf{f}\in\mathcal{S}} f_1^{\text{HV,LO}}. \tag{8.29}$$

Due to $\min_{\mathbf{f}\in\mathcal{S}} f_1^{\text{HV,HO}} \le \tilde{f}_1^{\text{HV,HO}}$, we have

$$\min_{\mathbf{f}\in\mathcal{S}} f_1^{\text{HV,HO}} \le \phi_1^* - \delta^{\text{AV,HO}} - \max_{\mathbf{f}\in\mathcal{S}} f_1^{\text{HV,LO}}, \tag{8.30}$$

which proves the left-side inequality of Eq. (8.28).

We now prove the right-side inequality. Let $\tilde{f}_1^{\text{HV,LO}}$ be any flow of human-driven vehicles with low occupancy on lane 1, at any $\mathbf{f} \in \mathcal{S}$, when the flow of human-driven vehicles with high occupancy on lane 1 equals $\min_{\mathbf{f}\in\mathcal{S}} f_1^{\text{HV,HO}}$. According to Equation (8.14), we must have

$$\phi_1^* - \delta^{\text{AV,HO}} - \min_{\mathbf{f}\in\mathcal{S}} f_1^{\text{HV,HO}} = \tilde{f}_1^{\text{HV,LO}} + \mu f_1^{+\text{AV,LO}}. \tag{8.31}$$

Since $\tilde{f}_1^{\text{HV,LO}} + \mu f_1^{+\text{AV,LO}} \le \max_{\mathbf{f}\in\mathcal{S}} f_1^{\text{HV,LO}} + \mu d^{\text{AV,LO}}$, we have

$$\phi_1^* - \delta^{\text{AV,HO}} - \min_{\mathbf{f}\in\mathcal{S}} f_1^{\text{HV,HO}} \le \max_{\mathbf{f}\in\mathcal{S}} f_1^{\text{HV,LO}} + \mu d^{\text{AV,LO}}, \tag{8.32}$$

which proves the right-side inequality of Eq. (8.28). Thus the proof is complete. $\square$

Theorem 10 provides the conditions under which there is a unique equilibrium, while Theorem 11 allows us to determine the best and worst case equilibria, in terms of the total commuter delay, when the conditions in Theorem 10 do not hold.

Example 2. We now provide a numerical example to illustrate how the results of theorems 10 and 11 can be used to characterize worst and best cases of the total commuter delay, $J(\mathbf{f})$ in Eq. (8.12), when a uniform toll is imposed on all vehicles traveling on lane 1, except for autonomous vehicles with high occupancy (AV,HO). Let $\mathbf{d} = \{d^{\mathrm{AV,HO}} = 4,\ d^{\mathrm{AV,LO}} = 3,\ d^{\mathrm{HV,HO}} = 4,\ d^{\mathrm{HV,LO}} = 5\}$ (in unit of passengers/minute). Assume the delay functions as BPR functions [62] in the form:

$$D_i(\phi_i) = \theta_i + \gamma_i \left(\frac{\phi_i}{m_i} \right)^{\beta_i},\ \ \forall i \in \mathcal{I}, \tag{8.33}$$

with parameters $\mathbf{D} = \{\theta_i = 3(\text{in minutes}),\ \gamma_i = 1,\ \beta_i = 1,\ m_i = 10(\text{in vehicles/minute}) : i \in \mathcal{I} = \{1, 2\}\}$. When $\{n = 4,\ \mu = 0.5\}$, the lane choice equilibrium always exists and is unique when $\tau \geq 0.7$. Setting $\tau = 0.5$, the resulting equilibria form a simplex. The best-case equilibrium in terms of the total commuter delay is $\left(f_1^{\mathrm{HV,LO}} = 0,\ f_1^{\mathrm{HV,HO}} = 1,\ f_1^{\mathrm{AV,LO}} = 0 \right)$, and the worst equilibrium lies at $\left(f_1^{\mathrm{HV,LO}} = 1,\ f_1^{\mathrm{HV,HO}} = 0,\ f_1^{\mathrm{AV,LO}} = 0 \right)$. When $\{n = 2,\ \mu = 0.4\}$, the equilibrium is unique when $\tau \geq 0.74$. Setting $\tau = 0.5$, we have the best equilibrium at $\left(f_1^{\mathrm{HV,LO}} = 0,\ f_1^{\mathrm{HV,HO}} = 0,\ f_1^{\mathrm{AV,LO}} = 3 \right)$, and the worst equilibrium at $\left(f_1^{\mathrm{HV,LO}} = 1.2,\ f_1^{\mathrm{HV,HO}} = 0,\ f_1^{\mathrm{AV,LO}} = 0 \right)$. All the vehicle flows are in unit of vehicles/minute. Notice that in order to mimic the real world scenario, the demands and delay parameters come with certain units, however, the validity of the examples are independent of the units of choice.

8.4   Design Applications

In this section, we explore and present several fields of application where the toll lane framework can be employed to facilitate the decision and optimization process such as to find the optimal toll/occupancy threshold/lane policy that minimizes the total commuter delay under a mixed autonomy.

Determining an appropriate uniform toll τ

One important transportation policy problem is to determine an appropriate toll, which ideally induces the Wardrop equilibrium to approximate a socially optimal one. The optimization problem can be formulated as

$$\min_{\tau \geq 0}\ \ J(\mathbf{f})$$

$$\text{subject to}\ \ \text{Conditions } (8.6) - (8.11).$$

Usually, these type of optimization problems with equilibrium conditions are difficult to solve. However, with the characterization of the equilibria in section 8.3, we propose a simple but effective algorithm to find the optimal toll that minimizes the total commuter delay.

At each toll value, according to Theorem 10, the equilibrium is either unique or in the simplex $\mathcal{S}$ in Eq. (8.15). The simplex is fully characterized by solving the single variable equation (8.13). Moreover, according to Theorem 11, the best and worst case equilibria, in terms of the total delay, can be easily selected from the contour of $\mathcal{S}$. Therefore, at each toll value, the total delay or the best/worst case total delays can be obtained and the toll optimization problem becomes a one dimensional search problem, which can be readily solved by well established algorithms such as golden section search.
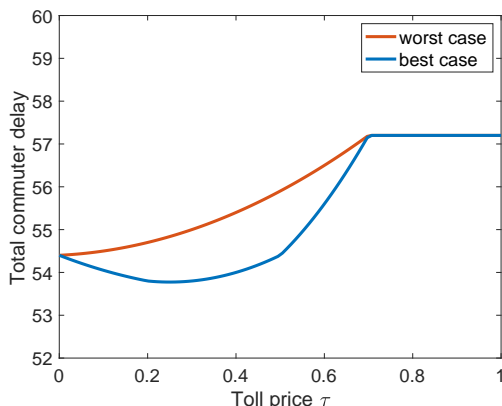
Figure 8.3: The best/worst-case total commuter delay versus different toll values, when a uniform toll is imposed on all vehicles traveling on lane 1, except for autonomous vehicles with high occupancy (AV,HO) (Examples 2 and 3).

Example 3. Consider again the numerical example described in Example 2 where $\{n = 4, \mu = 0.5\}$. The plot of the best/worst case total delay at different toll values is shown in Figure 8.3. As shown in the figure, the worst case total delay increases as the toll increases until the equilibrium becomes unique when $\tau \geq 0.7$. In contrast, the best case total delay first decreases with the increasing toll until it reaches a global minimum at $\tau = 0.25$, and then increases. We may choose the toll to be $\tau = 0$ to minimize the worst case total delay or we may choose the toll to be around $\tau = 0.25$ to minimize the best case total delay.

Determining the HOV passenger occupancy threshold n

Another interesting problem is to determine the passenger occupancy threshold n, at which a vehicle is considered a high occupancy vehicle (HOV). Given fixed total commuter demands, policy designers may want to set the value of n to be as high as possible to encourage a higher occupancy of vehicles. However, requiring occupancy level higher than $n = 2$, tends to disincentivize commuters from carpooling. To study this trade-off, in this section, we assume that the demand of commuters that take human-driven or autonomous vehicles are

fixed, and are respectively denoted by d^{HV} and d^{AV}. We also assume that, for an occupancy threshold $n \geq 2$, the probability of a commuter to carpool, $u(n) \in [0, 1]$, is the same for human-driven and autonomous vehicles, and $u(\cdot)$ is a non-increasing function. Thus, we have

$$d^{\mathrm{HV,HO}} = d^{\mathrm{HV}}u(n) \ \ \text{and} \ \ d^{\mathrm{HV,LO}} = d^{\mathrm{HV}}(1 - u(n)),$$
$$d^{\mathrm{AV,HO}} = d^{\mathrm{AV}}u(n) \ \ \text{and} \ \ d^{\mathrm{AV,LO}} = d^{\mathrm{AV}}(1 - u(n)). \tag{8.34}$$

To find the optimal passenger occupancy threshold n, we need to solve the optimization problem:

$$\min_{n \geq 2} \ \ J(\mathbf{f})$$

$$\text{subject to} \ \ \text{Conditions (8.6)} - \text{(8.11) and (8.34)}.$$

Similar to the toll design problem, we propose a simple solution algorithm with no convexity requirements on the delay functions. At each value of n, we either obtain the unique total delay for pure strategy equilibrium or, conversely, we obtain the best/worst case total delays, by utilizing Theorems 10 an 11. Thus, the passenger occupancy threshold optimization problem becomes a one-dimensional search, which can be solved by algorithms such as golden section search. Notice that the proposed approach can be used with any candidate range of n values, including a set of discrete integer values.

Example 4. We employ the following numerical example to illustrate the proposed passenger occupancy threshold optimization approach. Let $\{d^{\mathrm{AV}} = 7, \ d^{\mathrm{HV}} = 9, \ \mu = 0.5, \ \tau = 0.5\}$. Assume that the delay functions are given by the BPR function in Eq. (8.33), with parameters $\mathbf{D} = \{\theta_i = 3, \ \gamma_i = 1, \ \beta_i = 1, \ m_i = 10 : \ i \in \mathcal{I}\}$. We assume that the probability of a commuter to carpool is given by $u(n) = \frac{1}{n}$ for any $n \in [2, 4]$. The corresponding best/worst case total delay estimates for each value of n is shown in Figure 8.4. For this example, increasing the HOV occupancy threshold n does not significantly decrease the best case total commuter delay, whereas the worst case total commuter delay increases evidently.

Comparing the use of lanes reserved for high-occupancy vehicles with lanes reserved for autonomous vehicles

Currently many transit agencies have policies that allow high-occupancy vehicles (HOV) to travel freely on a dedicated HOV lane, while allowing other vehicles to travel on the HOV lane by paying a toll (henceforth referred to as the dedicated HOV lane (DHOVL) policy). With the upcoming deployment of autonomous and connected driving technologies that enable autonomous vehicles to transit with increased vehicle densities, it is interesting to compare the mobility efficiency gains that result from utilizing a dedicated HOV lane policy as opposed to using that lane to allow autonomous vehicles to transit freely on a dedicated
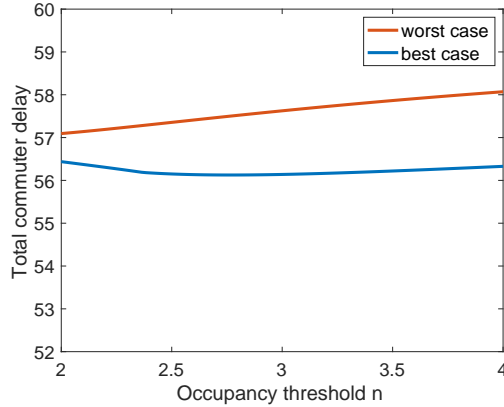
Figure 8.4: The best/worst case total commuter delay versus different values of the HOV occupancy threshold n in Example 4.

lane while charging a toll to other vehicles traveling in that lane (henceforth referred to as the dedicated autonomous vehicle lane (DAVL) policy). We can perform this comparison easily within the modeling framework proposed in the previous section.

The DHOVL policy can be modeled within our framework by setting all HOV flow to be in lane 1. Since we assume by default that all autonomous high occupancy vehicles are traveling on lane 1, we simply need to further set $f_1^{\text{HV,HO}} = \frac{d^{\text{HV,HO}}}{n}$.

Conversely, the DAVL policy can be modeled within our framework by setting $f_1^{\text{AV,LO}} = d^{\text{AV,LO}}$ and allowing the two human-driven vehicle classes (low occupancy and high occupancy) to make lane choices regarding which lane to travel. (Again, the implicit assumption is that toll lane 1 is capable enough to accommodate the prioritized vehicles free of toll, i.e., at least one of the tolled classes of vehicles pays a toll to join lane 1.) The properties of the resulting equilibria for either policy can be investigated using the results of theorems 10 and 11.

Example 5. Here we compare the DHOVL and the DAVL policies. Let $\{d^{\text{AV,HO}} = 4,\ d^{\text{AV,LO}} = 3,\ d^{\text{HV,HO}} = 4,\ d^{\text{HV,LO}} = 5,\ n = 4,\ \mu = 0.5\}$. Assume the delay functions as BPR functions with parameters $\mathbf{D} = \{\theta_i = 3,\ \gamma_i = 1,\ \beta_i = 1,\ m_i = 10 :\ i \in \mathcal{I}\}$. The best/worst case total commuter delay for each of the two policies is shown in Figure 8.5. For this highway configuration and any toll value, the dedicated HOV lane (DHOVL) policy outperforms the dedicated autonomous vehicle lane (DAVL) policy.

8.5   Differentiated Tolling

In this section we consider the scenario where each of the three tolled classes of vehicles is assigned with a distinct value of toll. We define the heterogeneous toll vector $\tau \in \mathbb{R}_+^3$
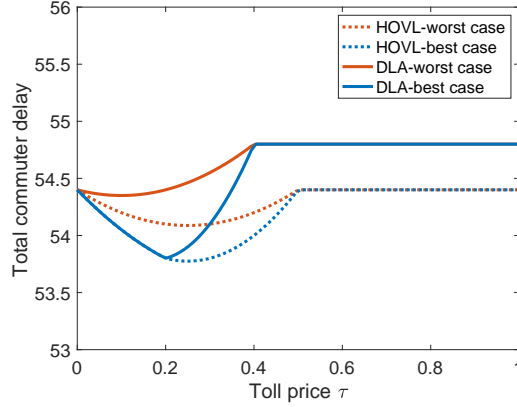
Figure 8.5: The best/worst case commuter total delay versus toll under the dedicated autonomous vehicle lane (DAVL) policy, or the dedicated HOV lane (DHOVL) policy in Example 5.

containing the tolls for the three tolled classes of vehicles as

$$\tau := \left(\tau^{\mathrm{HV,LO}}, \ \tau^{\mathrm{HV,HO}}, \ \tau^{\mathrm{AV,LO}} \right), \tag{8.35}$$

where for any class of vehicles $p \in \bar{\mathcal{P}}$, $\tau^p > 0$, and for $p \neq q \in \bar{\mathcal{P}}$, $\tau^p \neq \tau^q$.

Correspondingly, we let $J(\tau)$ be the total commuter delay under the heterogeneous toll vector τ. Let C_1^p be the travel cost for vehicles of class $p \in \bar{\mathcal{P}}$ on lane 1. Thus we have

$$C_1^p(\mathbf{f}) = D_1(\phi_1) + \tau^p, \ \ p \in \bar{\mathcal{P}}. \tag{8.36}$$

The travel cost for vehicles on lane 2 remains unchanged:

$$C_2(\mathbf{f}) = D_2(\phi_2). \tag{8.37}$$

Therefore, the lane choice equilibrium of the three classes of vehicles with differentiated tolls can then be modeled as a Wardrop equilibrium as follows.

Definition 11. For a segment of highway $G = (\mathbf{D}, \mathbf{d}, \tau, n, \mu)$ with differentiated tolls defined in Eq. (8.35), a feasible flow distribution vector $\mathbf{f}$ is a lane choice equilibrium if and only if, for all vehicles of class $p \in \bar{\mathcal{P}}$,

$$\begin{aligned} f_1^p(C_1^p(\mathbf{f}) - C_2(\mathbf{f})) &\leq 0, \\ f_2^p(C_2(\mathbf{f}) - C_1^p(\mathbf{f})) &\leq 0. \end{aligned} \tag{8.38}$$

When tolls are heterogeneous, the toll optimization problem as described in Section 8.4 is a nontrivial bi-level multi-dimensional optimization problem with equilibrium constraints,

which may potentially be solved by iterative optimization algorithms. However, iterative algorithms may take a long time to converge and for non-convex delay configurations, the convergence is not guaranteed. Therefore, we propose the following approach to effectively decrease the total commuter delay using differentiated tolling: first, assume uniform tolling and find the optimal uniform toll which produces the smallest best case total commuter delay according to the method described in Section 8.4. Subsequently, if the optimal uniform toll is non-zero and there are multiple equilibria, determine the heterogeneous toll vector that will induce the best case equilibrium under the optimal uniform toll. Specifically, we can determine the required heterogeneous toll vector τ in Eq. (8.35) according to the following proposition.

Proposition 10. *For a segment of highway $G = (\mathbf{D}, \mathbf{d}, \tau^*, n, \mu)$, where $\tau^* > 0$ is a predetermined optimal uniform toll that induces non-unique equilibria and let ϕ_1^* be the effective vehicle flow in lane 1 at the equilibria. Let $J^*(\tau^*)$ be the best total commuter delay under the uniform toll τ^*. Further, let $\tau_- > 0$ be any toll value satisfying $\tau_- < \tau^*$ and $\tau_+ > 0$ be any toll value satisfying $\tau_+ > \tau^*$. Then, an heterogeneous toll vector τ in Eq. (8.35) can be determined as follows that results in $J(\tau) = J^*(\tau^*)$:*

1) *If $n \leq \frac{1}{\mu}$, i.e., the required number of passengers for a vehicle to qualify as high-occupancy is smaller than the inverse of the capacity asymmetry degree of autonomous vehicles and, as a consequence, human-driven vehicles with high-occupancy (HV,HO) have a smaller mobility degree than autonomous vehicles with low occupancy (AV,LO), i.e., $\nu^{\mathrm{HV,HO}} < \nu^{\mathrm{AV,LO}}$,*

   a) *if $\phi_1^* \leq \delta^{\mathrm{AV,LO}} + \delta^{\mathrm{AV,HO}}$, then set $\tau = (\tau_+, \ \tau_+, \ \tau^*)$,*

   b) *if $\delta^{\mathrm{AV,LO}} + \delta^{\mathrm{AV,HO}} < \phi_1^* \leq \delta^{\mathrm{HV,HO}} + \delta^{\mathrm{AV,LO}} + \delta^{\mathrm{AV,HO}}$, then set $\tau = (\tau_+, \tau^*, \tau_-)$,*

   c) *if $\phi_1^* > \delta^{\mathrm{HV,HO}} + \delta^{\mathrm{AV,LO}} + \delta^{\mathrm{AV,HO}}$, then set $\tau = (\tau^*, \tau_-, \tau_-)$.*

2) *Conversely, if $n > \frac{1}{\mu}$, and as a consequence, $\nu^{\mathrm{HV,HO}} > \nu^{\mathrm{AV,LO}}$,*

   a) *if $\phi_1^* \leq \delta^{\mathrm{HV,HO}} + \delta^{\mathrm{AV,HO}}$, then set $\tau = (\tau_+, \tau^*, \tau_+)$,*

   b) *if $\delta^{\mathrm{HV,HO}} + \delta^{\mathrm{AV,HO}} < \phi_1^* \leq \delta^{\mathrm{AV,LO}} + \delta^{\mathrm{HV,HO}} + \delta^{\mathrm{AV,HO}}$, then set $\tau = (\tau_+, \tau_-, \tau^*)$,*

   c) *if $\phi_1^* > \delta^{\mathrm{AV,LO}} + \delta^{\mathrm{HV,HO}} + \delta^{\mathrm{AV,HO}}$, then set $\tau = (\tau^*, \tau_-, \tau_-)$.*

The general idea of this toll design proposition is to first identify the best equilibrium among all equilibria under a homogeneous toll, and then assign the optimal homogeneous toll τ^* to the vehicle class that uses both lanes under the best equilibrium, a toll higher than τ^* to the vehicle classes with a smaller mobility degree, and a toll lower than τ^* to vehicle classes with a larger mobility degree. We present a sketch of the proof below.

Proof. We give the detailed explanation for the first sub-case **a)** when $n \leq \frac{1}{\mu}$. According to Theorem 11, when $n \leq \frac{1}{\mu}$ and consequently all autonomous vehicles, including those with low occupancy, have a higher mobility degree than high occupancy human-driven vehicles, i.e. $\nu^{\text{AV,LO}} > \nu^{\text{HV,HO}}$, we should first prioritize autonomous vehicles with low occupancy on lane 1. When $\phi_1^* \leq \delta^{\text{AV,LO}} + \delta^{\text{AV,HO}}$, the best equilibrium under the optimal uniform toll would be $\mathbf{f}_1 = (0, 0, \frac{\phi_1^* - \delta^{\text{AV,HO}}}{\mu})$. One can check that $\mathbf{f}_1 = (0, 0, \frac{\phi_1^* - \delta^{\text{AV,HO}}}{\mu})$ is an equilibrium and is the only equilibrium that fulfills Definition 11 when tolls are selected as τ. The proofs for the other cases follow a similar logic and are thus omitted. $\square$

8.6   Effect of Vehicle Misbehavior

According to the previous section, the total commuter delay in a freeway segment can be significantly decreased by setting differentiated tolls for distinct classes of vehicles if they choose to enter the toll lane. However, the effectiveness of differentiated tolls may be undermined in real world scenarios because of deliberate vehicle misbehavior (i.e. toll cheating). For example, many toll-collection agencies determine whether a vehicle is either a high-occupancy or a low-occupancy vehicle via the signal transmitted by the toll collection transponder in the vehicle, which is often set by commuters themselves. Since toll-collecting agencies will not always validate the occupancy signals that they receive from vehicle transponders and may not consistently enforce fines to violating vehicles, some low-occupancy vehicles may decide to deceitfully send a high-occupancy transponder signal and enter the toll lane while paying the lower toll designed for high-occupancy vehicles. In this section, we will explore the impact of such misbehavior on the overall transportation system. Without loss of generality, we assume that misbehavior may take place among all classes of vehicles except autonomous vehicles with high occupancy (AV,HO), which are allowed to travel freely on the toll lane.

We will still consider inelastic commuter demands d^p and corresponding effective demand δ^p for every class of vehicles $p \in \mathcal{P}$. As in the previous section, we allow autonomous vehicles with high occupancy (AV,HO) to travel on the toll lane freely whereas differentiated nonzero tolls $\boldsymbol{\tau}$ as defined in (8.35) are charged to the other three classes of vehicles.

Let us now consider the possibility that a portion of ***misbehaving*** human-driven or low-occupancy autonomous vehicles may decide to travel on lane 1, without paying their prescribed toll. Denoting $0 \leq \alpha_{\text{m}}^p \leq 1$ as the proportion of misbehaving vehicles of class $p \in \bar{\mathcal{P}}$, we define the misbehaving proportion vector $\boldsymbol{\alpha}_{\text{m}} \in \mathbb{R}_+^3$ as

$$\boldsymbol{\alpha}_{\text{m}} := \left(\alpha_{\text{m}}^{\text{HV,LO}}, \alpha_{\text{m}}^{\text{HV,HO}}, \alpha_{\text{m}}^{\text{AV,LO}} \right). \tag{8.39}$$

These portions of misbehaving vehicles choose to travel on lane 1, without paying their assigned toll, at the risk of being caught by law enforcement and paying a fine.

Considering misbehaving vehicles, a feasible and meaningful flow distribution vector of **honest** vehicles $\hat{\mathbf{f}} := \left(\hat{\mathbf{f}}_1, \hat{\mathbf{f}}_2 \right) \in \mathbb{R}_+^6$, where $\hat{\mathbf{f}}_i := \left(\hat{f}_i^{\text{HV,LO}},\ \hat{f}_i^{\text{HV,HO}},\ \hat{f}_i^{\text{AV,LO}} \right) \in \mathbb{R}_+^3$ for lane $i \in \mathcal{I}$, must satisfy

$$
\begin{aligned}
\sum_{i \in \mathcal{I}} \hat{f}_i^{\text{HV,LO}} &= d^{\text{HV,LO}}(1 - \alpha_{\text{m}}^{\text{HV,LO}}), \\
\sum_{i \in \mathcal{I}} \hat{f}_i^{\text{HV,HO}} &= \frac{d^{\text{HV,HO}}}{n}(1 - \alpha_{\text{m}}^{\text{HV,HO}}), \\
\sum_{i \in \mathcal{I}} \hat{f}_i^{\text{AV,LO}} &= d^{\text{AV,LO}}(1 - \alpha_{\text{m}}^{\text{AV,LO}}), \\
\hat{f}_i^p &\geq 0, \quad \forall p \in \bar{\mathcal{P}}.
\end{aligned}
\tag{8.40}
$$

We also define $\hat{\phi}_i$ as the effective vehicle flow on lane $i \in \mathcal{I}$, accounting for misbehaving vehicles:

$$
\hat{\phi}_1 := \hat{f}_1^{\text{HV,LO}} + \hat{f}_1^{\text{HV,HO}} + \mu \hat{f}_1^{\text{AV,LO}} + \delta^{\text{AV,HO}} + \sum_{p \in \bar{\mathcal{P}}} \delta^p \alpha_{\text{m}}^p,
\tag{8.41}
$$

$$
\hat{\phi}_2 := \hat{f}_2^{\text{HV,LO}} + \hat{f}_2^{\text{HV,HO}} + \mu \hat{f}_2^{\text{AV,LO}},
$$

where we remind the reader that δ^p is the effective inelastic demand of vehicles of class $p \in \mathcal{P}$, as defined in Eq. (8.2). The travel delays D_i for lane $i \in \mathcal{I}$, is then a continuous and increasing function of $\hat{\phi}_i$, where we have $\hat{\phi}_1 \in \left[\delta^{\text{AV,HO}} + \sum_{p \in \bar{\mathcal{P}}} \delta^p \alpha_{\text{m}}^p, \sum_{p \in \mathcal{P}} \delta^p \right]$, and $\hat{\phi}_2 \in \left[0, \sum_{p \in \bar{\mathcal{P}}} \delta^p (1 - \alpha_{\text{m}}^p) \right]$, where $\sum_{p \in \bar{\mathcal{P}}} \delta^p \alpha_{\text{m}}^p$ is the effective total demand of misbehaving vehicles.

As in the previous section, let $\boldsymbol{\tau}$ be the vector of differentiated tolls, as defined in Eq. (8.35). Therefore, the travel cost experienced by **honest** vehicles, respectively traveling on lane 1 and 2 is given by

$$
C_1^p(\hat{\mathbf{f}}) = D_1(\hat{\phi}_1) + \tau^p,
\tag{8.42}
$$

$$
C_2(\hat{\mathbf{f}}) = D_2(\hat{\phi}_2).
\tag{8.43}
$$

Let the tuple $\hat{G} = (\mathbf{D}, \mathbf{d}, \tau, n, \mu, \boldsymbol{\alpha}_{\text{m}})$ represent a segment of highway shown in Figure 8.1 with the delay models $\mathbf{D}$, commuter demands $\mathbf{d}$, toll prices τ, an occupancy threshold n for high-occupancy vehicles, a capacity asymmetry degree μ for autonomous vehicles and misbehavior proportions $\boldsymbol{\alpha}_{\text{m}}$. The lane choice equilibrium for honest vehicles can be modeled by the following conditions.

Definition 12. For a segment of highway $\hat{G} = (\mathbf{D}, \mathbf{d}, \tau, n, \mu, \boldsymbol{\alpha}_{\mathrm{m}})$ with differentiated tolls and misbehaving vehicles, a feasible honest vehicle flow distribution vector $\hat{\mathbf{f}}$ is a lane choice equilibrium if and only if, for any vehicle class $p \in \bar{\mathcal{P}}$, we have

$$\hat{f}_1^p(C_1^p(\hat{\mathbf{f}}) - C_2(\hat{\mathbf{f}})) \leq 0, \tag{8.44}$$
$$\hat{f}_2^p(C_2(\hat{\mathbf{f}}) - C_1^p(\hat{\mathbf{f}})) \leq 0.$$

The total delay experienced by all commuters at a lane choice equilibrium $\hat{\mathbf{f}}$ can be calculated as

$$J(\hat{\mathbf{f}}) = \left(\hat{f}_2^{\mathrm{HV,LO}} + \hat{f}_2^{\mathrm{AV,LO}} + n\hat{f}_2^{\mathrm{HV,HO}} \right) D_2(\hat{\phi}_2) + \left[\hat{f}_1^{\mathrm{HV,LO}} + \hat{f}_1^{\mathrm{AV,LO}} + d^{\mathrm{HV,LO}}\alpha_{\mathrm{m}}^{\mathrm{HV,LO}} \right.$$
$$\left. + d^{\mathrm{AV,LO}}\alpha_{\mathrm{m}}^{\mathrm{AV,LO}} + n \left(\hat{f}_1^{\mathrm{HV,HO}} + \frac{d^{\mathrm{HV,HO}}}{n}\alpha_{\mathrm{m}}^{\mathrm{HV,HO}} + \frac{d^{\mathrm{AV,HO}}}{n} \right) \right] D_1(\hat{\phi}_1). \tag{8.45}$$

Notice that, in the extreme case where there exists no vehicle misbehavior, i.e. $\alpha_{\mathrm{m}}^p = 0$ for all $p \in \bar{\mathcal{P}}$, the lane choice equilibrium in Definition 12 will be the same as the lane choice equilibrium in Definition 11.

We intuitively expect that misbehavior of vehicles may deteriorate the traffic condition on the toll lane 1 since excessive demands of vehicles join lane 1. Furthermore, such misbehavior of vehicles may harm the traffic conditions of the whole transportation system. However, does such misbehavior actually always harm the traffic conditions? We will first discuss the impact of vehicle misbehavior on lane delays via the following theorem:

Theorem 12. *Consider a segment of highway* $\hat{G} = (\mathbf{D}, \mathbf{d}, \tau, n, \mu, \boldsymbol{\alpha}_{\mathrm{m}})$ *with differentiated tolls as given by Eq.* (8.35), *and proportions of misbehaving vehicles given by Eq.* (8.39). *The lane delays at the lane choice equilibrium* $\hat{\mathbf{f}}$, *as described in Definition 12, will remain the same as the lane delays of the lane choice equilibrium* $\mathbf{f}$ *without any vehicle misbehavior as described in Definition 11, if the following two conditions hold:*

1) *At the lane choice equilibrium* $\mathbf{f}$ *without any vehicle misbehavior, there exists a class of vehicles* $g \in \bar{\mathcal{P}}$ *that travel on both lanes, i.e., vehicles of class g experience the same travel cost on toll lane 1 and the regular lane 2. As a consequence, at the lane choice equilibrium* $\mathbf{f}$, *the effective total vehicle flow* ϕ_1^* *can be determined by the following equation:*

$$D_1(\phi_1^*) + \tau^g = D_2 \left(\sum_{p \in \mathcal{P}} \delta^p - \phi_1^* \right), \tag{8.46}$$

where τ^g is vehicle class g's assigned toll.

2) *Misbehaving vehicle proportions* $\boldsymbol{\alpha}_{\mathrm{m}}$ *satisfy*

$$\sum_{p \in \bar{\mathcal{P}} \backslash \mathcal{Q}_-^g} \delta^p \alpha_{\mathrm{m}}^p \leq \phi_1^* - \delta^{\mathrm{AV,HO}} - \sum_{q \in \mathcal{Q}_-^g} \delta^q, \tag{8.47}$$

> where the set $\mathcal{Q}_-^g \subset \bar{\mathcal{P}}$ contains all vehicle classes assigned a nonzero toll smaller than τ^g, and $\bar{\mathcal{P}} \setminus \mathcal{Q}_-^g \subset \bar{\mathcal{P}}$ contains all vehicle classes with a toll larger than or equal to τ^g.

The above theorem describes the conditions under which lane delays are unaffected by vehicle misbehavior, as long as the number of misbehaving vehicles remains sufficiently small. The underlying reason for the robustness is that, as the number of misbehaving vehicles entering toll lane 1 increases, honest vehicles will sense the potentially increased congestion in that lane, and will choose to travel on lane 2 instead. Thus, the selfish lane choices of all vehicles counter-intuitively are able to tolerate a certain amount of vehicle misbehavior, mitigating its resulting negative impact on lane delays.

Proof. We prove by contradiction that, under conditions (8.46) and (8.47), the effective total flow on lane 1 remains the same, i.e., $\hat{\phi}_1 = \phi_1^*$ and as a consequence, the lane delays remain the same.

Assume first that $\hat{\phi}_1 > \phi_1^*$. Since $C_1^g(\phi_1)$ are increasing functions of ϕ_1 and $C_2^g(\phi_1)$ are decreasing functions of ϕ_1, we conclude that it must be the case that $C_1^g(\hat{\phi}_1) > C_1^g(\phi_1^*)$ and $C_2^g(\hat{\phi}_1) < C_2^g(\phi_1^*)$. According to condition (8.46), since $C_2^g(\hat{\phi}_1) < C_1^g(\hat{\phi}_1)$, all class g vehicles must be traveling on lane 2. Correspondingly, all the other classes of vehicles, which are not misbehaving and whose assigned toll on lane 1 is larger than or equal to the toll assigned to vehicles of class g, must also be traveling on lane 2. Therefore, at the equilibrium $\hat{\mathbf{f}}$ described by Eq. (8.44), we have

$$\hat{\phi}_1 \leq \sum_{p \in \bar{\mathcal{P}} \setminus \mathcal{Q}_-^g} \delta^p \alpha_{\mathrm{m}}^p + \delta^{\mathrm{AV,HO}} + \sum_{q \in \mathcal{Q}_-^g} \delta^q, \tag{8.48}$$

since some vehicles belonging to $\mathcal{Q}_-^g$ could also be traveling on lane 2. However, due to condition (8.47), (8.48) implies that $\hat{\phi}_1 \leq \phi_1^*$, which contradicts our assumption.

Assume now that $\hat{\phi}_1 < \phi_1^*$ and, as a consequence, $C_1^g(\hat{\phi}_1) < C_1^g(\phi_1^*)$ and $C_2^g(\hat{\phi}_1) > C_2^g(\phi_1^*)$. According to condition (8.46), we have $C_2^g(\hat{\phi}_1) > C_1^g(\hat{\phi}_1)$. Thus, all honest vehicles of class g must be traveling on lane 1. Correspondingly, all the other honest vehicles whose toll is smaller than τ^g, the toll assigned to vehicles of class g, must also be traveling on lane 1. Therefore, at the equilibrium $\hat{\mathbf{f}}$, we have

$$\hat{\phi}_1 \geq \delta^{\mathrm{AV,HO}} + \sum_{q \in \mathcal{Q}_-^g} \delta^q (1 - \alpha_{\mathrm{m}}^q) + \sum_{q \in \mathcal{Q}_-^g} \delta^q \alpha_{\mathrm{m}}^q + \delta^g (1 - \alpha_{\mathrm{m}}^g) + \delta^g \alpha_{\mathrm{m}}^g, \tag{8.49}$$

since there are cheating vehicles belonging to the other classes traveling on lane 1. However, at equilibrium $\mathbf{f}$ described in (8.44) when there are no misbehaving vehicles, we have

$$\phi_1^* \leq \delta^{\mathrm{AV,HO}} + \sum_{q \in \mathcal{Q}_-^g} \delta^q + \delta^g, \tag{8.50}$$

since vehicles of class g are traveling on both lanes. Therefore, it must be the case that $\hat{\phi}_1 \geq \phi_1^*$, which contradicts our assumption. This proves that, Under conditions (8.46)

and (8.47), the effective total flow on lane 1 remains the same, i.e., $\hat{\phi}_1 = \phi_1^*$, and the lane delays remain the same.   □

In spite of the fact that, under the conditions of Theorem 12, lane delays remain unchanged under moderate vehicle cheating, the total commuter delay may still vary. This result is formalized in the next theorem.

Theorem 13. *Consider a highway segment $\hat{G} = (\mathbf{D}, \mathbf{d}, \tau, n, \mu, \boldsymbol{\alpha}_{\mathrm{m}})$ outlined in Theorem 12. Let $\mathcal{Q}_+^g \subset \bar{\mathcal{P}}$ be the set that contains all vehicle classes with an assigned nonzero toll that is higher than τ^g and let $\mathcal{M} := \{p \subseteq \bar{\mathcal{P}} : \alpha_{\mathrm{m}}^p > 0\}$ be the set that contains the vehicle classes in which misbehaving occurs.*
  Assuming that conditions 1) and 2) in Theorem 12 hold,

a) *if $\mathcal{Q}_+^g \cap \mathcal{M} = \emptyset$, then the total commuter delay of the lane choice equilibrium $\hat{\mathbf{f}}$ described in Definition 12, which results as a consequence of vehicle misbehavior, is larger than the total commuter delay of the lane choice equilibrium $\mathbf{f}$, which occurs without any vehicle misbehavior as described in Definition 11, i.e.,*

$$J(\hat{\mathbf{f}}) = J(\mathbf{f}). \tag{8.51}$$

b) *if $\mathcal{Q}_+^g \cap \mathcal{M} \neq \emptyset$ and every vehicle class $s \in \mathcal{Q}_+^g \cap \mathcal{M}$ has a mobility degree $\nu^s < \nu^g$, then*

$$J(\hat{\mathbf{f}}) > J(\mathbf{f}). \tag{8.52}$$

c) *if $\mathcal{Q}_+^g \cap \mathcal{M} \neq \emptyset$ and every vehicle class $s \in \mathcal{Q}_+^g \cap \mathcal{M}$ has a mobility degree $\nu^s > \nu^g$, then*

$$J(\hat{\mathbf{f}}) < J(\mathbf{f}). \tag{8.53}$$

Condition a) in Theorem 13 emphasizes that the total commuter delay is not affected by vehicle misbehavior if there are no cheating vehicles with an assigned toll that is higher than τ^g. The reader is reminded that vehicles belonging to class g experience the same travel cost whether they travel on toll lane 1 or on the regular lane 2, under the lane choice equilibrium $\mathbf{f}$, which occurs under no vehicle misbehavior, as described in Condition 1) in Theorem 12.

Condition b) in Theorem 13 corresponds to the situation when tolls are applied rationally. It is rational to assign a larger toll than τ^g to a vehicle class that has a mobility degree that is lower than the mobility degree of class g vehicles. Under rational tolling, the total commuter delay deteriorates with vehicle misbehavior, even if the amount of misbehavior is moderate as described in Eq. (8.47) in Theorem 12.

Proof. By Theorem 12 and its proof, the lane delays that result under a lane choice equilibrium $\hat{\mathbf{f}}$ (with vehicle misbehavior) will remain the same as the lane delays that result under the lane choice equilibrium $\mathbf{f}$ (without vehicle misbehavior). Specifically, for any lane $i \in \mathcal{I} = \{1, 2\}$, we have

$$\phi_i^* = \hat{\phi}_i \text{ and } D_i(\phi_i^*) = D_i\left(\hat{\phi}_i\right),$$

where $\hat{\phi}_i$ is the effective total flow on lane i at the lane choice equilibrium $\hat{\mathbf{f}}$ with vehicle misbehavior. Therefore, we have $D_1\left(\hat{\phi}_1\right) + \tau^g = D_2\left(\hat{\phi}_2\right)$, which implies that class g vehicles may possibly occupy both lanes, while vehicles that are charged a toll lower than τ^g will choose to travel on lane 1, and honest vehicles that are charged with a toll larger than τ^g will choose to travel on lane 2.

From Eqs. (8.12) and (8.45) we have

$$
J\left(\mathbf{f}\right) - J\left(\hat{\mathbf{f}}\right) = \left(\sum_{q \in \mathcal{Q}_-^g} d^q + nf_1^g + d^{\mathrm{AV,HO}}\right) D_1\left(\phi_1^*\right) + \left(\sum_{q \in \mathcal{Q}_+^g} d^q + nf_2^g\right) D_2\left(\sum_{p \in \mathcal{P}} \delta^p - \phi_1^*\right)
$$
$$
- \left[\left(\sum_{s \in \mathcal{M} \cap \mathcal{Q}_+^g} \alpha_{\mathrm{m}}^s d^s + \sum_{q \in \mathcal{Q}_-^g} d^q + \alpha_{\mathrm{m}}^g d^g + n\hat{f}_1^g + d^{\mathrm{AV,HO}}\right) D_1\left(\phi_1^*\right)\right.
$$
$$
\left. + \left(\sum_{q \in \mathcal{Q}_+^g} d^q - \sum_{s \in \mathcal{M} \cap \mathcal{Q}_+^g} \alpha_{\mathrm{m}}^s d^s + n\hat{f}_2^g\right) D_2\left(\sum_{p \in \mathcal{P}} \delta^p - \phi_1^*\right)\right], \qquad (8.54)
$$

where readers are reminded that the set $\mathcal{M}$ contains all misbehaving vehicles, i.e., for any vehicle class $s \in \mathcal{M}$, $\alpha_{\mathrm{m}}^s > 0$. Moreover, if class g vehicles are low occupancy vehicles, we just let $n = 1$ within this proof. Rearranging terms in (8.54), we have

$$
J\left(\mathbf{f}\right) - J\left(\hat{\mathbf{f}}\right) = \left(nf_1^g - \sum_{s \in \mathcal{M} \cap \mathcal{Q}_+^g} \alpha_{\mathrm{m}}^s d^s - \alpha_{\mathrm{m}}^g d^g - n\hat{f}_1^g\right) D_1\left(\phi_1^*\right)
$$
$$
+ \left(nf_2^g + \sum_{s \in \mathcal{M} \cap \mathcal{Q}_+^g} \alpha_{\mathrm{m}}^s d^s - n\hat{f}_2^g\right) D_2\left(\sum_{p \in \mathcal{P}} \delta^p - \phi_1^*\right). \qquad (8.55)
$$

Flow conservation implies that

$$
\hat{f}_1^g + \alpha_{\mathrm{m}}^g \delta^g + \hat{f}_2^g = f_1^g + f_2^g, \quad \text{when } g = \mathrm{HV,HO} \text{ or } \mathrm{HV,LO}, \qquad (8.56)
$$
$$
\text{or}
$$
$$
\mu\hat{f}_1^g + \alpha_{\mathrm{m}}^g \delta^g + \mu\hat{f}_2^g = \mu f_1^g + \mu f_2^g. \quad \text{when } g = \mathrm{AV,LO}, \qquad (8.57)
$$

Multiplying ν^g on both sides of either Eq. (8.56) or (8.57), we have $n\hat{f}_1^g + \alpha_{\mathrm{m}}^g d^g - nf_1^g = nf_2^g - n\hat{f}_2^g$, where ν^g is the mobility degree for vehicle class g defined in Eqs. (8.2) and (8.3).

Thus, we have

$$
J\left(\mathbf{f}\right) - J\left(\hat{\mathbf{f}}\right) = \left(n f_1^g - \sum_{s \in \mathcal{M} \cap \mathcal{Q}_+^g} \alpha_{\mathrm{m}}^s d^s - \alpha_{\mathrm{m}}^g d^g - n \hat{f}_1^g \right) D_1\left(\phi_1^*\right)
$$

$$
+ \left(n \hat{f}_1^g + \alpha_{\mathrm{m}}^g d^g + \sum_{s \in \mathcal{M} \cap \mathcal{Q}_+^g} \alpha_{\mathrm{m}}^s d^s - n f_1^g \right) D_2 \left(\sum_{p \in \mathcal{P}} \delta^p - \phi_1^* \right)
$$

$$
= \left(n f_1^g - \sum_{s \in \mathcal{M} \cap \mathcal{Q}_+^g} \alpha_{\mathrm{m}}^s d^s - \alpha_{\mathrm{m}}^g d^g - n \hat{f}_1^g \right) \left(D_1\left(\phi_1^*\right) - D_2 \left(\sum_{p \in \mathcal{P}} \delta^p - \phi_1^* \right) \right).
$$

$$(8.58)$$

According to condition 1) and Eq. (8.46) in Theorem 12,

$$
D_1\left(\phi_1^*\right) - D_2 \left(\sum_{p \in \mathcal{P}} \delta^p - \phi_1^* \right) < 0. \tag{8.59}
$$

Moreover, since $\phi_1^* = \hat{\phi}_1$, we have

$$
f_1^g - \alpha_{\mathrm{m}}^g \delta^g - \hat{f}_1^g = \sum_{s \in \mathcal{M} \cap \mathcal{Q}_+^g} \alpha_{\mathrm{m}}^s \delta^s, \quad \text{when } g = \mathrm{HV}, \mathrm{HO} \text{ or } \mathrm{HV}, \mathrm{LO}, \tag{8.60}
$$

or

$$
\mu f_1^g - \alpha_{\mathrm{m}}^g \delta^g - \mu \hat{f}_1^g = \sum_{s \in \mathcal{M} \cap \mathcal{Q}_+^g} \alpha_{\mathrm{m}}^s \delta^s, \quad \text{when } g = \mathrm{AV}, \mathrm{LO}. \tag{8.61}
$$

Multiplying ν^g on both sides of Eq. (8.60) or (8.61), we obtain $n \hat{f}_1^g + \alpha_{\mathrm{m}}^g d^g - n f_1^g = \nu^g \sum_{s \in \mathcal{M} \cap \mathcal{Q}_+^g} \alpha_{\mathrm{m}}^s \delta^s$. Thus,

$$
J\left(\mathbf{f}\right) - J\left(\hat{\mathbf{f}}\right) = \left(\nu^g \sum_{s \in \mathcal{M} \cap \mathcal{Q}_+^g} \alpha_{\mathrm{m}}^s \delta^s - \sum_{s \in \mathcal{M} \cap \mathcal{Q}_+^g} \alpha_{\mathrm{m}}^s d^s \right) \left(D_1\left(\phi_1^*\right) - D_2 \left(\sum_{p \in \mathcal{P}} \delta^p - \phi_1^* \right) \right).
$$

$$(8.62)$$

As described in Theorem 13, if $\mathcal{M} \cap \mathcal{Q}_+^g = \emptyset$, we have $J\left(\mathbf{f}\right) - J\left(\hat{\mathbf{f}}\right) = 0$. Otherwise if $\mathcal{M} \cap \mathcal{Q}_+^g \neq \emptyset$, for every vehicle class $s \in \mathcal{M} \cap \mathcal{Q}_+^g$ we have $d^s = \nu^s \delta^s$ and

$$
J\left(\mathbf{f}\right) - J\left(\hat{\mathbf{f}}\right) = \left((\nu^g - \nu^s) \sum_{s \in \mathcal{M} \cap \mathcal{Q}_+^g} \alpha_{\mathrm{m}}^s \delta^s \right) \left(D_1\left(\phi_1^*\right) - D_2 \left(\sum_{p \in \mathcal{P}} \delta^p - \phi_1^* \right) \right). \tag{8.63}
$$

If $\nu^s < \nu^g$, by Eqs. (8.63) and (8.59), $J\left(\mathbf{f}\right) - J\left(\hat{\mathbf{f}}\right) < 0$. Conversely, if $\nu^s > \nu^g$, $J\left(\mathbf{f}\right) - J\left(\hat{\mathbf{f}}\right) > 0$. $\qquad\square$

Theorem 12 states that lane delays are unaffected by vehicle misbehavior under moderate vehicle cheating volumes if the assumptions stated in the theorem apply. Theorem 13 states that the total travel cost becomes an increasing function of the proportion of vehicle toll violations, when rational tolling policies are utilized.

Example 6. We illustrate the above results with a simple scenario in which differentiated tolling is applied and vehicle misbehavior takes place. Consider a highway segment with the following commuter demands $\{d^{\text{AV,HO}} = 20, \ d^{\text{AV,LO}} = 30, \ d^{\text{HV,HO}} = 48, \ d^{\text{HV,LO}} = 36\}$, a vehicle occupancy of $n = 2$ to qualify as a high-occupancy vehicle, and an autonomy capacity asymmetry degree of $\mu = 0.3$. With these parameters, the class of autonomous vehicles with high occupancy (AV,HO) has the largest mobility degree given by $\nu^{\text{AV,HO}} = \frac{n}{\mu} \approx 6$. These vehicles travel freely on the toll lane 1. The other three classes of vehicles will be tolled while traveling on lane 1. Of these, the class of autonomous vehicles with low occupancy (AV,LO) has the largest mobility degree given by $\nu^{\text{AV,LO}} = \frac{1}{\mu} \approx 3$, followed by the class of human-driven vehicles with high occupancy (HV,HO) with a mobility degree $\nu^{\text{HV,HO}} = n = 2$. The class of human driven vehicles with low occupancy (HV,LO) has the smallest mobility degree $\nu^{\text{HV,LO}} = 1$.

A rational differentiated tolling policy should assign progressively higher tolls to vehicles as their mobility degrees decrease. Thus, in this example we assign the following tolls: $\tau^{\text{HV,LO}} = 0.3$, $\tau^{\text{HV,HO}} = 0.12$ and $\tau^{\text{AV,LO}} = 0.05$. The delay functions used in this example are the BPR functions in Eq. (8.33) with parameters $\mathbf{D} = \{\theta_i = 3, \ \gamma_i = 1, \ \beta_i = 1, \ m_i = 100 : \ i \in \mathcal{I} = [1, 2]\}$.

From Eq. (8.46) in Condition 1) of theorem 12, we can determine that the class of HV,HO vehicles will be traveling on both lanes at the lane choice equilibrium, when no vehicles misbehave, i.e. $g = \text{HV}, \text{HO}$. Correspondingly, according to the toll configuration, we have $\mathcal{Q}_{-}^{g} = \{\text{AV, LO}\}$ and $\mathcal{Q}_{+}^{g} = \{\text{HV, LO}\}$.

In this example, we consider the case when only human-driven vehicles with low occupancy (HV,LO) misbehave i.e., $\alpha_{\text{m}}^{\text{HV,LO}} > 0$, while $\alpha_{\text{m}}^{\text{HV,HO}} = \alpha_{\text{m}}^{\text{AV,LO}} = 0$. We then gradually increase the proportion of misbehaving HV,LO vehicles and plot the tendency curve of lane delays and the total commuter delay in Figure 8.6.

Fig. 8.6a plots lane delays as the proportion of misbehaving HV,LO vehicles, $\alpha_{\text{m}}^{\text{HV,LO}}$, increases from 0 to 1. As expected from the results of Theorem 12, lane delays remain robust to moderate levels of cheating vehicles until the proportion of cheating vehicles exceeds the bound given by Eq. (8.47), which in this example is $\alpha_{\text{m}}^{\text{HV,LO}} = 0.5$. When bound (8.47) is exceeded, lane delays indeed vary.

Fig. 8.6b plots the total commuter delay $J(\hat{\mathbf{f}})$ in Eq. (8.45) as $\alpha_{\text{m}}^{\text{HV,LO}}$, increases from 0 to 1. Notice that condition b) in theorem 13 is satisfied. Therefore, as expected from the results of this theorem, the total delay increases as $\alpha_{\text{m}}^{\text{HV,LO}}$ increases, until bound (8.47) is exceeded when $\alpha_{\text{m}}^{\text{HV,LO}} = 0.5$ and the total commuter delay $J(\hat{\mathbf{f}})$ is no longer guaranteed to be a monotonically increasing function of $\alpha_{\text{m}}^{\text{HV,LO}}$.

Figs. 8.6a and 8.6b also show that, when the proportion of human driven vehicles with
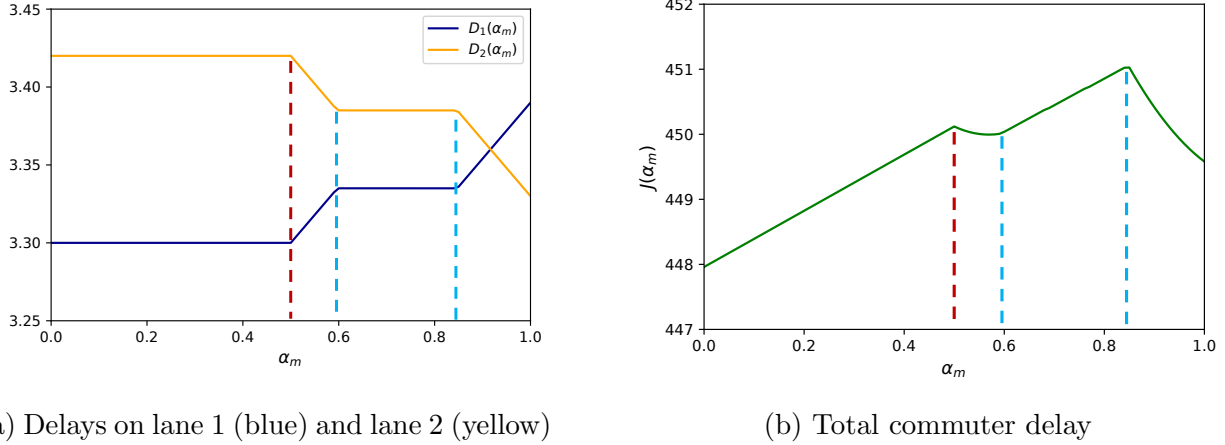
(a) Delays on lane 1 (blue) and lane 2 (yellow)   (b) Total commuter delay

Figure 8.6: The lane delays and the total commuter delay as a function of the proportion
of misbehaving human driven vehicles with low occupancy (HV,LO) $\alpha_m^{\text{HV,LO}}$, as described
in Example 6. While the conditions in Theorem 12, 13 and Proposition 11 hold, the total
commuter delay increases as $\alpha_m^{\text{HV,LO}}$ increases, while lane delays remain constant. As long as
the toll design is rational, the minimum total commuter delay occurs when vehicles do not
misbehave.

low occupancy toll violations, $\alpha_m^{\text{HV,LO}}$, increases beyond the bound given by Eq. (8.47), lane
travel delays no longer remain constant and the total commuter delay may in fact temporarily
decrease as the number of toll violations increases. This undesirable phenomenon persists
until another robust region is reached ($\alpha_m^{\text{HV,LO}} \in [0.6, 0.85]$ in Fig. 8.6a), in which lane
delays again remain constant and the total commuter delay becomes an increasing function
of the number of toll violations. The above results are formally described in the following
proposition.

Proposition 11. *Consider a highway segment* $\hat{G} = (\mathbf{D}, \mathbf{d}, \tau, n, \mu, \boldsymbol{\alpha}_{\mathrm{m}})$ *as outlined in The-
orem 12. Assume that, Condition 1) in Theorem 12 holds and there exists a vehicle class
$g_- \in \mathcal{Q}_-^g$, i.e., $\tau^{g-} < \tau^g$, then the lane delays remain constant when the misbehaving vehicle
proportions $\boldsymbol{\alpha}_{\mathrm{m}}$ lie in the following region:*

$$\tilde{\phi}_1 - \delta^{\mathrm{AV,HO}} - \sum_{q \in \mathcal{Q}_-^{g-}} \delta^q - \delta^{g-}(1 - \alpha_{\mathrm{m}}^{g-}) \leq \sum_{p \in \bar{\mathcal{P}} \backslash \mathcal{Q}_-^{g-}} \delta^p \alpha_{\mathrm{m}}^p \leq \tilde{\phi}_1 - \delta^{\mathrm{AV,HO}} - \sum_{q \in \mathcal{Q}_-^{g-}} \delta^q, \quad (8.64)$$

*where the set $\mathcal{Q}_-^{g-} \subset \bar{\mathcal{P}}$ contains all vehicle classes whose assigned toll in lane 1 is smaller
than τ^{g-}, and the value $\tilde{\phi}_1$ of the effective flow in lane 1 is determined by the following
equation:*

$$D_1(\tilde{\phi}_1) + \tau^{g-} = D_2(\sum_{p \in \mathcal{P}} \delta^p - \tilde{\phi}_1). \quad (8.65)$$

Furthermore, let $\mathcal{Q}_+^{g-} \subset \bar{\mathcal{P}}$ be the set that contains all vehicle classes with an assigned toll higher than τ^{g-} and consider the total commuter delay $J(\hat{\mathbf{f}})$ as a function of $\tilde{\alpha} := \sum_{p \in \mathcal{Q}_+^{g-}} \delta^p \alpha_m^p$ (the total number of cheating vehicles with a toll larger than τ^{g-}). We also remind the reader that the set $\mathcal{M} := \{p \subseteq \bar{\mathcal{P}} : \alpha_m^p > 0\}$ contains all misbehaving vehicle classes.

a) *If $\mathcal{Q}_+^{g-} \cap \mathcal{M} = \emptyset$, then $J(\tilde{\alpha})$ remains constant within the region characterized by Eq. (8.64).*

b) *If $\mathcal{Q}_+^{g-} \cap \mathcal{M} \neq \emptyset$ and every vehicle class $s \in \mathcal{Q}_+^{g-} \cap \mathcal{M}$, has a mobility degree $\nu^s < \nu^{g-}$, then $J(\tilde{\alpha})$ is an increasing function within the region characterized by Eq. (8.64).*

c) *If $\mathcal{Q}_+^{g-} \cap \mathcal{M} \neq \emptyset$ and every vehicle class $s \in \mathcal{Q}_+^{g-} \cap \mathcal{M}$, has a mobility degree $\nu^s > \nu^{g-}$, then $J(\tilde{\alpha})$ is a decreasing function within the region characterized by Eq. (8.64).*

Proof. The proof of the proposition can be obtained by replacing vehicle class g with vehicle class g_- within the proof of Theorem 12 and 13. Thus the proof is omitted here. $\square$

Example 7. We continue our analysis of the results in Example 6, when the proportion of cheating vehicles $\alpha_m^{\text{HV,LO}}$ is larger than bound (8.47) in theorem 12, i.e. $\alpha_m^{\text{HV,LO}} > 0.5$, and we use the results in proposition 11 to determine the robust region $\alpha_m^{\text{HV,LO}} \in [0.6, 0.85]$ in which lane delays again remain constant.

Since $\mathcal{Q}_-^g = \{\text{AV}, \text{LO}\}$, we have only one vehicle class $g_- = \text{AV}, \text{LO}$ (autonomous vehicles with low occupancy) and only expect one additional robust region. We first determine the value $\tilde{\phi}_1 = 33.5$ of the effective flow in lane 1 using Eq. (8.65), and then obtain the lower and upper bounds of the robust region $\alpha_m^{\text{HV,LO}} \in [0.6, 0.85]$ by calculating the respective lower and upper bounds in Eq. (8.64). Correspondingly, lane delays remain constant withing this region, as shown in Fig. 8.6a. Finally, since Condition b) in Proposition 11 is satisfied, the total commuter delay monotonically increases as a function of $\alpha_m^{\text{HV,LO}}$ within this region, as shown in Fig. 8.6b.

Notice that the undesirable and somewhat counter-intuitive phenomenon observed in the intervals $\alpha_m^{\text{HV,LO}} \in (0.5, 0.6)$ and $\alpha_m^{\text{HV,LO}} \in (0.85, 1]$ in Fig. 8.6b, where the total commuter delay decreases as the proportion of cheating vehicles increases, cannot be predicted by the results contained in the theorems and propositions presented in this chapter. However, in this somewhat simple example, this phenomenon can be explained as follows. As the number of cheating vehicles traveling on toll lane 1 increase, the other vehicle classes, which rightfully can travel on lane 1, choose instead to travel on lane 2, as their cost of traveling on lane 1 becomes larger than their cost of traveling in lane 2. The two critical proportions of vehicle misbehavior $\alpha_m^{\text{HV,LO}} = 0.5$ and $\alpha_m^{\text{HV,LO}} = 0.85$ observed in Fig. 8.6b, when total travel time becomes a local maximum function of vehicle misbehavior, occur when all honest vehicles of a certain vehicle class are driven out of lane 1. Thus, in this example all vehicles of class HV,HO are driven out of lane 1 when $\alpha_m^{\text{HV,LO}} = 0.5$, while all vehicles of class AV,LO are driven out of lane 1 when $\alpha_m^{\text{HV,LO}} = 0.85$. When this occurs, the decrease in the delay of the lane 2, due to cheating vehicles choosing to use lane 1, becomes the dominant factor

affecting the change of total commuter delay, causing its downward slope as a function of vehicle cheating proportion. We also stress that, even though increase cheating locally improves total commuter delay, it is still larger than the total delay under no cheating and vehicle cheating results in revenue loss on the part of the toll-collecting agencies.

8.7 Summary

We proposed a toll lane framework where four classes of vehicles are sharing a segment of highway with a restricted/tolled lane. In our framework autonomous vehicles with high occupancy, which have the largest mobility index and as a consequence have the largest impact in increasing commuter density in a lane, travel freely on the restricted/tolled lane. The other three classes of vehicles, human-driven vehicles with high occupancy, autonomous vehicles with low occupancy and human-driven vehicles with low occupancy, can choose to enter the restricted/tolled lane by paying a toll or instead use the regular lanes without paying a toll. We assume that all vehicles are selfish and will always minimize their own travel costs. We established desirable properties of the resulting lane choice Wardrop equilibria, by comparing high-occupancy vehicles with autonomous vehicles in terms of their capabilities to increase lane commuter densities, and establishing rational tolling policies accordingly. We also developed a framework for analyzing and designing a number of toll lane policies including the selection of an optimal uniform toll, the determination of the optimal vehicle occupancy threshold for classifying vehicles as high occupancy, and design parameters for guaranteeing that a differentiated tolling policy will minimize the total commuter delay in the freeway segment. We also considered the effects of toll violation by various classes of misbehaving vehicles on the lane and total commuter delays. Our analysis shows that, under rational tolling policies and moderate quantities of vehicle toll violations, lane delays remain unaffected but total commuter delay increases. However, when the number of vehicle toll violations increases beyond a prescribed bound, the total commuter delay may possibly decrease under increased vehicle toll violations under certain circumstances.

Part IV

Conclusions and Future Directions

Chapter 9

Conclusions

The rapid advancement of autonomous driving technology in both academic and industrial settings has spurred a widespread belief that autonomous vehicles will significantly transform future transportation systems. Nonetheless, the integration of autonomous vehicles into current transportation systems necessitates a comprehensive examination of their limitations and potential impacts. While aiming for "perfect" autonomous vehicles that can excellently perform any task on the roads is a less realistic goal, it is even more crucial to explore how specific features of autonomy can be applied in certain transportation scenarios to define the demand for autonomous vehicles. Therefore, the essence of this dissertation is to investigate the application of particular features of autonomous vehicles in specific transportation scenarios in order to induce societal benefits. The scenario-based control design for autonomous vehicles aims to address the potential benefit of autonomy while minimizing the dependence on "perfect" autonomy.

One novel approach proposed in the dissertation (Part II) is to utilize autonomous vehicles as altruistic decision-makers in traffic networks to address the issue of inefficiency and congestion, which is in contrast to the selfish behavior of human-driven vehicles. A systematic macroscopic behavioral model for human-driven vehicles is proposed to effectively and efficiently predict human-driven vehicles' selfish lane choice behavior in various transportation scenarios, such as traffic diverges with an upstream bifurcating lane in the middle targeting two exit directions (Chapter 3), and highway on-ramp areas (Chapter 4), and examine the level of inefficiency and congestion induced by human-driven vehicles' selfish behavior. To leverage the potential of autonomous vehicles as altruistic decision-makers, an approach is proposed to configure the local cost that autonomous vehicles evaluate in local scenarios to make it relevant to social efficiency (Chapter 5). This approach enables autonomous vehicles to make decisions that are aligned with the goal of enhancing social mobility, ultimately leading to a reduction in congestion and improved social traffic conditions.

Another approach investigated in the dissertation is to decrease the headway of autonomous vehicles on the roads. The potential of autonomous vehicles to increase road capacities by preserving a shorter headway compared to human-driven vehicles has been widely validated by previous literature and experiment results. Part III in the dissertation

examines the impact of autonomous vehicles' shortened headway in various transportation scenarios with a focus on the interaction between human-driven and autonomous vehicles in the mixed autonomy transportation system. The scenario where vehicles selfishly choose their route across a traffic network is first examined. In Chapter 6, a theoretic guarantee is established for traffic networks with a single origin-destination pair that better social traffic conditions can be obtained by decreasing autonomous vehicles' headway. A closed-form upper bound of the impact induced by autonomous vehicles' shortened headway related to the penetration rate and headway of autonomous vehicles is proved for networks with parallel roads. This proof has significant implications for policymakers and engineers, as it provides an important expectation for the potential impact of autonomous vehicles on traffic networks. Policymakers and engineers can better anticipate and evaluate the potential benefits and challenges of autonomous vehicles' integration into transportation systems and make informed decisions. Further in Chapter 7, the stability of the dynamic mixed autonomy system with queuing and signal controls is analyzed using dissipativity tools from population games. Chapter 8 presents an analysis of a typical toll lane scenario under mixed autonomy. In this scenario, autonomous vehicles and high-occupancy vehicles share the road, which leads to indeterminate and uncontrollable lane choice equilibria. To address this issue, a comprehensive study of the best and worst-case lane choice equilibria is conducted and an effective differentiated tolling scheme is proposed to enforce the appearance of the best lane choice equilibrium. The proposed toll lane framework provides an effective mechanism for comparing autonomous vehicles to high-occupancy vehicles in enhancing social mobility and transitioning established policies for high-occupancy vehicles to policies for autonomous vehicles.

Overall, this dissertation contributes to the understanding of how autonomous vehicles can be utilized in various specified transportation scenarios to enhance societal benefits and particularly emphasizes the crucial challenge in integrating autonomous vehicles into human-dominated transportation systems: developing suitable control and optimization strategies considering selfish human drivers' interaction and exploitation. The dissertation provides a theoretical and practical foundation for future studies in the application of autonomous vehicles and can assist policymakers in formulating effective regulations that promote a sustainable and efficient mixed autonomy transportation system.

Chapter 10

Future Directions

The application of autonomous vehicles in future transportation systems is a wide-ranging and interdisciplinary field that presents numerous challenges and opportunities across various research domains. These include but are not limited to human behavior modeling, multi-agent system modeling, and control and optimization. As a final remark, I would like to suggest several potential avenues for further exploration that could expand upon the findings of this dissertation.

A Unified Behavioral Modeling Framework. The lane choice modeling framework introduced in Part II is applicable to various scenarios, including traffic diverges with a bifurcating lane in the middle, highway on-ramps, and human drivers' crafty bypassing behavior at the end of diverges [44]. Although these scenarios share similar lane choice decision models, their cost functions have unique structures. Our current approach employs iterative design, whereby we propose cost functions, calibrate and validate them until satisfactory results are obtained. The framework shows a potential in the prediction of lane choice behavior in other gaming scenarios in traffic networks such as roundabouts and median U-turns. However, in more and more complex scenarios, discovering suitable cost functions becomes increasingly challenging, as the structure of cost functions can become less intuitive. As a result, it is beneficial and necessary to explore a unified model that is capable of learning the cost functions from human drivers' demonstrations either in a specified scenario or across multiple scenarios.

Human Agents' Bounded Rationality. The underlying assumption of this dissertation is that humans are inherently selfish, meaning that they strive to maximize their own benefits, which demonstrates rational behavior. However, it is important to acknowledge that in reality, humans have limited rationality. For instance, when selecting a route, humans may choose a familiar one without considering the possibility of traffic congestion. This type of behavior is known as heuristics. In modeling and control design, it is essential to consider the impact of heuristics, as they can drastically alter how humans react to autonomous agents. Therefore, it is imperative to consider human agents' heuristics and bounded rationality when designing future transportation systems that incorporate autonomous vehicles, and ensure the robustness and resilience of the control and the system.

Network Level Incentive Design. In Chapter 5, we have explored how autonomous vehicles can be programmed to make altruistic decisions, reducing system-level congestion. However, it is essential to consider the fairness and realism of such approaches, particularly at a larger scale network level. It may not be appropriate to always exploit the benefits from a certain subset of vehicles. Therefore, we must consider how we can motivate autonomous vehicles to align with social objectives more effectively. For instance, a certain subset of autonomous vehicles could sacrifice their interests in certain scenarios such as highway on-ramps but gain benefits elsewhere such as rewarded by reduced pricing in toll lanes. By considering the network-level altruism distribution and incentive design, we can create more equitable and efficient transportation systems.

An Even Broader Picture. The process of reshaping daily transportation requires input from multiple stakeholders, including the user market, public or private transit agencies, and authorities. However, in many cases, stakeholders may have different or even conflicting interests or goals. Therefore, it is necessary to account for interactions of different stakeholders and find solutions that align goals of various parties when designing policies and reforming the system. Various mechanisms in the interaction, collaboration and communication between stakeholders, shall be properly designed in order to create transportation systems that are more efficient, reliable, equitable, and sustainable.

Bibliography

[1] INRIX Research. "Inrix 2022 global traffic scorecard." (2022), [Online]. Available: https://inrix.com/scorecard/.

[2] M. Papageorgiou and A. Kotsialos, "Freeway ramp metering: An overview," *IEEE transactions on intelligent transportation systems*, vol. 3, no. 4, pp. 271–281, 2002.

[3] A. Hegyi, B. De Schutter, and H. Hellendoorn, "Model predictive control for optimal coordination of ramp metering and variable speed limits," *Transportation Research Part C: Emerging Technologies*, vol. 13, no. 3, pp. 185–209, 2005.

[4] G. Gomes and R. Horowitz, "Optimal freeway ramp metering using the asymmetric cell transmission model," *Transportation Research Part C: Emerging Technologies*, vol. 14, no. 4, pp. 244–262, 2006.

[5] P. Hunt, D. Robertson, R. Bretherton, and M. C. Royle, "The scoot on-line traffic signal optimisation technique," *Traffic Engineering & Control*, vol. 23, no. 4, 1982.

[6] N. H. Gartner, *OPAC: A demand-responsive strategy for traffic signal control*, 906. 1983.

[7] M. Smith and T. Van Vuren, "Traffic equilibrium with responsive traffic control," *Transportation science*, vol. 27, no. 2, pp. 118–132, 1993.

[8] P. Varaiya, "Max pressure control of a network of signalized intersections," *Transportation Research Part C: Emerging Technologies*, vol. 36, pp. 177–195, 2013.

[9] K. Button and E. Verhoef, *Road pricing, traffic congestion and the environment*. Edward Elgar Publishing, 1998.

[10] A. de Palma and R. Lindsey, "Traffic congestion pricing methodologies and technologies," *Transportation Research Part C: Emerging Technologies*, vol. 19, no. 6, pp. 1377–1399, 2011.

[11] N. Mehr and R. Horowitz, "Pricing traffic networks with mixed vehicle autonomy," in *2019 American Control Conference (ACC)*, IEEE, 2019, pp. 2676–2682.

[12] J. Lioris, R. Pedarsani, F. Y. Tascikaraoglu, and P. Varaiya, "Doubling throughput in urban roads by platooning," *IFAC-PapersOnLine*, vol. 49, no. 3, pp. 49–54, 2016.

[13] ——, "Platoons of connected vehicles can double throughput in urban roads," *Transportation Research Part C: Emerging Technologies*, vol. 77, pp. 292–305, 2017.

[14] C. Wu, A. Kreidieh, E. Vinitsky, and A. M. Bayen, "Emergent behaviors in mixed-autonomy traffic," in *Conference on Robot Learning*, 2017, pp. 398–407.

[15] N. Mehr and R. Horowitz, "How will the presence of autonomous vehilces affect the equilibrium state of traffic networks?" *IEEE Transactions on Control of Network Systems*, vol. 7, no. 1, pp. 96–105, 2019.

[16] S. W. Smith, Y. Kim, J. Guanetti, *et al.*, "Improving urban traffic throughput with vehicle platooning: Theory and experiments," *IEEE Access*, vol. 8, pp. 141 208–141 223, 2020.

[17] P. N. Brown, "Partial altruism is worse than complete selfishness in nonatomic congestion games," *arXiv preprint arXiv:2007.05591*, 2020.

[18] R. Li, N. Mehr, and R. Horowitz, "The impact of autonomous vehicles' headway on the social delay of traffic networks," in *2020 59th IEEE Conference on Decision and Control (CDC)*, IEEE, 2020, pp. 268–273.

[19] C. M. Farmer, "Crash avoidance potential of five vehicle technologies," *Insurance Institute for Highway Safety*, 2008.

[20] S. A. Bagloee, M. Tavana, M. Asadi, and T. Oliver, "Autonomous vehicles: Challenges, opportunities, and future implications for transportation policies," *Journal of modern transportation*, vol. 24, no. 4, pp. 284–303, 2016.

[21] B. Asadi and A. Vahidi, "Predictive cruise control: Utilizing upcoming traffic signal information for improving fuel economy and reducing trip time," *IEEE transactions on control systems technology*, vol. 19, no. 3, pp. 707–714, 2010.

[22] L. Luo, H. Liu, P. Li, and H. Wang, "Model predictive control for adaptive cruise control with multi-objectives: Comfort, fuel-economy, safety and car-following," *Journal of Zhejiang University SCIENCE A*, vol. 11, no. 3, pp. 191–201, 2010.

[23] I. H. Zohdy, R. K. Kamalanathsharma, and H. Rakha, "Intersection management for autonomous vehicles using icacc," in *2012 15th international IEEE conference on intelligent transportation systems*, IEEE, 2012, pp. 1109–1114.

[24] A. Talebpour and H. S. Mahmassani, "Influence of connected and autonomous vehicles on traffic flow stability and throughput," *Transportation Research Part C: Emerging Technologies*, vol. 71, pp. 143–163, 2016.

[25] Z. Zheng, "Recent developments and research needs in modeling lane changing," en, *Transportation Research Part B: Methodological*, vol. 60, pp. 16–32, Feb. 2014, ISSN: 01912615. DOI: 10.1016/j.trb.2013.11.009.

[26] M. Rahman, M. Chowdhury, Y. Xie, and Y. He, "Review of microscopic lane-changing models and future research opportunities," *IEEE transactions on intelligent transportation systems*, vol. 14, no. 4, pp. 1942–1956, 2013.

[27] P. G. Gipps, "A model for the structure of lane-changing decisions," *Transportation Research Part B: Methodological*, vol. 20, no. 5, pp. 403–414, 1986.

[28]   A. Halati, H. Lieu, and S. Walker, "Corsim - corridor traffic simulation model," in *Traffic Congestion and Traffic Safety in the 21st Century: Challenges, Innovations, and Opportunities*, 1997.

[29]   K. I. Ahmed, "Modeling drivers' acceleration and lane changing behavior," in *Thesis (Sc. D.)–Massachusetts Institute of Technology*, 1999.

[30]   T. Toledo, H. N. Koutsopoulos, and M. E. Ben-Akiva, "Modeling integrated lane-changing behavior," in *Transportation Research Record: Journal of the Transportation Research Board, Volume: 1857 issue: 1*, 2003, pp. 30–38.

[31]   A. Kesting, M. Treiber, and D. Helbing, "General lane-changing model mobil for car-following models," *Transportation Research Record: Journal of the Transportation Research Board*, no. 1999, pp. 86–94, 2007.

[32]   H. Kita, "A merging–giveway interaction model of cars in a merging section: A game theoretic analysis," *Transportation Research Part A: Policy and Practice*, vol. 33, no. 3-4, pp. 305–312, 1999.

[33]   P. Hidas, "Modelling vehicle interactions in microscopic simulation of merging and weaving," in *Transportation Research Part C: Emerging Technologies Volume 13, Issue 1*, Elsevier, 2005, pp. 37–62.

[34]   A. Talebpour, H. S. Mahmassani, and S. H. Hamdar, "Modeling lane-changing behavior in a connected environment: A game theory approach," *Transportation Research Part C: Emerging Technologies*, vol. 59, pp. 216–232, 2015.

[35]   F. Meng, J. Su, C. Liu, and W.-H. Chen, "Dynamic decision making in lane change: Game theory with receding horizon," in *2016 UKACC 11th International Conference on Control (CONTROL)*, IEEE, 2016, pp. 1–6.

[36]   A. C. Pigou, *The economics of welfare*. Palgrave Macmillan, 2013.

[37]   T. Roughgarden and É. Tardos, "How bad is selfish routing?" *Journal of the ACM (JACM)*, vol. 49, no. 2, pp. 236–259, 2002.

[38]   G.-L. Chang and Y.-M. Kao, "An empirical investigation of macroscopic lane-changing characteristics on uncongested multilane freeways," in *Transportation Research Part A: General Volume 25, Issue 6*, Elsevier, 1991, pp. 375–389.

[39]   M. Brackstone, M. McDonald, and J. Wu, "Lane changing on the motorway: Factors affecting its occurrence, and their implications," in *Ninth International Conference on Road Transport Information and Control*, 1998, pp. 160–164.

[40]   C. F. Daganzo, "A behavioral theory of multi-lane traffic flow. part ii: Merges and the onset of congestion," in *Transportation Research Part B: Methodological Volume 36, Issue 2*, Elsevier, 2002, pp. 159–169.

[41]   B. Coifman, S. Krishnamurthy, and X. Wang, "Lane-change maneuvers consuming freeway capacity," in *Traffic and Granular Flow 03*, Springer, 2005, pp. 3–14.

[42] J. A. Laval and C. F. Daganzo, "Lane-changing in traffic streams," *Transportation Research Part B: Methodological*, vol. 40, no. 3, pp. 251–264, 2006.

[43] J. Laval, M. Cassidy, and C. Daganzo, "Impacts of lane changes at merge bottlenecks: A theory and strategies to maximize capacity," in *Traffic and Granular Flow'05*, Springer, 2007, pp. 577–586.

[44] N. Mehr, R. Li, and R. Horowitz, "A game theoretic model for aggregate bypassing behavior of vehicles at traffic diverges," in *21st International Conference on Intelligent Transportation Systems*, IEEE, 2018.

[45] J. G. Wardrop, "Some theoretical aspects of road traffic research," in *Proceedings of the Institution of Civil Engineers, Volume 1 Issue 3*, 1952, pp. 325–362.

[46] M. Cassidy, P. Chan, B. Robinson, and A. May, "A proposed analytical technique for the design and analysis of major freeway weaving sections. final report," Tech. Rep., 1990.

[47] R. Cole, Y. Dodis, and T. Roughgarden, "Pricing network edges for heterogeneous selfish users," in *Proceedings of the thirty-fifth annual ACM symposium on Theory of computing*, 2003, pp. 521–530.

[48] L. Fleischer, K. Jain, and M. Mahdian, "Tolls for heterogeneous selfish users in multi-commodity networks and generalized congestion games," in *45th Annual IEEE Symposium on Foundations of Computer Science*, IEEE, 2004, pp. 277–285.

[49] B. L. Ferguson, P. N. Brown, and J. R. Marden, "Utilizing information optimally to influence distributed network routing," in *2019 IEEE 58th Conference on Decision and Control (CDC)*, IEEE, 2019, pp. 5008–5013.

[50] P. N. Brown and J. R. Marden, "Can taxes improve congestion on all networks?" *IEEE Transactions on Control of Network Systems*, 2020.

[51] M. J. Beckmann, C. B. McGuire, and C. B. Winsten, "Studies in the economics of transportation," 1955.

[52] W. H. Sandholm, "Evolutionary implementation and congestion pricing," *The Review of Economic Studies*, vol. 69, no. 3, pp. 667–689, 2002.

[53] E. Bıyık, D. A. Lazar, R. Pedarsani, and D. Sadigh, "Altruistic autonomy: Beating congestion on shared roads," in *International Workshop on the Algorithmic Foundations of Robotics*, Springer, 2018, pp. 887–904.

[54] Q. Jin, G. Wu, K. Boriboonsomsin, and M. Barth, "Platoon-based multi-agent intersection management for connected vehicle," in *16th International IEEE Conference on Intelligent Transportation Systems (ITSC 2013)*, IEEE, 2013, pp. 1462–1467.

[55] A. I. M. Medina, N. Van de Wouw, and H. Nijmeijer, "Automation of a t-intersection using virtual platoons of cooperative autonomous vehicles," in *2015 IEEE 18th International Conference on Intelligent Transportation Systems*, IEEE, 2015, pp. 1696–1701.

[56] G. Antonelli and S. Chiaverini, "Fault tolerant kinematic control of platoons of autonomous vehicles," in *IEEE International Conference on Robotics and Automation, 2004. Proceedings. ICRA'04. 2004*, IEEE, vol. 4, 2004, pp. 3313–3318.

[57] D. J. Stilwell, B. E. Bishop, and C. A. Sylvester, "Redundant manipulator techniques for partially decentralized path planning and control of a platoon of autonomous vehicles," *IEEE Transactions on Systems, Man, and Cybernetics, Part B (Cybernetics)*, vol. 35, no. 4, pp. 842–848, 2005.

[58] G. Antonelli and S. Chiaverini, "Kinematic control of platoons of autonomous vehicles," *IEEE Transactions on Robotics*, vol. 22, no. 6, pp. 1285–1292, 2006.

[59] S. Gong, J. Shen, and L. Du, "Constrained optimization and distributed computation based car following control of a connected and autonomous vehicle platoon," *Transportation Research Part B: Methodological*, vol. 94, pp. 314–334, 2016.

[60] S. Gong, A. Zhou, and S. Peeta, "Cooperative adaptive cruise control for a platoon of connected and autonomous vehicles considering dynamic information flow topology," *Transportation Research Record*, vol. 2673, no. 10, pp. 185–198, 2019.

[61] M. Mavronicolas and P. Spirakis, "The price of selfish routing," in *Proceedings of the thirty-third annual ACM symposium on Theory of computing*, 2001, pp. 510–519.

[62] Bureau of Public Roads, *Traffic assignment manual*. U.S. Department of Commerce, Urban Planning Division, 1964.

[63] D. A. Lazar, S. Coogan, and R. Pedarsani, "Capacity modeling and routing for traffic networks with mixed autonomy," in *2017 IEEE 56th Annual Conference on Decision and Control (CDC)*, IEEE, 2017, pp. 5678–5683.

[64] M. Smith and M. Wisten, "A continuous day-to-day traffic assignment model and the existence of a continuous dynamic user equilibrium," *Annals of Operations Research*, vol. 60, no. 1, pp. 59–79, 1995.

[65] M. Smith, "Traffic signal control and route choice: A new assignment and control model which designs signal timings," *Transportation Research Part C: Emerging Technologies*, vol. 58, pp. 451–473, 2015.

[66] M. J. Fox and J. S. Shamma, "Population games, stable games, and passivity," *Games*, vol. 4, no. 4, pp. 561–583, 2013.

[67] S. Park, N. C. Martins, and J. S. Shamma, "From population games to payoff dynamics models: A passivity-based approac," in *2019 IEEE 58th Conference on Decision and Control (CDC)*, IEEE, 2019, pp. 6584–6601.

[68] M. Arcak and N. C. Martins, "Dissipativity tools for convergence to nash equilibria in population games," *IEEE Transactions on Control of Network Systems*, vol. 8, no. 1, pp. 39–50, 2021. DOI: 10.1109/TCNS.2020.3029990.

[69] H. S. Mahmassani, "50th anniversary invited article—autonomous vehicles and connected vehicle systems: Flow and operations considerations," *Transportation Science*, vol. 50, no. 4, pp. 1140–1162, 2016.

[70] L. Ye and T. Yamamoto, "Impact of dedicated lanes for connected and autonomous vehicle on traffic flow throughput," *Physica A: Statistical Mechanics and its Applications*, vol. 512, pp. 588–597, 2018.

[71] J. Ivanchev, A. Knoll, D. Zehe, S. Nair, and D. Eckhoff, "A macroscopic study on dedicated highway lanes for autonomous vehicles," in *International Conference on Computational Science*, Springer, 2019, pp. 520–533.

[72] A. Talebpour, H. S. Mahmassani, and A. Elfar, "Investigating the effects of reserved lanes for autonomous vehicles on congestion and travel time reliability," *Transportation Research Record*, vol. 2622, no. 1, pp. 1–12, 2017. DOI: 10.3141/2622-01. eprint: https://doi.org/10.3141/2622-01. [Online]. Available: https://doi.org/10.3141/2622-01.

[73] Z. Zhong, *Assessing the effectiveness of managed lane strategies for the rapid deployment of cooperative adaptive cruise control technology*. New Jersey Institute of Technology, 2018.

[74] Z. Liu and Z. Song, "Strategic planning of dedicated autonomous vehicle lanes and autonomous vehicle/toll lanes in transportation networks," *Transportation Research Part C: Emerging Technologies*, vol. 106, pp. 381–403, 2019.

[75] L. Xiao, M. Wang, and B. van Arem, "Traffic flow impacts of converting an hov lane into a dedicated cacc lane on a freeway corridor," *IEEE Intelligent Transportation Systems Magazine*, vol. 12, no. 1, pp. 60–73, 2019.

[76] Y. Guo and J. Ma, "Leveraging existing high-occupancy vehicle lanes for mixed-autonomy traffic management with emerging connected automated vehicle applications," *Transportmetrica A: Transport Science*, vol. 16, no. 3, pp. 1375–1399, 2020.

[77] R. Li, N. Mehr, and R. Horowitz, "An extended game–theoretic model for aggregate lane choice behavior of vehicles at traffic diverges with a bifurcating lane," in *2019 IEEE Intelligent Transportation Systems Conference (ITSC)*, IEEE, 2019, pp. 2226–2231.

[78] R. Li, J. Liu, and R. Horowitz, "A game-theoretic model for aggregate lane choice behavior of highway mainline vehicles at the vicinity of on-ramps," in *2020 American Control Conference (ACC)*, IEEE, 2020, pp. 5376–5381.

[79] R. Li, P. N. Brown, and R. Horowitz, "Employing altruistic vehicles at on-ramps to improve the social traffic conditions," in *2021 American Control Conference (ACC)*, IEEE, 2021, pp. 4547–4552.

[80] R. Li and R. Horowitz, "Dynamic routing and queuing for mixed autonomy with traffic responsive intersection signaling," in *2022 American Control Conference (ACC)*, IEEE, 2022, pp. 144–155.

[81] R. Li, P. N. Brown, and R. Horowitz, "A highway toll lane framework that unites autonomous vehicles and high-occupancy vehicles," in *2021 IEEE International Intelligent Transportation Systems Conference (ITSC)*, IEEE, 2021, pp. 3482–3489.

[82] D. Braess and G. Koch, "On the existence of equilibria in asymmetrical multiclass-user transportation networks," *Transportation Science*, vol. 13, no. 1, pp. 56–63, 1979.

[83] D. Krajzewicz, J. Erdmann, M. Behrisch, and L. Bieker, "Recent development and applications of SUMO - Simulation of Urban MObility," *International Journal On Advances in Systems and Measurements*, International Journal On Advances in Systems and Measurements, vol. 5, no. 3&4, pp. 128–138, Dec. 2012. [Online]. Available: http://elib.dlr.de/80483/.

[84] V. Raman, A. Donzé, M. Maasoumy, R. M. Murray, A. Sangiovanni-Vincentelli, and S. A. Seshia, "Model predictive control with signal temporal logic specifications," in *2014 IEEE 53rd Annual Conference on Decision and Control (CDC)*, IEEE, 2014, pp. 81–87.

[85] L. Leclercq, J. A. Laval, and N. Chiabaut, "Capacity drops at merges: An endogenous model," *Procedia-Social and Behavioral Sciences*, vol. 17, pp. 12–26, 2011.

[86] A. Srivastava and N. Geroliminis, "Empirical observations of capacity drop in freeway merges with ramp control and integration in a first-order model," *Transportation Research Part C: Emerging Technologies*, vol. 30, pp. 161–177, 2013.

[87] *California Driver Handbook*, https://www.dmv.ca.gov/web/eng_pdf/dl600.pdf, California Department of Motor Vehicles, 2019.

[88] Trans Res Board, *Highway Capacity Manual*. Washington, D.C.: Transportation Research Board, National Research Council, 2000.

[89] *Aimsun 8 users' manual*, Transportation Simulation Systems, S.L., 2015.

[90] R. Li, N. Mehr, and R. Horowitz, *An extended game-theoretic model for aggregate lane choice behavior of vehicles at traffic diverges with a bifurcating lane*, 2019. arXiv: 1904.08358 [cs.GT].

[91] M. A. Hall, "Properties of the equilibrium state in transportation networks," *Transportation Science*, vol. 12, no. 3, pp. 208–216, 1978.

[92] H. Spiess, "Conical volume-delay functions," *Transportation Science*, vol. 24, no. 2, pp. 153–158, 1990.

[93] D. Hearn, "Bounding flows in traffic assignment models," *Research Report*, pp. 80–4, 1980.